YOLLANDA E. MOREIRA FRANCO

Estudo da via da glutaminólise em astrocitomas e mecanismo de ação do gene *GLSiso2* (GAC)

São Paulo

2023

YOLLANDA E. MOREIRA FRANCO

Estudo da via da glutaminólise em astrocitomas e mecanismo de ação do gene *GLSiso2* (GAC)

Tese apresentada à Faculdade de Medicina da Universidade de São Paulo para obtenção de título de Doutor em Ciências.

Programa de Neurologia

Orientadora: Profa. Dra. Suely Kazue Nagahashi Marie

São Paulo

2023

Ficha Catalográfica

Dedicatória

À minha família, em especial às minhas avós
pelas orações, carinho e ensinamentos.

Ao meu marido Thomas, pelo carinho,
incentivo e apoio incondicional.

Com todo meu amor dedico a vocês.

Agradecimentos

À minha orientadora Profa. Dra. Suely Kazue Nagahashi Marie, que me deu todo apoio e incentivo, nos momentos que mais precisei. Obrigada por me ajudar tanto, confiar e não desistir de mim. A você fica minha eterna gratidão e respeito.

À Dra. Sueli Mieko Oba-Shinjo por toda atenção, mentoria e ajuda.

À Dra. Roseli da Silva e Paula Sola pela ajuda no desenvolvimento desse trabalho.

Ao Dr. Antonio Lerário por todas as análises de transcriptoma e pelas sugestões relevantes no desenvolvimento desse trabalho e de tantos outros no nosso laboratório.

Ao Prof. Dr. Esper Kallas e equipe, por me permitir e ajudar a realizar os ensaios de citometria de fluxo.

Ao laboratório de sequenciamento em larga escala (SELA), principalmente a Amanda Narcizo.

Ao MSKCC, Brown Laboratory e principalmente à Dr. Chrysothemis Brown, por me permitir realizar parte dos ensaios apresentados nesse trabalho.

À Dra. Patricia Oliveira de Carvalho e Dra. Giovanna Barbarini Longato por estarem comigo nessa jornada cientifica desde sempre e por me permitirem realizar ensaios celulares e metabolomicos.

Às queridas alunas do LIM-15 Adaliana, Camila, Isabelle, Stella e Talita. Obrigada pelo companheirismo, por toda ajuda e conselhos compartilhados.

Aos funcionários do LIM15, Dra. Christiane Ohzaki, Luís Roberto Silva, Maria Eunice, Camila, Darcy e Eliene, principalmente a funcionária Rosa Martins, por sempre me acolher e me fazer sentir em casa. A todos funcionários do departamento de Neurologia principalmente à secretária Thais Figueira.

Resumo

Franco YEM. Estudo da via da glutaminolise em astrocitomas e mecanismo de ação do gene Glsiso2 (GAC) [tese]. São Paulo: Universidade de São Paulo, Faculdade de Medicina; 2023.

O glioblastoma (GBM) é o tumor maligno de alto grau mais frequente no do sistema nervoso central e com pior prognóstico, mesmo com uso da terapia combinada envolvendo ressecção cirúrgica máxima, radioterapia e quimioterapia com temozolomida (TMZ). As células tumorais têm capacidade de reprogramar sua maquinaria metabólica para atender às suas necessidades biosintéticas e bioenergéticas, por meio de uma variedade de vias alternativas de produção de energia, dependendo da disponibilidade de nutrientes. A glutaminólise, o processo pelo qual a glutamina é transportada para dentro da célula e é convertida em α-cetoglutarato para entrar no ciclo do ácido tricarboxílico, é regulada positivamente em vários tipos de câncer, incluindo GBM. A glutaminase (GLS) é o principal regulador desta via e apresenta duas formas em humanos: GLS tipo rim (KGA ou GAC) e GLS2 tipo fígado (LGA ou GAB), com distribuição, regulação e funções distintas. O gene *GLS* apresenta duas isoformas: *GLSiso1* e *GLSiso2* e sua regulação em células tumorais ainda não é bem compreendida. No presente estudo, analisamos os níveis de expressão gênica relacionada à glutaminólise em nossa coorte de 153 astrocitomas de diferentes graus de malignidade e 22 amostras cerebrais não neoplásicas por meio de qRT-PCR. Adicionalmente, investigamos o perfil de expressão proteica dos principais reguladores da glutaminólise: GLS, glutamato desidrogenase (GLUD1), glutamato piruvato transaminase (GPT2); e reguladores da biossíntese de glutationa (GSH): GSH sintase (GS) e níveis de GSH em diferentes graus de astrocitoma estratificados pelo estado mutacional de *IDH1*. As expressões gênicas diferenciais foram validadas in silico no banco de dados TCGA GBM-RNASeq. Em GBM, o acúmulo de Glu devido ao aumento da expressão de GPT2 e GLUD1 correlacionou-se com o aumento da expressão de genes relacionados à síntese de GSH que poderiam favorecer a sobrevivência de células tumorais, principalmente no subtipo de GBM mesenquimal mais agressivo. Em contraste, a análise de correlação *in silício* do conjunto de dados TCGA mostrou que GLUD1 pode levar à diminuição da síntese de GSH em astrocitoma de baixo grau *IDH1*mut, aumentando a suscetibilidade ao estresse oxidativo, tornando-os mais sensíveis à radioterapia e à terapia alquilante. Sendo assim, a monitoração dos níveis de expressão de GLUD1 e GPT2 medindo enzimas e produtos de seus metabolitos, como amônia e alanina, utilizando técnica de imagem não invasiva, poderia potencialmente detectar a progressão de astrocitoma de baixo grau com mutação *IDH1* para GBM secundário. Além disso, o aumento gradual da expressão de ambas as isoformas GLS, GLSiso1 e GLSiso2, foi observado em paralelo ao aumento da malignidade do astrocitoma. É importante ressaltar que a expressão de GLSiso2 no tecido cerebral normal foi menor do que GLSiso1, apontando *GLSiso2* como alvo terapêutico interessante. O papel de *GLSiso2* na tumorigênese foi analisado através do silenciamento gênico da isoforma utilizando a técnica de siRNA em células U87MG-GBM. O silenciamento de *GLSiso2* levou à diminuição da proliferação celular, parada do ciclo na fase G1 e aumento da resposta das células tumorais para o tratamento com TMZ. Os dados do transcriptoma de RNAseq e ensaios funcionais mostraram a associação de *GLSiso2* com um shift metabólico em direção ao efeito Warburg, interferindo principalmente no nível de lactato no microambiente tumoral. Além disso, uma diminuição de 48,6% do processo angiogênico foi observada pelo ensaio de sprouting utilizando esferoides

provenientes da linhagem endotelial HUVEC que foram expostos ao meio condicionado de células U87MG silenciadas com *GLSiso2*. Tal diminuição angiogênica foi provavelmente mediada por VEGF-A, TNF-α e ANGPTL2 cujos níveis foram reduzidos no meio condicionado de células *GLSiso2* silenciadas em relação ao NTC. Esses achados de ensaios funcionais *in vitro* corroboraram com a hipótese de que o GLSiso2 e um potencial novo alvo terapêutico para pacientes com GBM.

Palavras-chave: Glioblastoma. GLS. GLSiso2. Glutaminolise. IDH1. Angiogênese. Metabolismo.

Abstract

Franco YEM. Glutaminolysis dynamics in astrocytomas and *GLSiso2* (GAC) gene silencing: mechanism of action [thesis]. São Paulo: " Universidade de São Paulo, Faculdade de Medicina"; 2023.

Glioblastoma (GBM) is the most frequent and high-grade adult malignant central nervous system tumor, with poor prognosis despite the combined therapy involving maximal surgical resection, radiotherapy, and chemotherapy with temozolomide (TMZ). Tumor cells can reprogram their metabolic machinery to meet their biosynthetic and bioenergetic needs, through a variety of alternative energy production pathways depending on the availability of nutrients. Glutaminolysis, the process by which the glutamine is transported into cell and converted into α-ketoglutarate to enter into the tricarboxylic acid cycle, is upregulated in several cancer types, including GBM. Glutaminase (GLS) is the main regulator of this pathway and presents two forms in humans: kidney-type GLS (KGA or GAC) and liver-type GLS2 (LGA or GAB), with distinct tissue distribution, regulation and functions. The *GLS* gene presents two isoforms: *GLSiso1* and *GLSiso2* and their regulation in tumor cells is still not well understood. In the present study, we analyzed the glutaminolysis-related gene expression levels in our cohort of 153 astrocytomas of different malignant grades and 22 non-neoplastic brain samples through qRT-PCR. Additionally, we investigated the protein expression profile of the key regulator of glutaminolysis: GLS, glutamate dehydrogenase (GLUD1), glutamate pyruvate transaminase (GPT2); and regulators of glutathione (GSH) biosynthesis: GSH synthase (GS) and GSH levels in different grades of astrocytoma stratified by the IDH1 mutational status. The differential gene expressions were validated *in silico* on the TCGA GBM-RNASeq database. Particularly in GBM, the accumulation of Glu due to *GPT2* and *GLUD1* downregulation correlated to upregulation of genes related to GSH synthesis which could favor tumor cell survival, mostly in the most aggressive mesenchymal GBM subtype. In contrast, *in silico* TCGA dataset correlation analysis showed that *GLUD1* may lead to decrease in GSH synthesis in $IDH1^{mut}$ low-grade astrocytoma increasing the susceptibility to oxidative stress, rendering them more sensitive to radiation therapy and to alkylating therapy. Thus, monitoring GLUD1 and GPT2 expression levels by measuring their end metabolites enzymes such as ammonia, and alanine by a non-invasive imaging technique may potentially detect the progression of lower-grade astrocytoma harboring *IDH1* mutation towards secondary GBM. Additionally, gradual expression increase of both GLS isoforms, *GLSiso1* and *GLSiso2,* was observed in parallel to the increase of astrocytoma malignancy. Importantly, *GLSiso2* expression in normal brain tissue was lower than *GLSiso1*, which pointed *GLSiso2* more eligible as therapeutic target. *GLSiso2* role in tumorigenesis was analyzed by silencing this isoform through siRNA in U87MG-GBM cells. *GLSiso2* silencing led to decrease of tumor cell proliferation, cycle arrest at G1 phase and increase of tumor cell response for TMZ. The RNAseq transcriptome data and functional assays showed the association of *GLSiso2* with metabolic shift towards Warburg effect, mainly interfering with lactate level in tumor microenvironment. Moreover, a decrease of 48.6% of angiogenic process was observed by sprouting assay of HUVEC spheroids exposed to *GLSiso2* silenced U87MG cells conditioned media. Such angiogenic decrease was probably mediated by VEGF-A, TNF-α and ANGPTL2 which levels were reduced in the conditioned media

of GLSiso2 silenced cells compared to NTC. These findings of *in vitro* functional assays corroborated *GLSiso2* as a potential new therapeutic target for GBM patients.

Summary

1. Introduction

1.1. Cancer, glioma, and glioblastoma

Cancer is a multifactorial heterogeneous disease and one of the major causes of mortality worldwide (1). It is characterized by disordered growth of cells that invade surrounding normal tissues and can spread to other organs of the body. According to the WHO, the estimate for the year 2030 is about 26 million new cases and 17 million cancer deaths worldwide due to aging and population growth (2). Some physiological changes that characterize cancer are sustaining proliferative signaling, evading growth suppressors, resisting cell death, enabling replicative immortality, inducing angiogenesis, and activating invasion and metastasis (3). In addition, changes may lead to genomic instabilities, which generate genetic diversity and accelerate the process of cell mutation; as well as inflammation, reprogramming of energy metabolism and immune system evasion. Additionally, the tumor microenvironment also plays a role as it propitiates an appropriate ambience for growth, maintenance, and malignant progression of tumor cells (4). Therefore, deep understanding on tumor characteristics helps in identifying new drugs and in new treatment strategies for this disease.

Brain tumors account for about 3% of all types of malignancies, being one of the least prevalent, although they are more worrying because of their poor outcome (5,6). Among them, gliomas present the highest frequency (above 80%) and are among the most fatal types of cancers. The annual incidence of glioma is around 6 per 100.000 worldwide. Being 1.6 fold more incident in men than woman (5). They are qualified as lesions originating from glial cells, which have support, protection, and nutrition roles of neurons in the central nervous system (CNS) (7). Gliomas have been historically classified based on morphological and immunohistochemical resemblance to differentiated glial lineages, including astrocytic, oligodendrocytic and ependymal lineages and have been graded according to histological features of biological aggressiveness. Stem–like cells within the CNS are now thought to be the cells of origin of several primary brain tumor types, including glioblastoma (GBM) (8,9). GBM is the most lethal type of glioma, accounting for 70–75% of all diffuse gliomas. This tumor presents the median overall survival of 14–17 months even after current standard of care, consisting in surgical resection, irradiation, and chemotherapy with Temozolomide (TMZ) (6,8,9). The recurrence of GBM is also high, with an average rate of more

than 90%, by regrowth of surgically not-resected cells that invaded the surrounding normal brain parenchyma, partially induced by hypoxic and acidic environment (10–13).

1.2. Classification of astrocytomas: molecular classification and *IDH1* mutation

Due to The Cancer Genome Atlas (TCGA) team´s efforts a refined glioma classification system was proposed based on in-depth tumor genomic characterization, which allowed the integration of histologic and genomic features (14–16). As a result of this integration of pheno and genotypic features, gliomas are classified into two major categories: *IDH1*-wildtype (*IDH1*^{wt}) and *IDH1*-mutant (*IDH1*^{mut}) gliomas (17). The IDH status separates low-grade gliomas from high-grade GBM, impacting the overall survival of patients and it is considered a strong prognostic marker of gliomas. GBM is the most frequent glioma, classified as astrocytoma grade 4 with the poorest outcome. Histologically, GBM is a heterogenous, mitotically active with high proliferative rate, characterized by nuclear atypia, microvascular proliferation, and necrosis (18,19). In the past decade, many efforts have been made to better understand the molecular basis of GBM (6,8). Verhaak and colleagues classified GBM into 4 molecular subtypes according to transcriptomic profile: proneural, neural, classical and mesenchymal subtypes (20), which was later refined into three subtypes: proneural, classical and mesenchymal (21). The proneural subtype is characterized by the presence of *IDH1*, *PDGFRA* and *TP53* gene mutations and has been associated with better prognosis (22). The classical subtype is characterized by the presence of proliferative markers such as amplification of EGFR, deletion in chromosome 10 and amplification in chromosome 7 (23). The mesenchymal subtype shows *NF1* or *RB1* mutations and presents the worst prognosis, with an average overall survival of 8–11 months (24). Metabolic reprogramming (25,26), invasion, and angiogenesis are major hallmarks of GBM (27–29).

Isocitrate dehydrogenase (IDH) enzymes are essential enzymes that participate in major metabolic processes as Krebs cycle, glutamine metabolism and lipogenesis (30). IDH1 is found mainly in the cytoplasm and peroxisomes, whereas IDH2 is located in the mitochondrial matrix (31). The *IDH1* gene encodes an enzyme that catalyzes oxidative carboxylation of isocitrate to α-ketoglutarate (α-KG) and is a major cellular source of cytoplasmic NADPH (32). *IDH* mutations occurs most frequently at exon 4 codon 132 (R132H) and are prevalent in gliomas, as 80% of low-grade gliomas, grades 2 and 3, harbor this mutation. In GBMs, the *IDH* mutations are mainly found

in secondary GBM (73%), whereas only 3.7% on primary GBM are *IDH*[mut] (30). The presence of *IDH* mutations is correlated with favorable outcome with a prolonged median survival. Low grade gliomas *IDH1*[mut] present 7-year overall survival (33), and primary *IDH1*[mut] GBMs present 46 months of overall survival compared to 13 months in *IDH1*[wt] GBMs (34,35). Consequently, the *IDH* mutational status is relevant for glioma diagnosis, prognosis and establishment of treatment strategy (36–38).

1.3. Metabolic reprogramming in GBM: relevance of glutaminolysis

The deregulated cellular energetics metabolism is known for affecting the transition from normal to cancer cells (3,39). Glioma cells, like many other cancer cells, acquire abilities to reprogram the metabolic machinery to satisfy their biosynthetic and bioenergetic needs (Figure 1A) (40–42). Hypoxia, mutation in oncogenes and changes in signaling pathways induce hyperregulation of anabolic processes and suppression of catabolic pathways in tumor cells (43). The most well documented metabolic alteration in cancer is the activation of aerobic glycolysis, known as the Warburg effect, where glycolysis is uncoupled from the mitochondrial tricarboxylic acid (TCA) cycle and oxidative phosphorylation (OXPHOS). Consequently, the majority of glycolysis-derived pyruvate is diverted to lactate fermentation and kept away from mitochondrial oxidative metabolism (44–46). Furthermore, cancer cells, including gliomas cells, shift their metabolic pathways to increase nutrient availability, including intracellular lipids, amino acids and nucleotides through several molecular mechanisms as incrementing extracellular uptake, increasing *de novo* synthesis and orchestrating carbon and nitrogen availability from different metabolic pathways (28,40,41,47,48). Since the description of the Warburg effect in 1925, glucose has been considered as the main metabolic source for energy production in cancer (49). However, cumulative evidences have demonstrated that tumor cells may also resort of alternative energy production pathways. Glutaminolysis, the process by which glutamine is converted to α-KG, a key substrate of TCA cycle, has emerged as a relevant anaplerotic metabolic pathway in cancer cells (40,50–52).

1.3.1 Glutaminolysis

Glutamine (Gln) is a non-essential amino acid that maintains cell survival by supporting the anaplerosis, as a source of carbon to replenish the TCA cycle, and of nitrogen for *de novo*

biosynthesis of nucleotides and other nonessential amino acids, via glutaminolysis (41,53). Gln is also involved in other cellular processes, including antioxidative stress, as a source of glutathione, mTOR signaling and autophagy for anaplerosis (53–57). Both Gln uptake and the rate of glutaminolysis are known to be increased in tumors (50,51,58), including gliomas (42,51,59,60). In addition, upregulation of Gln transporters in astrocytomas was previously described by our group (61). Therefore, the dependence of cancer cells on Gln makes glutaminolysis an attractive cancer therapy target (58,62–64).

Glutaminolysis starts when Gln is transported into the cells via transporters such as SLC1A5 (ASCT2) and SLC7A5 (LAT1) and is converted into glutamate (Glu) and ammonia through deamination by the enzyme glutaminase (GLS). Glu is then converted to α-KG, an intermediate substrate in the TCA cycle, to produce ATP and anabolic carbons for the synthesis of amino acids, nucleotides, and lipids. The conversion of Glu to α-KG is catalyzed by glutamate dehydrogenase (GLUD) or transaminases such as glutamate pyruvate transaminases (GPT-alanine aminotransferases) and glutamate oxaloacetate transaminases (GOT-aspartate aminotransferases), which convert α-keto acids to their corresponding amino acids (Figure 1B). This mechanism provides nitrogen, sulfur, and carbon skeletons to produce biosynthetic precursors necessary for the growth and proliferation of cancer cells (16,50,65). The main regulator of this pathway is the glutaminase (GLS) enzyme that converts Gln to Glu (Figure 1B). High rates of glutaminolysis support rapid proliferation by supplying precursors to low–flux biosynthetic pathways (66). Current attempts to target glutaminolysis clinically have focused largely on inhibiting glutaminase. Such chemical inhibitors, as BPTES (bis-2- (5-phenylacetamido-1,3,4-thiadiazol-2-yl)ethyl sulfide), have presented impact in cancer cell decreasing proliferation both in *in vitro*/*in vivo* models (67,68).

The glutaminolysis is also essential for maintaining cellular redox homeostasis by controlling the reactive oxygen species (ROS) level by the glutathione (GSH) synthesis pathway (69). GSH is an important intracellular antioxidant, acting as a regulator of cellular redox state, and protecting cells from damage caused by ROS (70). GSH biosynthesis is a well-conserved pathway that occurs exclusively in the cytosol, involving two enzymes, glutamate cysteine ligase (GCL) and glutathione synthetase (GS) (71), in which three amino acid precursors, cysteine, Glu, and glycine, are combined to form the tripeptide GSH. Gln is a direct fuel source of Glu and cysteine uptake occurs via the System XC-transporter, which takes up cysteine and simultaneously secretes Glu (72). Consistent with this mechanism, Gln starvation has been associated with impaired uptake of

cysteine through the System XC and with decreased intracellular GSH level (73). Recent studies have highlighted the GSH involvement in key signal transduction reactions as a controller of cell differentiation, proliferation, and apoptosis. Molecular changes in the GSH antioxidant system and disruptions in GSH homeostasis have been implicated in tumor initiation, progression, and treatment response (74,75). Importantly, GSH has been considered as the main factor responsible for treatment resistance in cancer, including gliomas, because of its antioxidant effect (76,77). Hence, GSH has both protective and pathogenic roles: in healthy cells, it is crucial for the removal and detoxification of carcinogens, and in tumor cells, elevated GSH levels are associated with tumor progression and increased resistance to chemotherapeutic drugs (70). Therefore, several attempts have been aimed GSH depletion by inhibiting the XC–transporter (78) to limit GSH synthesis by reducing cysteine availability (76,77).

1.3.2 Glutaminases and *GLSiso2*

Glutaminase (GLS) is the first enzyme of the glutaminolysis which converts Gln in Glu. Two GLS enzymes are described in human: kidney-type GLS and liver-type GLS2 (LGA or GAB), which exhibit distinct tissue distributions and are regulated differently (50,79,80). Tumor cells present higher activity of GLS, being associated with tumor growth, malignancy and regulated by the oncogene c-MYC. GLS2 presents tumor suppressive characteristics and its expression is associated with resting or quiescent cell states, being regulated by p53 (81–85). Upregulation of GLS at mRNA and protein levels has been observed in cancers including liver, lung, breast, colorectal and brain tumors, and its enzymatic activity correlates with poor outcome (86–89). Therefore, upregulation of GLS has been considered as a metabolic adaptation by which cancer cells gain selective advantages for the use of alternative carbon sources, replenishing metabolic requirements for tumor growth (68).

The GLS presents two isoforms: *GLSiso1*- KGA and *GLSiso2*-GAC, and the regulation of both GLS isoforms is not yet completely understood. Previous studies have reported *GLSiso2* (GAC) in the mitochondria and *GLSiso1* (KGA) in the cytoplasm. The *GLSiso2* is derived from an alternative exon splicing at the 3'-end terminal, replacing the last four exons in the KGA transcript, resulting in the lack of ankyrin repeats that are present at the C-terminus of the KGA. Thus, the isoform 2 is shorter than isoform 1, with a distinct C-terminal (Figure 1C).
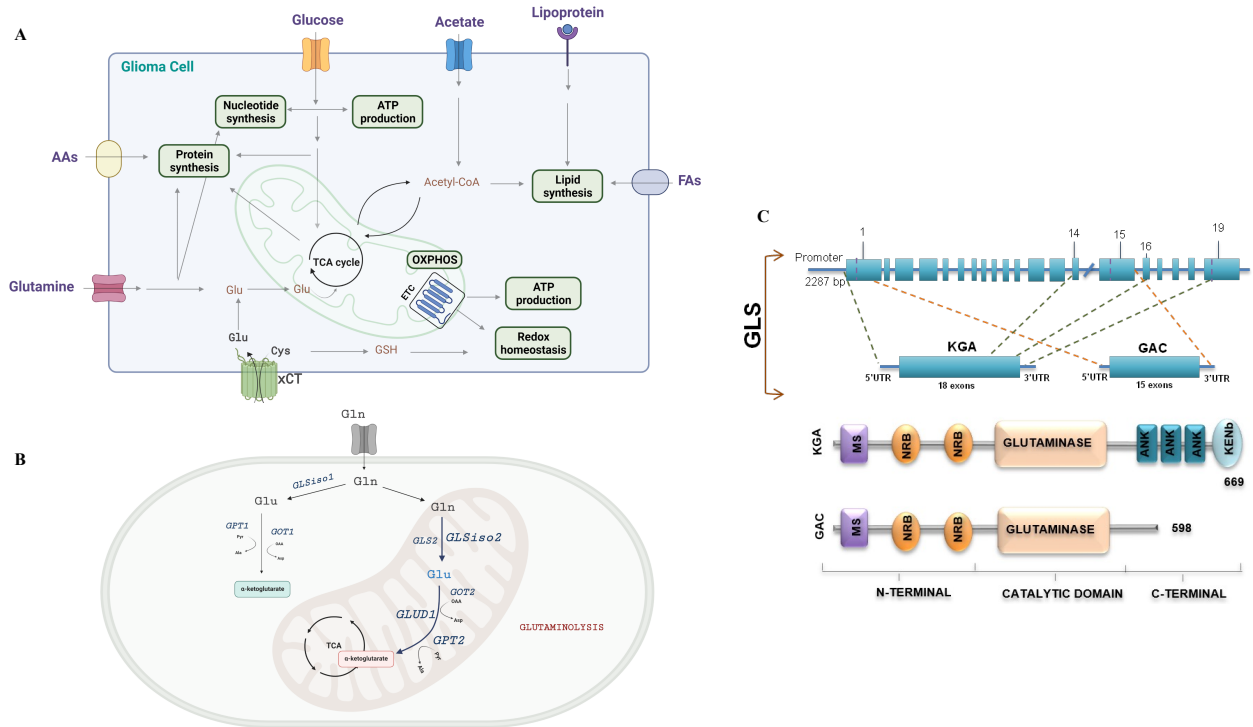
Figure 1- **Main metabolic pathways used by glioma cells, glutaminolysis pathway, and glutaminase isoforms. (A)** Glioma cells take up nutrients including glucose, acetate, and glutamine, as well as other amino acids (AAs), fatty acids (FAs), and lipoproteins from the extracellular environment, and use these nutrients for energy and biomass production by fueling the glycolysis, the tricarboxylic acid (TCA) cycle and the oxidative phosphorylation (OXPHOS). The increased metabolic activity of proliferating glioma cells generates reactive oxygen species as by-products that necessitate antioxidant production, including the production of reduced glutathione (GSH). **(B)** Glutaminolysis pathway: The main destination of glutamine (Gln), after its conversion to glutamate (Glu) is the conversion of glutamate to α-ketoglutarate. The glutaminolysis contributes to the production of mitochondrial NADH, which is used to sustain ATP production by OXPHOS. The enzyme glutaminase (GLS) is the main regulator of this pathway. The pyruvate transaminase (GPT) and glutamate oxaloacetate transaminase (GOT) catalyze the transfer of the amino group from glutamate to pyruvate and oxaloacetate to produce alanine and aspartate. **(C)** Structural organization of *GLS* isoforms. KGA and GAC are alternative splicing products of the *GLS* gene. GAC and KGA have the localization signal for mitochondria (MS). In common, both present glutaminase catalytic domains, in addition to NR box domains for possible interaction with nuclear receptors. KGA presents ankyrin domains (ANK) of interaction with other proteins. In the region C-terminal, KGA also has a KENbox sequence. There is no known motif prediction for the GAC C-terminal region.

1.4. GBM and Angiogenesis

One of the hallmarks of cancer is angiogenesis, the capacity of tumor cells to induce formation of new blood vessels from an already existing vasculature through tumor-stromal signaling. Endothelial cells (ECs) is the major lining component of blood and lymphatic vessels and they respond to metabolic demands during the physiological growth of organs, supplying the required nutrients and oxygen (95,96). Over time, ECs remain mostly inactive in the human body; however, they retain the ability to rapidly initiate the formation of new vessels in response to injury or in pathological conditions, phenomenon known as angiogenic switch. Evidences indicate that metabolic changes may trigger this switch (91,92). During tumor progression, this switch occurs in support for the high demands of proliferative cancer cells (47). Tumor and stromal cells secrete high levels of pro-angiogenic factors, as vascular endothelial growth factor (VEGF), angiopoietins, platelet-derived growth factor (PDGF-B) and transforming growth factor (TGF-b), that induce neovascularization (98,99). The dysfunctional new vessels impact profoundly the tumor cell and its microenvironment, leading to hypoxia, decreased infiltration and activity of immune cells, remodeling of extracellular matrix (ECM), and metastatic dissemination (45,46).

Angiogenesis is increased in GBM and it is associated with poor prognosis (25,26). The angiogenic process involves various mechanisms such as: growth of new blood vessels by coopting existing host vessels (94); *de novo* angiogenesis through extension of nearby vessels (95); differentiation of bone marrow-derived endothelial progenitors (96); splitting of the existing vasculature known as intussusception (97); and vascular mimicry by glioma stem cells that form luminal cylinders resembling vessels (98–101). Hypoxia is the main trigger of angiogenesis and glioma cells are able to sense and adapt to hypoxic environments (98). The hypoxia-inducible factor-1 (HIF1) is key nuclear transcription factor induced by hypoxia, a heterodimeric factor composed by two subunits, HIF1α and HIF1β. The HIF1α subunit regulates HIF1 activity in response to changes in local O_2 levels. Under normoxic conditions, the α subunit is rapidly degraded; however, under hypoxic conditions, this subunit remains intact and binds to the constitutively expressed β subunit to form HIF1complex in the nucleus, where it induces the expression of several genes, including multiple proangiogenic factors. HIF-1 can also be activated by non-canonic pathways such as a pseudo-hypoxic state caused by the Warburg effect and through the lactate production (102–105). High lactate level has been related to tumor recurrence,

metastases, and poor prognosis (106–108). It enhances tumor cells motility and can contribute to angiogenesis through induction of IL-8 and VEGF/VEGF-A (109,110).

VEGF promotes tumor angiogenesis through different mechanisms such as increased migration and invasion of EC and increased permeability of existing vessels (111,112). Besides, its proangiogenic effect has independent autocrine effects of survival, migration, and invasion of tumor cells (113). High VEGF expression level has been correlated with increased angiogenesis and higher histological grade in various human cancers, including GBM (120-124). Thus, these clinical findings supported the attempts to develop anti-angiogenic therapies to control tumor growth by triggering tumor cell death via deprivation of oxygen and nutrients, as well as leading to the transient normalization of the tumor vasculature and improved delivery of cytotoxic chemotherapy (115). Given the importance of VEGF in tumor angiogenesis, several different approaches to suppress VEGF signaling have been searched, including monoclonal antibodies as Bevacizumab, and small molecule inhibitors (116). However, anti-VEGF approach returned no benefits to GBM patients (117,118).

In the context of tumor metabolic reprogramming and the previous findings of our group about the amino transporters related to glutaminolysis (61), the aim of the present study was to deepen the understanding of the role of glutaminolysis in the astrocytoma malignant progression, analyzing the involved signaling pathways with emphasis to angiogenesis.

2. Aims

2.1 Evaluate the glutaminolysis dynamics during astrocytoma malignant progression

- Analyze the expression of glutaminolysis related genes
- Analyze the impact of glutaminolysis in tumor cell fitness according to *IDH1* mutational status

2.2 Evaluate the relevance of *GLS* isoforms, *GLSiso1* and *GLSiso2*, in astrocytoma

- Analyze the impact of *GLSiso2* on tumor cell behavior in *in vitro* model of GBM
- Validate the impact of GLS by chemical inhibition
- Analyze the signaling pathways associated with GLSiso2
- Validate the identified pathways in *in vitro* 3D model

3. Materials and methods

3.1. Tissue sample and Ethical statement: We analyzed 153 human astrocytoma samples stratified according to the WHO classification (2007) (119) as: 23 astrocytomas grade 1 (AG1), 26 astrocytomas grade 2 (AG2), 18 astrocytomas grade 3 (AG3), and 86 GBM. Non–neoplastic brain samples (NN) were used as control (22 cases). Tumor samples were obtained from surgery of patients treated by the Neurosurgery Group of Department of Neurology at Hospital das Clinicas at the School of Medicine of University of São Paulo, in the period of 2000 to 2007. NN brain tissue samples were collected from epilepsy patients subjected to temporal lobectomy.

3.2. Cell Culture: The human GBM cell line U87MG was obtained from American Type Culture Collection (ATCC) and was cultured in Dulbecco's Modified Eagle's medium (DMEM) (Thermo Fisher Scientific, Whatham, MA), supplemented with 10% heat-inactivated fetal bovine serum (FBS) (Cultilab, Campinas, Sao Paulo, Brazil), and antibiotics (100 units/ml penicillin, 100μg/ml streptomycin). The HUVEC cell line was kindly donated by Prof. F. Laurindo´s research group. This cell line was cultured with RPMI supplemented with 10% FBS, and antibiotics (100 units/ml penicillin, 100μg/ml streptomycin). Both cell lines were maintained in a humidified atmosphere of 5% CO_2 in air at 37°C. The cell lines were authenticated by short tandem repeats (STR) analysis using GenePrint 10 System (Promega, Madison, WI).

3.3. RNA extraction and cDNA synthesis: Samples were snap–frozen in liquid nitrogen immediately following surgical removal and macro dissected prior to RNA extraction. A 4μm–thick cryosection of each sample was stained with hematoxylin–eosin and analyzed under a light microscope for assessment of necrotic, cellular debris and hemorragic areas (in tumoral samples) in order to only include samples with more than 80% of tumor cell density. Total RNA was extracted from frozen tissues (tumor and NN) using the RNeasy Mini Kit (Qiagen, Hilden, Germany) following the manufacturer's instructions. The RNA concentration and purity were evaluated by NanoDrop, and ratios of 260/280 measures ranging from 1.8 to 2.0 were considered satisfactory for purity standards. RNA quality was checked by electrophoresis in agarose gel. A conventional reverse transcription reaction was performed to yield single–stranded cDNA. The first strand of cDNA was synthesized from 1 μg of total RNA previously treated with 1 unit of DNase I (FPLC– pure, GE Healthcare, Uppsala, Sweden) using random and oligo (dT) primers, RNase inhibitor, and

SuperScript III reverse transcriptase according to the manufacturer's recommendations (Thermo Fisher Scientific, Carlsbad, CA). The resulting cDNA was subsequently treated with 1 unit of RNase H (GE Healthcare), diluted with TE buffer, and stored at −20°C until later use.

3.4. Analysis of Gene Expression by quantitative real–time PCR (qRT–PCR): The relative expression levels of genes involved in glutaminolysis pathway *GLS, GLSiso1, GLSiso2, GLS2, GLUD1, GOT1, GOT2, GPT2* were analyzed by qRT–PCR, using the SYBR Green approach. The expression of *ASCT2* and *LAT1* genes were previously described by our group (61). A geometric mean of three suitable reference genes was used for normalizing the quantitative data: hypoxanthine phosphoribosyl transferase (*HPRT*), glucuronidase beta (*GUSβ*) and TATA box binding protein (*TBP*) (120). The primers were designed to amplify 80–120 bp amplicons, with a melting temperature of 60°C and were synthesized by IDT (Integrated DNA Technologies, Coralville, IA). The primers information is described in Table 1:

Table 1: The primer sequences and the concentration used in qRT–PCR

Genes	Forward Primer (5'–3')	Reverse Primer (5'–3')	Concentration (nM)
GLS	CAGGGCAGTTTGCTTTCCAT	GAGACCAGCACATCATACCCAT	200
GLSiso1	GCAGAGGGTCATGTTGAAGTTGT	GGTGTCCAAAGTGCAGTGCTT	200
GLSiso2	ATCCTCGAAGAGAAGGTGGTGA	GCAAGTTCTTGTTGGAGACTTTCA	400
GLS2	ATCCTCGAAGAGAAGGTGGTGA	ATGGCTGACAAGGCAAACCT	200
GLUD1	TGGCATACACAATGGAGCGT	TCTCAATGGCATTAACATAGGCA	400
GOT1	CTGTGCCCAGTCCTTCTCCA	GATGCTCTCAGGTTCTTTTCCAA	400
GOT2	CTTGAGGTTGGAGACCAGTTGAGT	GATTGCTGCTGCCATTCTGA	400
GPT2	GGCTTTGGGCAGAGGGAA	TCACGCGTACTTCTCCAGGAA	200
HPRT	TGAGGATTTGGAAAGGGTGT	GAGCACACAGAGGGCTACAA	200
GUSβ	AAATACGTGGTTGGAGAGCTCATT	CCGAGTGAAGATCCCCTTTTTA	400
TBP	AGGATAAGAGAGCCACGAACCA	CTTGCTGCCAGTCTGGACTGT	200

To ensure the efficiency of amplification and analysis of melting curves, which gave a single peak for all PCR products, standard curves with varying concentrations of the primer pairs of each gene were performed. The optimal primer concentration was determined as the lower concentration which did not affect the cycle threshold (Ct) and displayed the maximum amplification efficiency while minimizing non–specific amplification. Additionally, the amplified PCR product sizes were checked by agarose gel electrophoresis. The SYBR Green I amplification mixtures (12 µl) were composed by cDNA, Power SYBR Green I Master Mix (Thermo Fisher Scientific), and the reverse and forward primers. The qRT–PCR was done in duplicate using the ABI Prism 7500 (Thermo Fisher Scientific) as follows: 2min at 50°C, 10 min of polymerase activation at 95°C, and 40 cycles

of 15s at 95°C and 1min at 60°C. The following equation was applied to calculate gene expression in tumor and NN tissue samples: $2^{-\Delta Ct}$, where ΔCt = Ct of a specific gene – geometric mean Ct of housekeeping genes (121).

3.5. Analysis of protein expression by Western Blotting: The protein extracts from NN (5), AG1 (4), AG2 (4), AG3 (2), GBM (6), and U87MG glioma cell line were analyzed. Cells were cultured in monolayer with DMEM medium (Dulbecco's Modified Eagle's Medium, (Thermo Fisher Scientific, Carlsbad, CA), 10% FBS and 100 µg/ml streptomycin and 100 IU/ml penicillin. The samples were homogenized with RIPA lysis buffer (50mM Tris–HCl, 1%NP–40, 0.25% Na deoxycholate, 150mM NaCl, 1mM EDTA) supplemented with a cocktail of protease inhibitors (Sigma–Aldrich, St Louis, MO). The protein concentration was determined using Bradford reagent. All samples (20 µg protein) were resolved by electrophoresis on 4–12% gradient gels in SDS–PAGE using electrophorese buffer NuPAGE MOPS SDS (Thermo Fisher Scientific) and transferred onto PVDF membrane by iBlot Dry Blotting System (Thermo Fisher Scientific). Then the remaining binding sites of the membranes were blocked with skimmed milk powder solution at 5% diluted in Tris–buffered saline and 0.1%Tween 20 (TBST). Subsequently, the membranes were incubated overnight with the primary antibody, anti–GLS (1:1000, Abcam, Cambridge, MA), anti-GS (1:2000) from Abcam (Cambridge, MA), and anti-GLUD1, anti-GPT2 (1:1000) from Thermo Fisher diluted in TBST with 5% bovine serum albumin (BSA) solution. β–actin (Sigma–Aldrich) was used as loading control (dilution 1:5000). The membranes were incubated with peroxidase–conjugated secondary antibody anti–rabbit and anti–mouse (1:5000) (Sigma–Aldrich), also diluted in TBST 5% BSA. The proteins levels were detected using the chemiluminescence detection method (Western Lightning Plus–ECL, Enhanced Chemiluminescence Substrate, Perkin Elmer, Waltham, MA). The detection of the chemiluminescent signal was performed in the Photo QuantLAS 4000 mini (GE Healthcare) photo documentation system and the bands were analyzed and quantified using Image J software (obtained from imagej.nih.gov/ij/download/).

3.6. GSH measurement: Tissue samples were resuspended in PSB–0.5% NP40 (pH 6) and homogenized in syringes with an insulin needle 10 times. An aliquot of each sample was separated for protein quantification. Eighty µL were processed with 250 µL of cold GSH extraction buffer (KClO$_4$ 50 mM; EDTA 10 mM; H$_3$PO$_4$ 0.1% (v/v), pH 5) and 40 µL of cold metaphosphoric acid 5% (v/v). The samples were vortexed for 1 min and centrifuged at 8000×g (10 min, 4 °C). The

supernatants were used as 1:10 dilutions. GSH was measured using a fluorometric detection assay kit (ab138881, Abcam) according to the manufacturer's instructions. This assay is based on the fluorescent properties of thiol green, which is a non-fluorescent dye that becomes strongly fluorescent upon reacting directly with GSH. The fluorescence intensity was evaluated at an excitation wavelength of 490 nm and an emission wavelength of 520 nm using a 96-well plate in a spectrofluorometer (SpectraMAX M2, Molecular Devices, Sunnyvale, CA). GSH concentration was calculated by interpolation of a standard curve and results were expressed as pmol/μg of total protein.

3.7. Lactate quantification: U87MG cells were cultured in monolayer (5×10^4 cells/well) and then challenged with siRNA*GLSiso2* and NTC. The supernatants were collected 72 hours after silencing (day 4), centrifuged (5 min, 2500 rpm) and then transferred (200uL/ replicate) to a 96 wells clear plate. The extra cellular lactate level was quantified using the L-Lactate Assay Kit (Eton Bioscience Inc., Research Triangle Park, NC) following the manufacturer's instructions. The plates were read using a SpectroStar plate reader.

3.8. Analysis of growth factor expression: U87MG cells were cultured in monolayer (5×10^4 cells/well) and then challenged with siRNA*GLSiso2* and NTC. The supernatants were collected 72 hours after silencing (day 4), centrifuged (5 min, 2500 rpm) and then transferred (200uL/ replicate) to a 96 well clear plate. The profiling of growth factors/angiogenesis panel (LEGENDplex, BioLegend, San Diego, CA) was performed according to the manufacturer's instructions using a Cytek Aurora Flow cytometer. The mix and match fluorescence-encoded beads Angiogenesis human Panel 1 (VEGF Cat#: 740710 TNF-α Cat#: 740711 and Angiopoietin-2 Cat#: 741217) were selected.

3.9. TCGA data analysis: The gene expression from TCGA GBM-RNAseq dataset was downloaded (Genomics Data Commons Data Portal - https://portal.gdc.cancer.gov/) and normalized by DEseq R software. Normalized read counts were converted to z-score for heat map visualization.

3.10. *GLS*iso2 gene silencing of U87MG cells by siRNA: *A* sequence of small interference RNA (siRNA) for *GLSiso2* silencing (5'-AUAUAGAAUGGAAAGUCUGGGAGAG-3') and non-target control (NTC) siRNA were synthesized by Integrated DNA technologies (IDT, Coralville, IA). The

oligos were diluted in RNAse free duplex buffer provided by IDT. U87MG cells (1×10^5 cells/well) were seeded in a six-well plate and transfected after 24 h with Lipofectamine RNAiMax (Thermo Fisher Scientific). siRNA and NTC oligos were utilized at a final concentration of 10 nM and the knockdown were evaluated after 2-, 4- and 7-days following transfection. The efficiency was verified by RT-qPCR and Western blot.

3.11. Cell Viability/Proliferation: U87MG cells were seeded (1.10^3/well- 96wells plate) after 24h of incubation the cells were challenged with siRNA*GLSiso2* and NTC. The cell viability was analyzed for 7 days (168h). After each day, the cells were incubated with PrestoBlue reagent (Invitrogen, Carlsbad, CA, USA) for 2 h, and the fluorescence was measured on a GloMax® 96 Microplate Luminometer (Promega Corporation, Madison, WI, USA).

3.12. Apoptosis assay: This experiment was done using FITC Annexin V Apoptosis Detection Kit I (Thermo Fisher Scientific), following the fabricant's instructions. U87MG cells (5×10^5 cells / well) were seeded in 6-well plates with complete medium and incubated at 37 °C with 5% CO_2, for 24h. After that, the cells were challenged with siRNA*GLSiso2* and NTC, and additionally, they were also treated with Temozolomide (1mM) diluted in DMSO and with DMSO as a negative control. The samples were collected after 72 hours after silencing (day 4). The cells were harvested, collected, centrifuged (5 min, 2500 rpm) and the supernatant collected. After trypsinization and washing, each cell suspension was stained with FITC Annexin V Apoptosis Detection Kit I (Thermo Fisher Scientific) for 20 min at room temperature in the dark and then analyzed (at least 5000 events/replicate) by flow cytometry. Using the FACS Canto II; BD Biosciences software each cell population was registered and quantified at four cell subpopulations named as viable cells [(-) annexin (-) 7-AAD]; only PS externalization [(+) annexin (-) 7-AAD]; both PS externalization and membrane permeabilization [(+) annexin (+) 7-AAD]; only membrane permeabilization [(-) annexin (+) 7-AAD].

3.13. Cell cycle assay: U87MG cells (5×10^5 cells / well) were seeded in 6-well plates with complete medium and incubated at 37 °C with 5% CO2, for 24h. Cells were synchronized by incubation with FBS-free DMEM with 0.5% bovine serum albumin for 24 h. After that, the cells were challenged with siRNA*GLSiso2* and the NTC and the samples were collected at 3, 6, 12 and 24 hours after silencing and fixed with cold ethanol in increasing concentrations (25, 50, 75, 90%). After fixation,

cells were washed and incubated with PI. PI fluorescence was accessed by flow cytometry FACSCanto (Beckton Dickinson). Analysis was performed using FlowJo version 10, using the cell cycle interface.

3.14. Chemical inhibition of GLS by BPTES: The U87MG cell line was exposed to BPTES (Sigma-Aldrich), a total GLS inhibitor, at different concentrations and time intervals to define the best response for chemical blockade. First, the stock solution of BPTES (7.5mM) was prepared aseptically using DMSO followed by serial dilution in complete medium. The cells were seeded ($1x10^4$ cells/mL, 100 µL/well) in 96-well plates incubated for 24 h and treated with BPTES at final concentrations of 0.8 - 50 µM (100 µL/well), in quadruplicate, and then incubated for 48 h at 37°C in 5% CO_2. A second plate, named T0, was prepared to infer the absorbance value of untreated cells at the sample addition moment. The final concentration of DMSO was used as a control and did not affect cell viability. The cell viability was analyzed for 24, 48, 72 and 96 hours. After each day, the cells were incubated with PrestoBlue reagent (Invitrogen, Carlsbad, CA, USA) for 2 h, and the fluorescence was measured on a GloMax® 96 Microplate Luminometer (Promega Corporation, Madison, WI, USA).

3.15. Analyze of GLS expression by immunohistochemistry: Paraffin embedded tissue of AG1, AG2, AG3 and GBM cases, and NN brain tissues from surgical epilepsy cases were immunostained for GLS using the Novolink kit (Novolink; Novocastra, Newcastle-upon-Tyne, UK), following the manufacture guide. The sections were processed to antigen retrieval, by citrate buffer (10mM, pH6.0) for 3 minutes at 122ºC, using an electric cooker (BioCare Medical, Walnut Creek, USA). After protein blocking, the tissue was incubated with anti-GLS (ab180798, rabbit polyclonal, 1:1000 diluted) at 20° for 16 hours. The reaction performed by the kit uses diaminobenzidine, and for nuclear staining Harris hematoxylin was used. To obtained optimal dilution tonsil sections was used. The immunoreactions for the GLS were analyzed according to a semi-quantitative score system considering the intensity of staining (0: negative, 1: weak, 2: moderate and 3: strong). An immunolabeling score (ILS) was obtained by the product of the intensity of stained cells, by two independent investigators (YFP and SKNM), and simultaneous revision were performed to obtain the final score in case the concordance was not achieved. Digital photomicrographs of representative fields were captured and processed using Adobe Illustrator CS6 (Adobe System, San Jose, CA).

3.16. Analyze of GLS expression by Immunofluorescence: The immunofluorescence was assessed to confirm the GLSiso2 protein expression in U87MG after 2, 4 and 7 days after silencing with *siRNA-GLSiso2* and to evaluate the GLS expression in HUVEC cells. For this, cells were cultured in monolayer (5×10^4 cells/well) in coverslip pre-treated with poli-L-lisine. The mitochondrial staining with MitoTracker Deep Red (Thermo Fisher Scientific) was performed according to manufacturer's recommendation. After each day, cells were fixed with paraformaldehyde (4%), the membrane was permeabilized with Triton-X-100 (0.1%), and, to avoid unspecific reactions, the cells were blocked with 4% of goat serum. The primary antibody GLS (ab180798, rabbit polyclonal, 1:1000 diluted), was incubated overnight at 4ºC. The secondary antibody (Thermo Fisher Scientific, Carlsbad, CA) goat anti-Rabbit IgG H&L (Alexa Fluor 568) and goat anti-Mouse IgG H&L (Alexa Fluor 568 and 488) were incubated for one hour, and nuclei were stained with DAPI (Thermo Fisher Scientific, Carlsbad, CA). The preparations were analyzed in confocal microscopic Zeiss 510 LSM META and Zeiss 780-NLO (Thornwood, NY). The retrieved images were analyzed by Image J/Fiji.

3.17. RNA-Seq analysis of U87MG cells silenced for *GLSiso2*: The libraries were constructed with SureSelect Strand-Specific RNA Prep for Illumina Multiplexed Sequencing following the manufacturer protocol (Ilumina, CA, USA). Total RNA of each sample in duplicates were used to start the library prep. The mean size of each library was determined on the Tapestation 2200 (Agilent Technologies), and quantification was performed by qRT-PCR using Kapa Library Quantification Kit (Kapa Biosystems, Wilmington, MA). The DNA libraries were pooled and sequenced on a HiSeq 2500 (Illumina) with 100 bp pair-ended reads in the SELA Facility Core of Rede Premium of School of Medicine, University of Sao Paulo.

3.18. Analysis of signaling pathways associated with *GLSiso2*: Sequencing generated an average of 51 million reads per sample. Quality control analysis was performed by FASTQC software. Raw reads were aligned to the hg38 through STAR software [122] . Quantification of the gene expression data was performed through RSEM software [123] and the data were normalized according to two different methods: Reads per kilobase million (RPKM) and counts per million (CPM). Differential expression analysis (Bioconductor portal) was analyzed by the Limma-voom framework [124]. The raw data were initially log-transformed and normalized. Subsequently, differential expression between groups was analyzed by linear models and the application of moderate t statistics. This

analysis was performed with the RNA-Seq tool (125). The *GLSiso2* silencing showed log [fold change] = -0,7. Finally, the analysis of RNA-Seq data (genes differentially expressed in cells silenced by siRNA compared with the NTC) was performed in genes related to altered processes observed in functional assays. logCPM values were transformed to z-scores for heat map visualization.

3.19. Functional validation of angiogenesis by sprouting assay: This assay was performed based on HUVECs cells (1.10^3/spheroid) were resuspended in DME F-12 culture media containing 0.20% (w/v) methylcellulose and seeded by using the hanging drop method. After for 24 h each spheroid was transferred to an embedded media containing collagen and methocel (1:1) into a 96 well plate and allowed to polymerize for 30 min prior adding conditioned media on top of the gel. Each well/condition containing at least 4 spheroids was treated with a different conditioned media being: basal media with VEGF-A (250ug/mL) the positive control, and the media from U87MG cells silenced with and NTC (negative control) at day 4. After 24 h, the spheroids were fixed using PFA 4% and pictures of the sprouting were taken with an inverted light microscope (Invitrogen EVOS™). Sprouting was quantified by counting the number of the sprouts that had grown out of each spheroid using Fiji v1.5.2, with at least 4 spheroids analyzed per experimental group and the experiment was done in duplicates.

3.20. Statistical analysis: Statistical analysis was conducted with SPSS for Windows, version 20.0 (IBM Corporation, Armonk, NY) and GraphPad Prism (version 5.02, San Diego, CA). Comparisons were considered statistically significant when $p < 0.05$. The non-parametric Kruskal-Wallis and post hoc Dunn tests were used to analyze the differences in mRNA relative expression in different grades of astrocytomas. The correlation analysis between gene expression values was assessed by the non-parametric Spearman-rho correlation test. The variation of specificity and sensibility of gene expression levels was analyzed using the receiver operating characteristic (ROC) curve. Among the continuous variables categorized through the ROC curve, the value with the best sensitivity and specificity was chosen as the cut-off value. The area under the ROC curve (AUC) was used to measure how the expression levels could distinguish between two groups. The gene expressions were classified as hyper or hypoexpressed based on this cut-off value. The comparison of protein expression and functional assays were carried by Two–way ANOVA and Bonferroni post-test. The

data was provided as the result with mean $\pm$ standard error and we considered statistically significant when $p < 0.05$. The analysis was done in biological triplicate of at least two experiments.

4. Results

4.1. Expression analysis of coding transcripts for the key enzymes involved in glutaminolysis

Expression analysis of transcript coding for the key enzymes involved in glutaminolysis, *GLSiso1, GLSiso2, GLS2, GLUD1, GOT1, GOT2*, and *GPT2* was performed in our series of astrocytomas of different malignant grades and NN brain samples.

4.2. *GAC* (*GLSiso2*) expression increases in parallel to astrocytoma malignancy

Interestingly, although no significant differential expression of the total *GLS* transcripts was observed among different grades of astrocytoma compared to NN, a significant *GLSiso2* (GAC) hyperexpression was observed in all grades of astrocytoma when compared to NN ($p < 0.0001$ Kruskal–Wallis test, and $p < 0.001$ Dunn test), with the highest expression levels detected in a set of GBM samples (Figure 2A). Of note, GLSiso2 expression increased in parallel to the grade of malignancy ($p < 0.0001$ AG1 vs. AG3, $p < 0.05$ AG2 vs. GBM, $p < 0.05$ AG3 vs. GBM; Dunn test) which reflected an increase of its correlation with the gene expression levels of the glutaminolysis pathway from NN to GBM (Figure 2A). When gene expression level correlations were analyzed, *GLSiso2* expression correlated weakly only with *GPT2* expression in NN, while no correlation was detected in AG1. GLSiso2 correlated negatively with *GLS2, GOT1*, and *GOT2* in AG2 and positively with *GLS2* and *GLSiso1* in AG3, whereas *GLSiso2* correlated positively with all genes of the glutaminolysis pathway in GBM (Figure 2B). Additionally, as shown in Figure 3, the *GLSiso2* expression levels presented high discriminatory power to distinguish between GBM and NN samples by ROC curve analysis (AUC = 0.919; 95% CI, 0.867–0.971) and between GBM and AG2, although with lower discriminatory power (AUC = 0.675; 95% CI, 0.569–0.781).
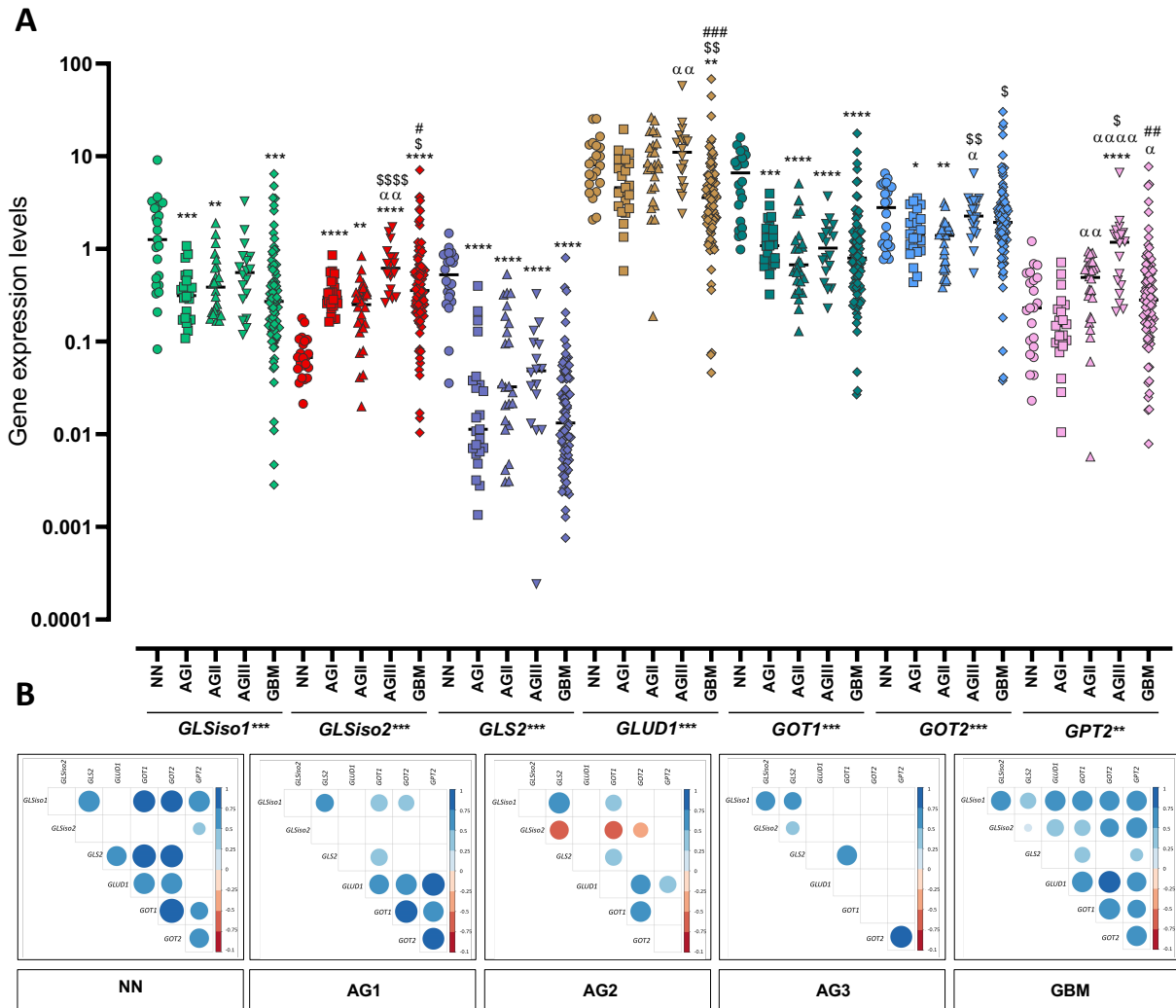
Figure 2. Expression analysis of genes coding for glutaminolysis in astrocytomas of different malignant grades. (A) *GLSiso1*, *GLSiso2*, *GLS*, *GLS2*, *GLUD1*, *GOT1*, *GOT2* and *GPT2* expression levels in non-neoplastic brain tissue (NN) compared to pilocytic astrocytoma (AG1), low grade astrocytoma (AG2), anaplastic astrocytoma (AG3) and glioblastoma (GBM). The expression levels differ significantly among the groups for all genes analyzed (**p = 0.002, ***p < 0.0001, Kruskal-Wallis test) and between NN and each tumor group (post-hoc Dunn test, where ****p < 0.0001, ***p < 0.0005, **p < 0.005, and *p < 0.05. The significant comparison between the groups are represent by different symbols: NN (*), AG1 (α), AG2 ($), and AG3 (#). Horizontal bars show the median of each group. The results are presented in log10 scale**. (B)** Correlation matrix showing the gene expression correlations with each other in all groups analyzed. Positive correlations are shown in blue and negative correlations in orange. The color intensiveness and the size of the circle are proportional to the value of r by Spearman test. Only the correlations with p < 0.05 were plotted.

In contrast, *GLSiso1* mRNA expression was significantly lower in AG1, AG2 and GBM compared to NN (p < 0.0001 Kruskal–Wallis test, and p < 0.05 Dunn´s test) (Figure 2A), with discriminatory power to distinguish between GBM and NN (AUC = 0.796; 95% CI, 0.1–0.308). No significant difference of its expression was detected in a pairwise comparison among different

grades of astrocytoma. However, we observed a strong positive correlation between *GLSiso1* and *GLS2* in AG2 and with *GLSiso2* in AG3, as well as with *GLSiso2, GLUD1, GOT1, GOT2* and *GPT2* in GBM cases. Similarly, *GLS2* hypoexpression was observed in astrocytoma of all malignant grades compared to NN (p < 0.0001 Kruskal–Wallis test, and p < 0.00001 for all astrocytoma grades and NN Dunn test) (Figure 2), and its expression level presented the power to distinguish between GBM and NN (AUC = 0.791; 95% CI, 0.000–0.06) and to distinguish between GBM and AG2, but with lower discriminatory power (AUC = 0.65; 95% CI, 0.221–0.48) (Figure 3)
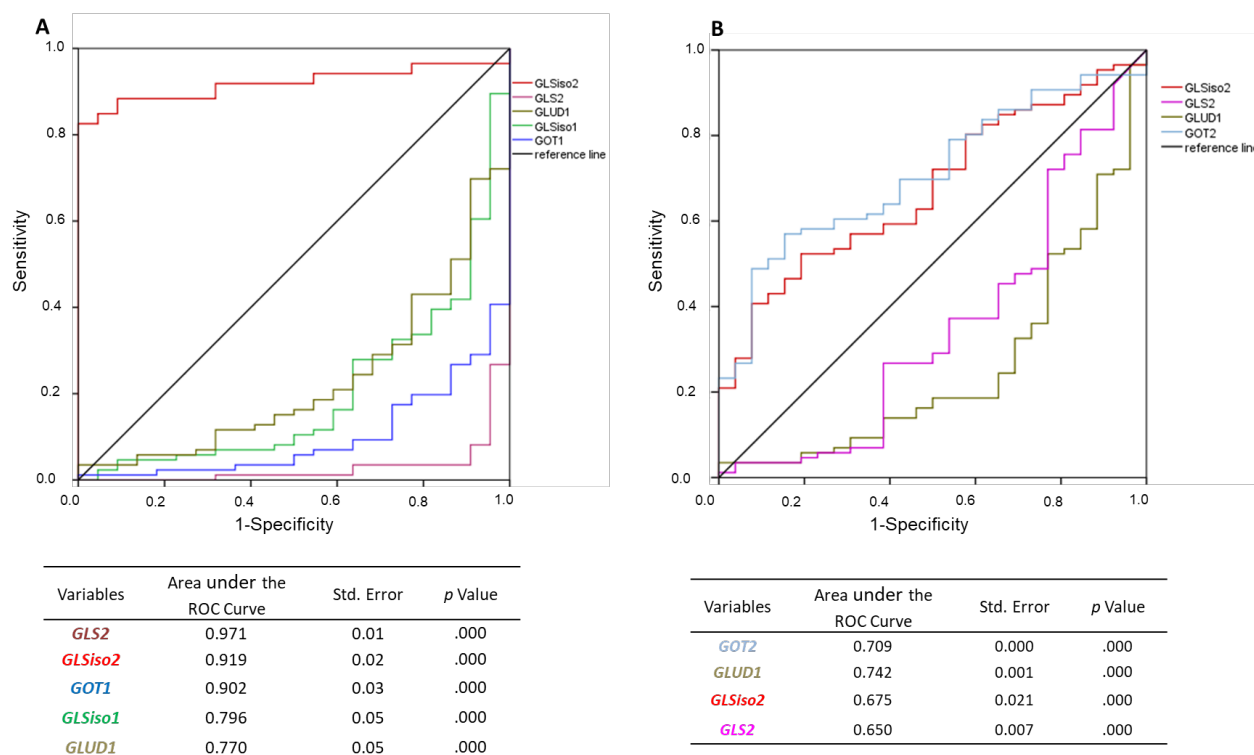

Variables	Area under the ROC Curve	Std. Error	p Value
GLS2	0.971	0.01	.000
GLSiso2	0.919	0.02	.000
GOT1	0.902	0.03	.000
GLSiso1	0.796	0.05	.000
GLUD1	0.770	0.05	.000

Variables	Area under the ROC Curve	Std. Error	p Value
GOT2	0.709	0.000	.000
GLUD1	0.742	0.001	.000
GLSiso2	0.675	0.021	.000
GLS2	0.650	0.007	.000

Figure 3. ROC curves for glutaminolysis pathway gene expressions. ROC curves for *GLSiso1, GLSiso2, GLS2, GLUD1 and GOT1* and *GOT2* expression levels, showing sensitivity and specificity of gene expression. The AUC values represent the accuracy of the individual gene for distinguishing between GBM and non–neoplastic tissue in **A**, and between GBM and AG2 samples in **B**.

4.3. *GPT2* downregulation in the GBM mesenchymal subtype correlated to upregulation of genes involved in glutathione synthesis

Once Glu is synthesized it can be converted to α–KG, an intermediate of the TCA cycle, by glutamate dehydrogenase (GLUD1) and glutamate transaminases, as glutamate oxaloacetate

transaminases (GOT1–cytosolic and GOT2–mitochondrial) and glutamate pyruvate transaminases (GPT1–cytosolic and GPT2–mitochondrial), which transfer amino groups from oxaloacetate or from pyruvate to generate α–KG and aspartate or alanine, respectively (50). The expressions levels of *GLUD1, GOT1, GOT2*, and *GPT2* were differentially expressed in astrocytomas compared to NN ($p < 0.0001$ Kruskal–Wallis test for *GLUD1, GOT1, and GPT2* and $p < 0.002$ for *GOT2*) (Figure 2A). Interestingly, *GLUD1* expression was significantly decreased in GBM compared to AG2 ($p < 0.005$ Dunn test), and its expression level presented discriminatory power to distinguish between GBM and NN (ROC AUC = 0.770; 95% CI, 0.128–0.332) and between GBM and AG2 (ROC AUC = 0.742; 95% CI, 0.147–0.368) (Figure 3).
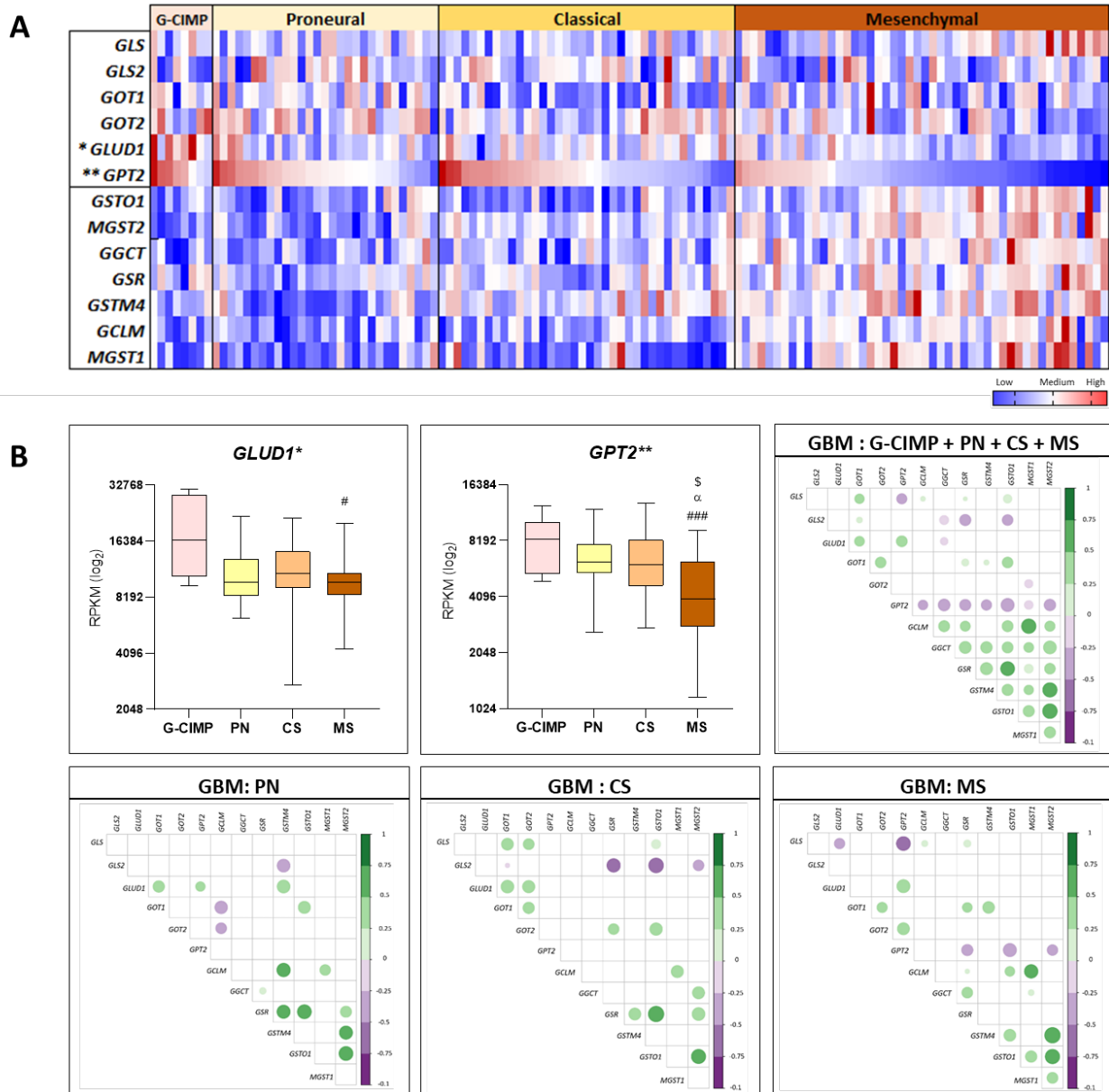
In contrast, *GOT2* expression increased according to malignancy ($p < 0.001$ AG2 vs. AG3 and $p < 0.01$ AG2 vs. GBM, Dunn test) (Figure 2A) and presented discriminatory power to distinguish between GBM and AG2 (AUC = 0.709; 95% CI, 0.608–0.810) (Figure 3). *GPT2* expression also increased significantly according to malignancy (AG1 relative to AG2 $p < 0.001$, to AG3 $p < 0.0001$, to GBM $p < 0.05$; AG2 vs AG3 $p < 0.05$, AG3 vs GBM $p < 0.005$; Dunn test), in addition, the only different expression level was observed in AG3 compared with NN ($p < 0.0001$) (Figure 2A). Although *GOT1* expression levels differed significantly between NN and astrocytomas, with discriminatory power to distinguish GBM from NN (ROC AUC = 0.902; 95% CI, 0.038–0.159), no significant difference of *GOT1* expression levels was detected among the astrocytoma grades of malignancy (Figure 2A).

Considering the natural history of malignancy progression from AG2 to GBM, an upregulation of *GLSiso2, GOT2,* and *GPT2* expression levels were observed, in contrast to the downregulation of *GLUD1*. However, a large spreading of their expressions was detected in GBM, consistent with the well–known heterogeneity observed in GBM. Therefore, we analyzed the expression levels in GBM cases classified according to the molecular subtypes in proneural (PN), classical (CS), and mesenchymal (MS) subtypes (126). Our cohort comprised of 14 PN, 38 CS, and 14 MS cases. We found a statistical difference for *GLS2* expression among the groups ($p < 0.005$, Kruskal–Wallis test) and comparing two groups: PN vs MS ($p < 0.05$, Dunn test) and CS vs MS ($p < 0.05$, Dunn test), with lower expression detected in the MS subtype.

To validate these findings, we analyzed gene expression *in silico* in a larger database. The TCGA GBM database with gene expression from RNAseq comprised of 37 PN (8 G-CIMP and 29 non-G-CIMP), 38 CS, and 48 MS cases. *GPT2* expression levels varied significantly among the

GBM subtypes (p < 0.0001, Kruskal–Wallis test) with lower levels in MS than G-CIMP (p < 0.0005), PN (p < 0.05), and CS (p < 0.05, Dunn test). *GLUD1* expression levels also varied significantly amongst GBM subtypes (p = 0.05, Kruskal–Wallis test) with significant higher levels in G-CIMP compared to PN (p < 0.01) and to MS (p < 0.005, Dunn test). Although no statistical significance was observed of *GLS* expression among GBM subtypes, a trend of increase of its expression was noted in MS subtype (Figure 4A). The expression levels of *GLS* isoforms were not available in this dataset. The TCGA data analysis showed the downregulation of *GLUD1* and *GPT2* involved in the conversion of Glu to α–KG. *GLUD1* differed statistically in G–CIMP to MS (p < 0.01). Particularly, *GPT2* differed when comparing all groups with the MS subtype of GBM (G–CIMP vs. MS p < 0.001; PN vs. MS p < 0.01; CS vs. MS p < 0.05).

The downregulation of both genes *GLUD1* and *GPT2* suggests that the intracellular availability of Glu is increased, especially in the MS subtype of GBM, which led us to investigate another important Glu metabolism pathway: GHS. To this purpose, we selected the genes related to glutathione pathway, glutamate–cysteine ligase modifier subunit (*CGLM*), gamma–glutamylcyclotransferase (*GGCT*), glutathione S–transferase mu 4 (*GSTM4*), glutathione S–transferase omega 1 (*GSTO1*), microsomal glutathione S–transferase 1 (*MGST1*), and microsomal glutathione S–transferase 2 (*MSGT2*), and analyzed the expression levels in the GBM database of TCGA (Figure 4A). Additionally, the expression values were correlated to the expression data of glutaminolysis genes (Figure 4B). The seven genes related to GSH synthesis presented differential expression levels among the GBM molecular subtypes, with statistical differences for all genes (p < 0.0005, Kruskal–Wallis test). Particularly, the expression of these genes was higher in the MS subtype compared to the other subtypes. Moreover, the gene expression levels of GSH synthesis were highly correlated among themselves when all groups of GBM were analyzed together (GBM: G–CIM+PN+CS+MS), and interestingly, an inverse correlation was noted with *GPT2* expression. Particularly in the MS subtype, *GPT2* expression correlated inversely to the expression levels of *GSTO1*, *GSR*, and *MGST2*, suggesting the possibility of Glu not converted to α–KG being used for GHS synthesis (Figure 4B).

Figure 4. TCGA dataset: Glutaminolysis– and Glutathione synthesis–related gene expressions and their correlation in GBM subtypes. (A) Heatmap representing gene expression levels in G-CIMP, proneural (PN), classical (CS), mesenchymal (MS) GBM subtypes. Up-regulated values are in red and down-regulated in blue. The RPKM values were normalized by z-score (*p =0.05, **p < 0.0001, Kruskal-Wallis test). **(B)** Box and whisker plots of *GLUD1* and *GPT2* expression levels in different GBM subgroups. The lines in the middle of the boxes show the median expression in each group, and the top and the bottom of boxes represent the first and third quartiles. The results are presented in log2 scale of RPKM values. (Kruskal-Wallis: *p < 0.05, **p < 0.005, Dunn test: MS vs PN (α); MS vs CS ($); G-CIMP vs MS: (#). Spearman correlation matrices of gene expression levels in different GBM molecular subtypes. The color bar on the right indicates the level of correlation (r) ranging from dark purple (negative correlation) to green (positive correlation). The color intensiveness and the circle size are proportional to r values. Only the correlation with p < 0.05 are plotted.

4.4. *GLUD1* upregulation in *IDH1*^mut AG3 correlated to downregulation of genes involved in glutathione synthesis

G-CIMP cases of PN molecular subtype of GBM presented the highest *GLUD1* and *GPT2* expression levels when compared to the other subgroups. Additionally, genes related to GSH synthesis presented the lowest expression levels in G-CIMP cases. These data and the information that increased conversion of Gln to Glu has been described in glioma cells harboring *IDH1* mutation (127) motivated us to investigate the *IDH1* mutation status influence in the expression levels of genes involved in the glutaminolysis pathway and GSH. Gene expression levels previously analyzed in GBM cases were also analyzed in AG2 and AG3 cases of TCGA, separating cases with and without *IDH1* mutation (Figure 5A). In our cohort, 20 AG2 out of 26 cases (77%) presented *IDH1* mutation, and 11 out of 18 AG3 cases harbored *IDH1* mutation (61%). Interestingly, upregulated *GLUD1* and *GPT2* expressions were observed in *IDH1*^mut AG2 cases, with significant difference compared to *IDH1*^wt AG2 cases for *GPT2* expression (p < 0.05, Mann-Whitney test), and a trend of increase for *GLUD1* (Figure 5B). In a larger TCGA dataset, with 51 *IDH1*^mut AG2 out of 63 cases (86%), and 80 *IDH1*^mut AG3 out of 129 cases (63%), a significant higher *GLUD1* and *GPT2* expression levels were observed both in AG2 and AG3 harboring *IDH1* mutation when compared to cases without *IDH1* mutation (p < 0.01 and p < 0.0001 for *GLUD1* in AG2 and AG3 respectively; p < 0.01 and p < 0.001 for *GPT2* in AG2 and AG3, respectively, Mann-Whitney test) (Figure 5B). Correlation analyzes of expression level of all genes demonstrated that *IDH1*^mut AG2 cases presented activation of both glutaminolysis and GSH synthesis in contrast to *IDH1*^wt AG2, with an inverse correlation between *GLS2* and *MSGT2* expressions in *IDH1*^mut AG2 (Figure 5C). On the other hand, *IDH1*^mut AG3 cases presented a significant high correlation between *GLUD1* and *GPT2* expression levels, and inverse correlations with several genes related to GSH synthesis. Of note, *GLUD1* expression level was inversely correlated to *GSR, GCLM, GSTO1* and *GSMT2* expression levels, indicating the downregulation of these gene expressions when *GLUD1* was upregulated in *IDH1*^mut AG3 cases (Figure 5C).
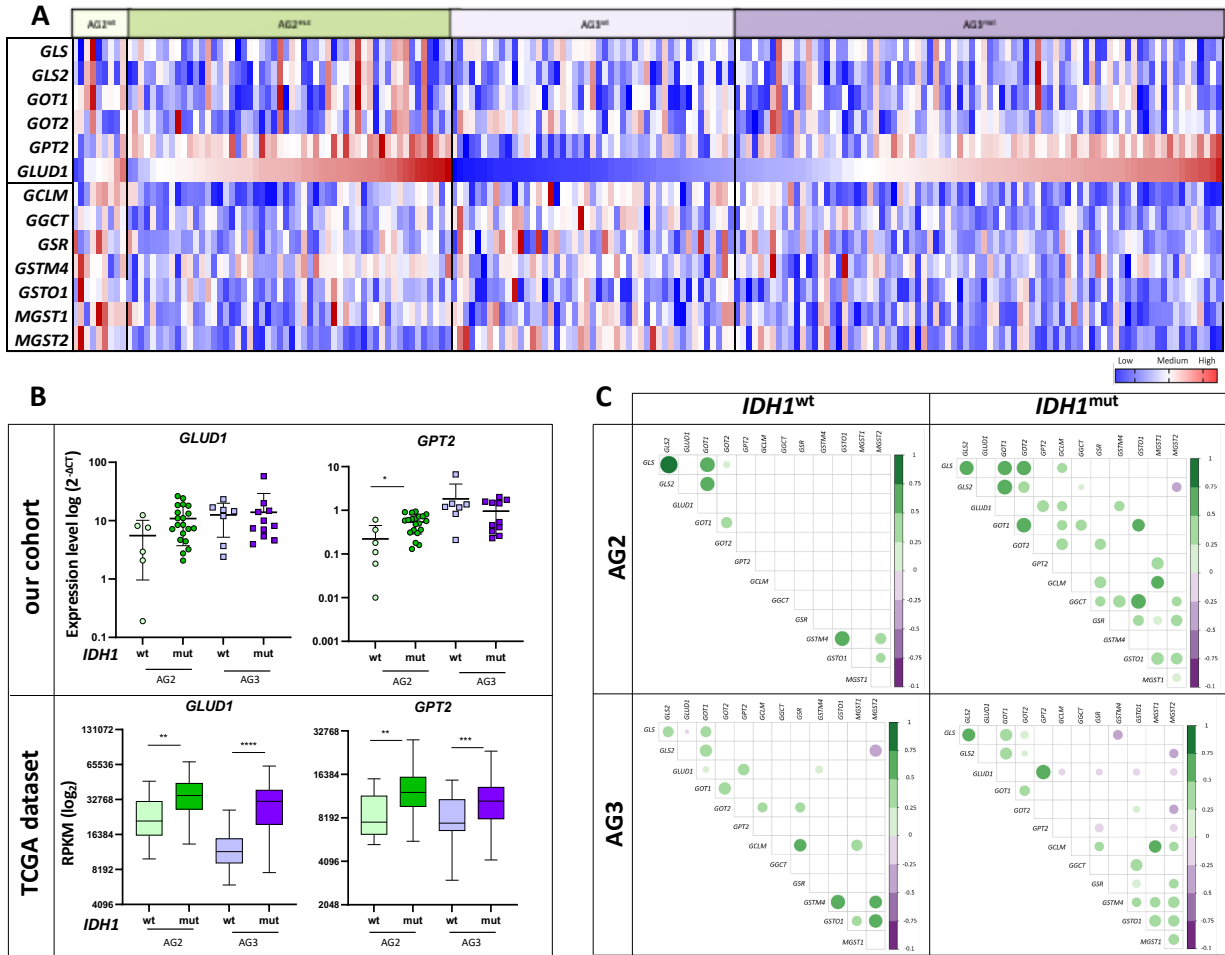
Figure 5. AG2, AG3 TCGA dataset: Glutaminolysis– and Glutathione synthesis–related gene expressions according to IDH1 mutation. (A) Heatmap representing the expression levels of genes presenting statistical significance in AG2 and AG3 with wild type (wt) and mutated (mut) *IDH1*. Upregulated values are represented in red and downregulated in blue. The RPKM values were normalized by z-score. **(B)** The differential expression levels of *GLUD1* and *GPT2* in each stratified group. (Mann-Whitney test: *p < 0.05, **p < 0.01; ***p < 0.0005, ****p < 0.0001). Horizontal bars show the median expression in each group for the up panels, while the bottom panels boxes represent the first (top) and third (bottom) quartiles, and the median are represented by the middle line in the boxes. The results are presented in log2 scale of RPKM values. **(C)** Spearman correlation matrix among the gene expression levels of each group. The color bar on the right indicates the level of correlation ranging from dark purple (negative correlation) to green (positive correlation). The color intensiveness and the circle sizes are proportional to r values. Only the correlations with p < 0.05 are plotted.

4.5. GLUD1 and GPT2 protein downregulation in GBM-MS and GLUD1 downregulation in AG2-IDH^{wt} correlated with upregulation of GS activity

35

The GBM-MS presented lower GLUD1 and GPT2 protein levels when compared to the GBM-PN cases ($p < 0.05$ and $p < 0.001$, respectively). Although statistical significance was not reached, AG2-IDH^{wt} presented low GLUD1 protein level (Figures 6A, B). Additionally, we evaluated whether the level of these proteins correlated with GS expression. Interestingly, a significant increase of GS expression was observed in GBM-MS and AG2-IDH^{wt} in comparison with GBM-PN and AG2-IDH^{mut} ($p < 0.01$ and $p = 0.05$, respectively) (Figures 6C, D).
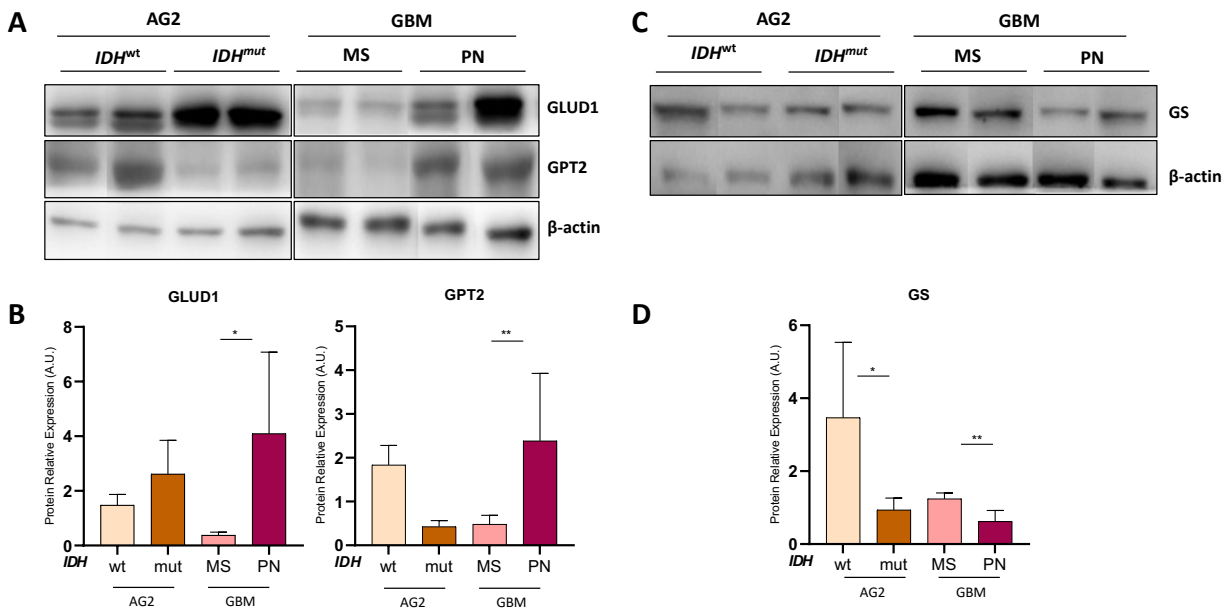

Figure 6: GLUD1, GPT2, and GS protein expression analysis in GBM and low-grade astrocytomas according to IDH mutation status. (A) Western blotting analysis of the expression of GLUD1 and GPT2 in AG2-IDH^{wt}, AG2-IDH^{mut,} GBM-MS (IDH^{wt}) and GBM-PN (IDH^{mut}) samples, and GS in **(C).** β-actin was used as the loading control. **(B, D)** Quantification of each protein relative to β-actin protein by ImageJ, represented by mean values ± standard deviation. The graph is representative of at least four replicates of one experiment. *$p < 0.05$, **$p < 0.001$, one-way ANOVA, Bonferroni post-test

4.6. The relevance of the GAC (*GLSiso2*) in malignant progression of astrocytomas

GLS isoforms expression was investigated at the protein level, and we confirmed a differential expression of GLSiso1 and GLSiso2 in astrocytomas of different malignant grades compared to NN cases (Figure 7). Whereas GLSiso1 was clearly present in all NN and in diffusely infiltrative astrocytoma (grade 2 to 4) samples, with higher abundance in NN samples in comparison to GBM samples ($p < 0.001$ ANOVA two–way, with Bonferroni post–test), GLSiso2 expression was mostly

detected in GBM cases and only slightly detected in NN samples. Both GLS isoforms were detected in the U87MG cell line, a GBM cell line of MS subtype (Figure 7).
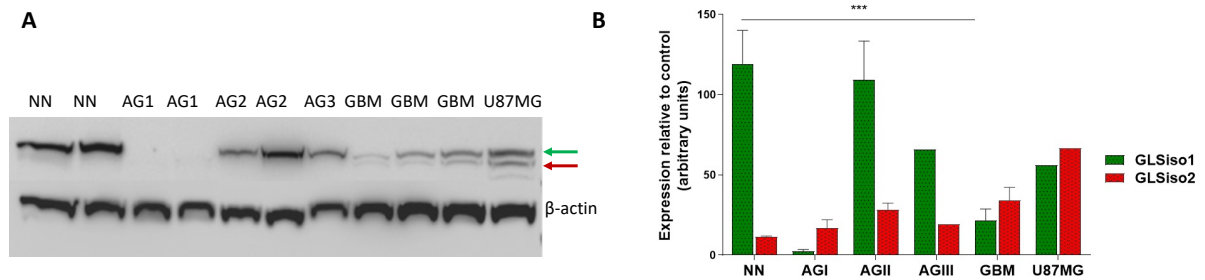

Figure 7. GLS isoforms expression profile during astrocytoma progression and U87MG human GBM cells. (A) Western blot analysis of the expression of GLS isoforms in non-neoplastic (NN), pilocytic astrocytoma (AG1), low grade astrocytoma (AG2), anaplastic astrocytoma (AG3), glioblastoma (GBM), and U87MG GBM cell line. GLSiso1 and GLSiso2 are indicated by green arrow and red arrows, respectively. β-actin was used as loading control. **(B)** Quantification of proteins by ImageJ represented by mean values ± standard deviation. The graph is representative of at least two replicates of one experiment. ***p < 0.001, Two-way ANOVA, Bonferroni post-test.

The high expression of *GLSiso2* in astrocytomas, especially in GBM, with its low expression in NN tissue pointed out this isoform as a potential candidate for new therapeutic strategies for GBM patients. Therefore, we analyzed the roles of *GLSiso2* in *in vitro* GBM cell model to better understand the reach of this target for clinical applicability. Initially, we performed a *GLSiso2* silencing in the human GBM cell line (U87MG). The analysis was assessed using a small interfering RNA against *GLSiso2* and a non-target (NTC) as negative control. We tested three different concentrations (0.1, 1 and 10nM) and the efficiency of *GLSiso2* silencing was evaluated at mRNA level through qPCR-RT (Figure 8A). The inhibition rate was more efficient on day four and day seven at concentration of 10nM (15.7% and 8.4% of *GLSiso2* expression in *siRNA-GLSiso2* compared to NTC, respectively) (Figure 8B). We also evaluated the protein expression through Western Blotting (Figures 8C, D) and we observed a higher inhibition at day 4 (D4). Thus, all further experiments were performed at D4. In addition, protein expression level and its cellular distribution were evaluated through immunofluorescence. A decrease of GLS protein expression was observed in tumor cells silenced for *GLSiso2* compared to control (NTC). Beyond the reduction in the protein quantity, it was observed the GLS localization in mitochondria. The zoomed-in regions-of-interest in images (ROI) confirmed the GLS, presumably GLSiso2, localization in mitochondria, as previously reported in literature (Figure 8E) (128).
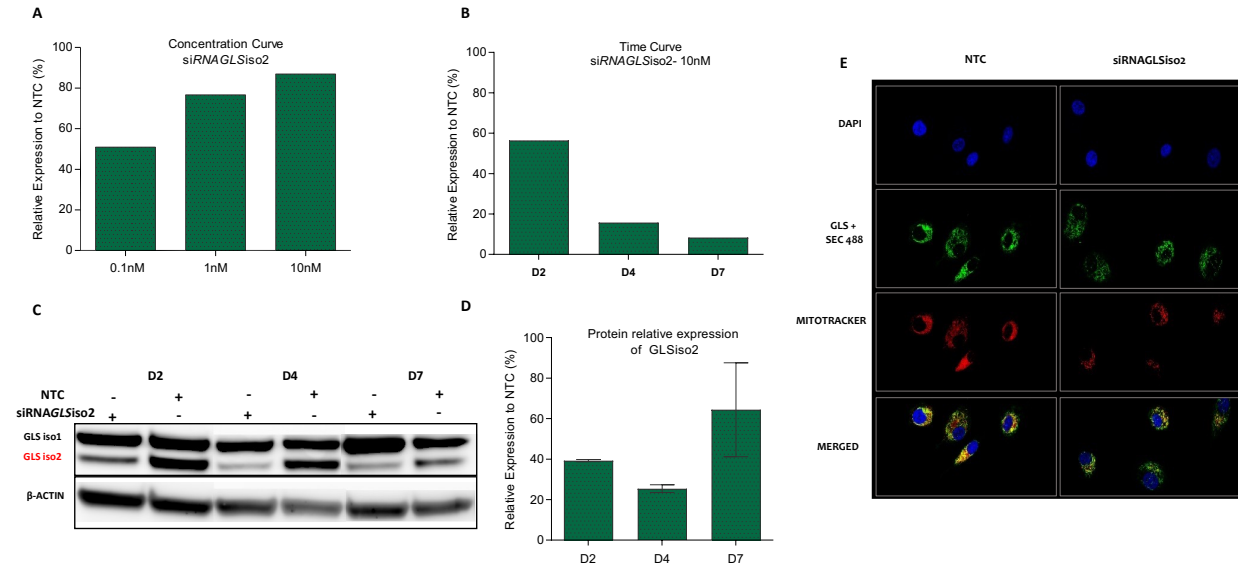
Figure 8. GLS isoforms expression analysis in U87MG cell line. (A) Expression of *GLSiso2 silencing* after transfection in different concentrations (10, 1 and 0,1 nM). **(B)** Expression of *GLSiso2* after transfection in different times (2, 4 and 7 days). Transcript levels was analyzed by quantitative real-time PCR. **(C)** Protein expression of GLS isoforms in U87MG cell line analyzed by Western blotting. Endogenous control: β-actin. **(D)** Densitometry results of the Western blotting presented in **(C)** representative of one experiment. **(E)** Double immunofluorescence analysis for GLS (green) and mitochondria (red mitoTracker) in U87MG cells showed their co-localization in 63x STACK. Nuclei were counterstained with DAPI (blue). The cells were fixed and stained after 4 days of silencing.

4.7. Silencing of *GLSiso2* decreased cell proliferation rate

The cell proliferation rate after silencing *GLSiso2*, and NTC showed a significant decrease of cell viability from D4 (50%), D5 (51.7%), D6 (70.3%) and D7 (59.4%) (Figure 9A). Moreover, a cell cycle arrest at G1 phase was observed in the *GLSiso2*-silenced cells (69.5%) in comparison with the control NTC (36.9%), as well as a significant difference between G1-S phases (25.77%) and G2/M (8.5%) in the *GLSiso2* silenced cells compared to NTC, confirming the G1 cell cycle arrest (Figures 9B, C). Additionally, as a specific chemical inhibitor for the GLS isoforms is not commercially available yet, we decided to perform the chemical blockage using different concentrations of BPTES, a total GLS inhibitor. A decreased tumor cell viability was observed after 24, 48, 72 and 96 h with BPTES at IC_{50} of 6μM in comparison with the control using DMSO (Figure 9D).
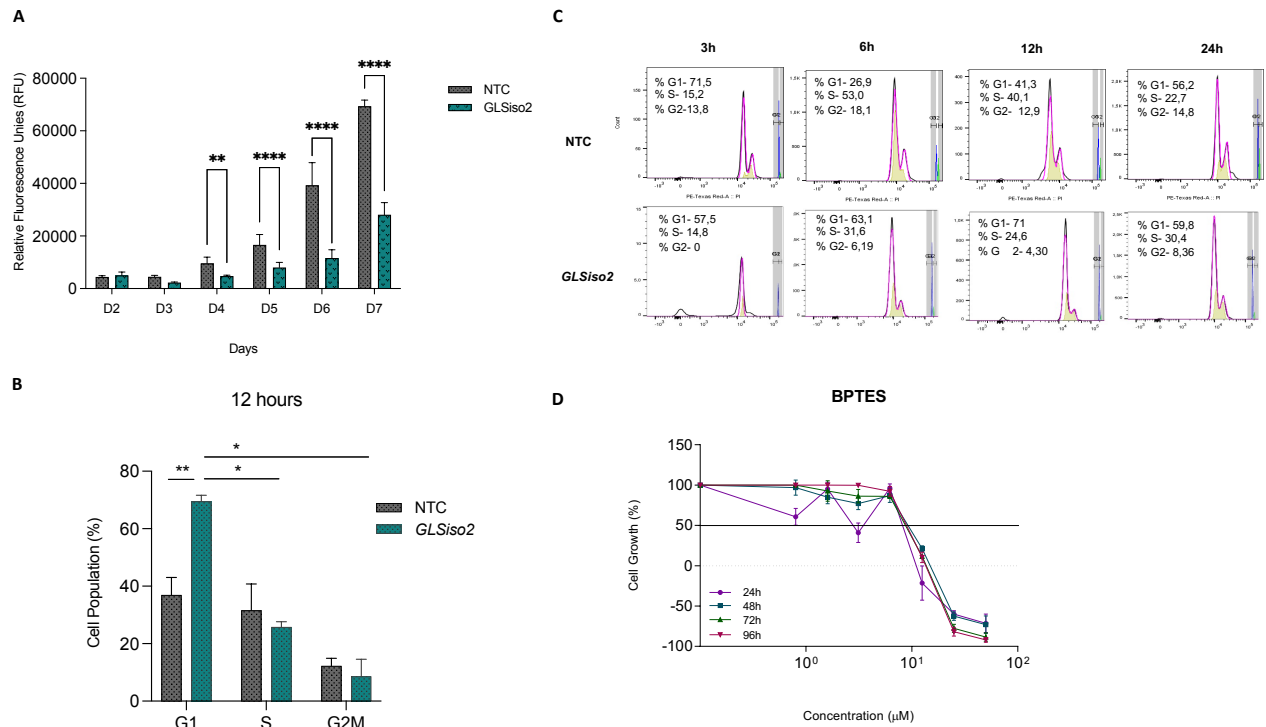
Figure 9. Proliferation rates in U87MG cell line after *GLSiso2* silencing. (A) Data comparing U87MG cells silenced for *GLSiso2* and control (NTC) after 2 (D2), 4 (D4) and 7 (D7) days. Viability of cells was accessed by Presto Blue reagent. *** p <0.001 * p <0.05 (two-way ANOVA: Bonferroni). **(B)** Quantification of U87MG cells in phases G1, S, and G2 after 12 h of silencing. **(C)** Histograms of quantification of U87MG cells in phases G1, S, and G2 after 3, 6, 12 and 24 h after silencing. The values were expressed as mean ± standard deviation of one replicate of three different experiments. * p < 0.05; ** p < 0.01, and **** p < 0.0001 (Two–way ANOVA: Bonferroni). **(D)** Proliferation assay comparing U87MG at 24, 48, 72 and 96 h after treatment with GLS inhibitor (BPTES 0,1-50uM) and control DMSO. Cell viability accessed by Presto Blue reagent. The values were expressed as mean ± standard deviation of four replicates of two different experiments.

4.8. Silencing of *GLSiso2* sensitized U87MG cells to Temozolomide

The decrease of tumor cell proliferation by *GLSiso2* silencing was enhanced in temozolomide-sensitized tumor cells, which was demonstrated by photomicrographs showing enhancement of cell death of siRNA*GLSiso2* cells when treated with TMZ in comparison to non-treated parental control cells, and NTC cells (Figure 10A). Moreover, a significant decrease of viable cells was observed for all conditions: NTC (91.0%) x siRNAGLSiso2 (77.2%); NTC+ DMSO (91.5%) x siRNA*GLSiso2* + DMSO (73.8%) and NTC+ TMZ (62.1%) x siRNA*GLSiso2* + TMZ (47.5%). Additionally, a trend of increasing annexin positive cells was observed (Figure 10B, C) in *GSLiso2* silenced+TMZ cells compared with controls. No differences were observed in double staining/late apoptosis and 7AAD (7-Aminoactinomycin D) staining/necrosis.
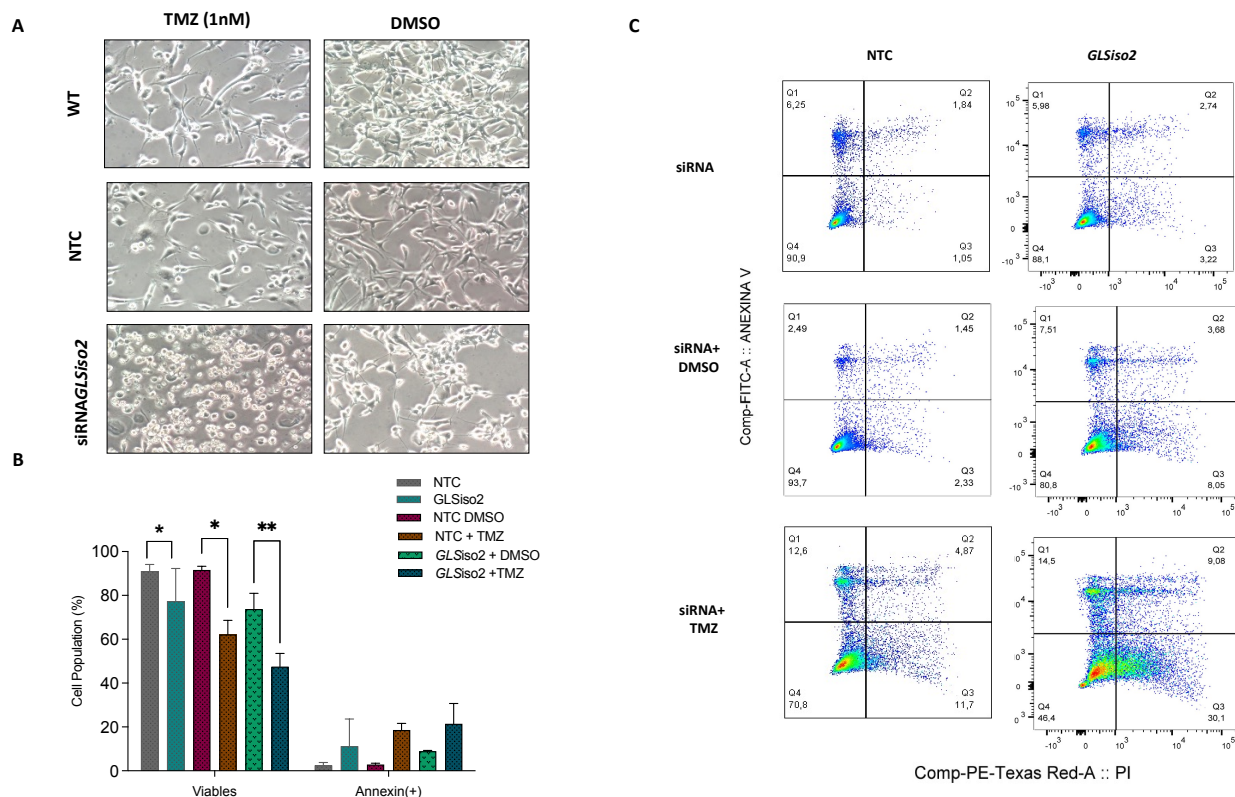
Figure 10. *GLSiso2* silencing sensitized U87MG cell to Temozolomide treatment. (A) Proliferation assay photomicrographs comparing the U87MG cell line treated with TMZ (1mM) and non-treated in different conditions: WT (parental cells), NTC (control) and silenced cells (siRNA*GLSiso2*). **(B)** Quantification of U87MG cells stained for annexin V–PE and 7–AAD after *GLSiso2* silencing, control (NTC) after 4 (D4) days and treated with TMZ (1mM-72h). Scatter plots of flow cytometry results are presented at **(C).** The values are expressed as mean ± standard deviation of two replicates of three different experiments. * p < 0.05 and *** p < 0.001. (Two–way ANOVA: Bonferroni).

4.9. GLS protein distribution in human Astrocytomas and HUVEC endothelial cell line

Total GLS protein distribution was also analyzed in different grades of human astrocytomas by immunohistochemistry. We observed that the higher the malignant grade, the higher the GLS protein expression in tumor cells. Interestingly, tumor ECs presented higher GLS expression in grade 4-GBM cases compared to lower grade astrocytomas and NN brain tissues (Figure 11A, B). As antibodies for specific GLS isoforms are not commercially available, the distribution of both isoforms in each tumor cell compartment, including ECs, awaits the development of these specific reagents.

We analyzed the differential expression of GLS isoforms in HUVEC immortalized umbilical EC line by qPCR and WB to verify whether this cell line was suitable to study the impact of GLS

isoforms on the vessel compartment. HUVEC cells presented higher expression of GLSiso2 than GLSiso1 (Figure 11D, E). Therefore, chemical blockade of the total GLS by BPTES was tested in HUVEC cells, and a significant decrease of EC proliferation was observed (Figure 11F). In addition, GLS protein distribution was evaluated through immunofluorescence in HUVEC cells. GLS (green) colocalized with mitochondria (red), suggesting the presence and abundance of GLSiso2 (mitochondrial isoform) in ECs (Figure 11C).
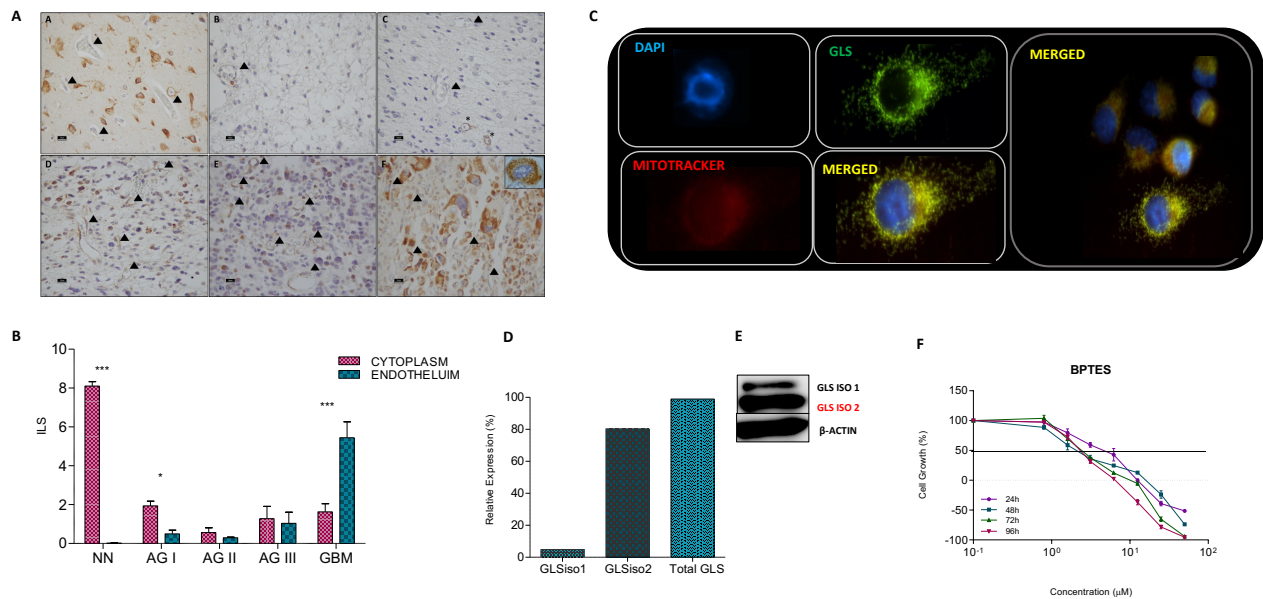

Figure 11. GLS protein distribution in different grades of astrocytomas and GLS isoform expressions in HUVEC cell line. (A, B) GLS protein expression in AG1-4 and NN: Representative images of GLS in (A-NN), (B-AG1), (C-AG2), (D-AG3), and (E, F-GBM). GLS positive staining was detected in neurons but not ECs in NN. AG1 and AG2 tumor cells (TUs) and ECs did not present positivity whereas few AG3 TUs and ECs presented positivity. Interestingly, GLS immunoreaction was quite heterogeneous in GBM: cases with ECs+/TU- (E-GBM) and ECs-/TU+ with strong positivity in granular pattern (F-GBM, insert 600x) were observed. Arrowheads = vessels. * In C point to neurons within the AG2 tumor bulk. Bars = 10µm scale. **(C)** Double immunofluorescence analysis for GLS (green) and mitochondria (red MitoTracker) in HUVEC cells showed their co-localization. Nuclei were counterstained with DAPI (blue). **(D)** Expression of total *GLS* and *GLSiso1 and 2* in HUVEC cell line. Transcript levels was analyzed by quantitative real-time PCR. **(E)** Protein expression of GLS isoforms in HUVEC cell line analyzed by Western blotting. Endogenous control: β-actin. **(F)** Proliferation assay comparing HUVEC at 24, 48, 72, and 96 after treatment with GLS inhibitors (BPTES 0,1-50uM) and control DMSO. Cell viability accessed by Presto Blue reagent. The values were expressed as mean ± standard deviation of four replicates of two different experiments.

4.10. The *GLSiso2* related signaling pathways identified by RNASeq: metabolic reprogramming and angiogenesis

To better understand the role of *GLSiso2* in GBM, we analyzed the transcriptome of U87MG *GLSiso2*-silenced cells by RNASeq. The transcriptomic analysis showed 352 downregulated genes (logFC<-0.7, p<0.05, and adjusted p<0.5) in comparison to NTC. The enrichment analysis by WebGestalt using the ORA methodology and Gene Ontology Pathways database revealed 10 biological processes with FDR <0.05 including, regulation of RNA polymerase II transcriptional complex assembly, post- embryonic animal organ development, response to hydrogen peroxide, muscle cell development, regulation of actin filament organization, cellular response to platelet-derived growth factor stimulus, response to platelet-derived growth factors, coronary vasculature morphogenesis , coronary vasculature development, and artery development (Figure 12A). The gene set from these pathways were analyzed and twenty-one differentially expressed genes, including important genes related to angiogenesis (129) such as pro-angiogenic factors *VEGFA, TGFA*, *PDGFβ*, and *ANGPTL2,4* were downregulated in the silenced cells compared to NTC cells (Figure 12B). Additionally, the analysis of the String Consortium tool showed high connectivity among this set of genes (130) (Figure 12C). Moreover, the system biology analysis revealed an interesting net among *GLS*, *TP53*, *PDGFR-B*, *TGFA*, *VEGFA*, *ANGPTL2,4* connecting metabolism, and angiogenesis (Figure 12D).
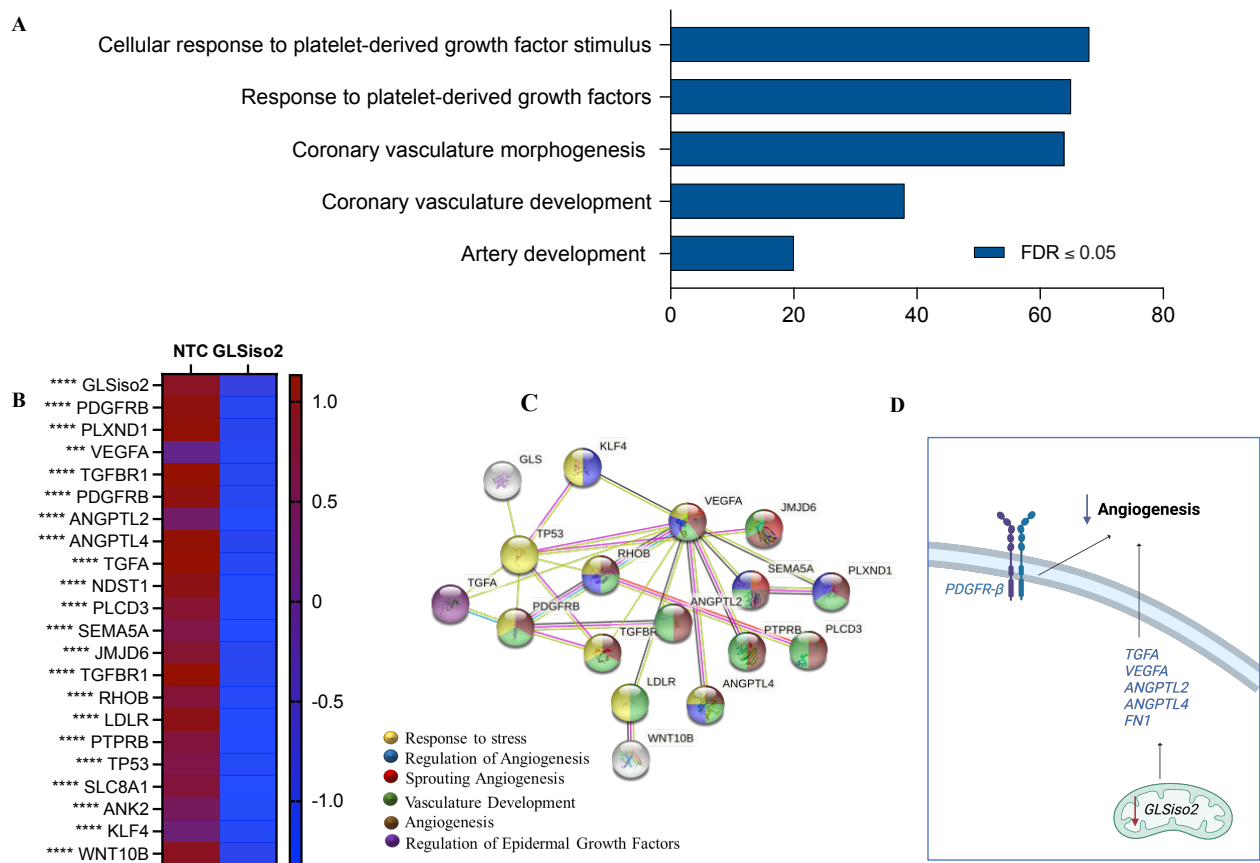
Figure 12- Transcriptome analysis of U87MG *GLSiso2*-silenced cells. **(a)** Ten most enriched pathways of ORA methods for GO biological process pathways of downregulated genes in comparison to NTC. The bars represent a score determined by the gene pool (FDR) and related fold change. FDR: false discovery rate. **(b)** Heatmap of 21 genes involved in pathways related to angiogenesis. Downregulated values are presented in blue and upregulated values in red. The values are expressed as mean three replicates ***p < 0.001 and **** p < 0.0001. (Two–way ANOVA: Bonferroni). The logCPM (counts per million) values were normalized by z-score. **(c)** The differentially expressed genes were plotted in a network according to the biological function- Gene Ontology Resource (130) by the String Consortium tool. **(d)** Proposed influence of *GLSiso2* siRNA and angiogenesis related genes in U87MG cells.

4.11. *GLSiso2* association with metabolic reprogramming

As GLS is a key regulator of the glutaminolysis, an important metabolic pathway, we analyzed the metabolic related genes in U87MG *GLSiso2*-silenced compared with NTC cells based on the KEGG pathway database (131). A set of 17 downregulated genes were detected in different metabolic pathways (Figure 13A), strongly connected as shown by the String Consortium tool (Figure 13B). Important genes related to glycolysis pathway such as *LDHA*, *ENO1*, *GAPDH* and *ALDOA* as well as glucose transporters, *GLUT1* and *GLUT3*, were downregulated in *GLSiso2*

silenced cells. Moreover, *GPT2* related to glutaminolysis, and *IDH3B* and *IDH3G*, genes responsible for converting α-KG in isocitrate in TCA cycle were downregulated. Lastly, two lactate transporters (*MCT1* and *MCT4*) were downregulated in comparison to the NTC. The above cited genes are involved in the Warburg effect (132).

The lactate is an end product of glycolysis, and its abundance increases during Warburg effect. Therefore, we measured lactate in siRNA*GLSios2* and NTC cell samples, and a decreased of 48.6% in the siRNA*GLSiso2* samples was observed (Figure 13D), corroborating the downregulation of important metabolic genes involved in the Warburg effect, including genes associated with the glycolytic pathway, glucose and lactate transporters leading to a decreased lactate production in *GLSiso2* silencing cells (Figure 13C).
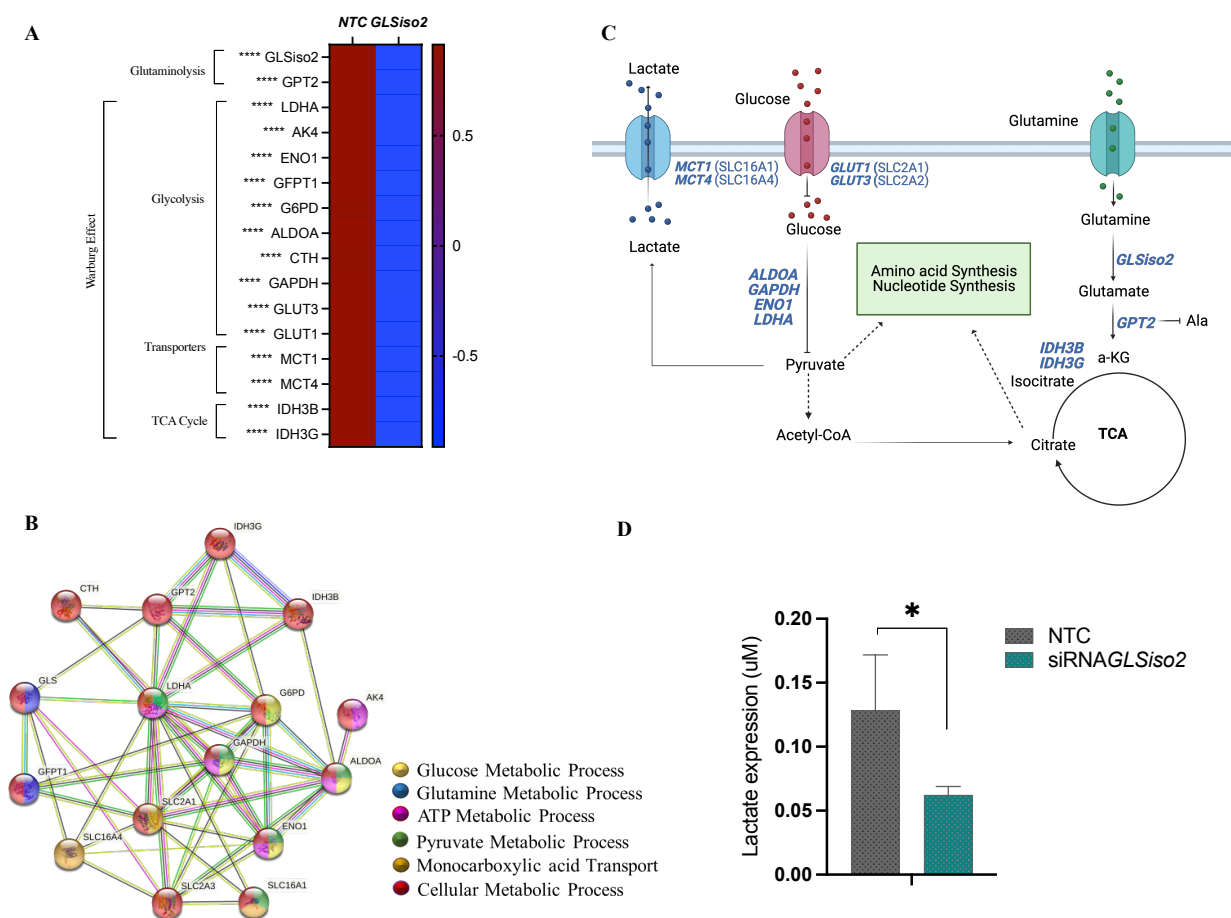

Figure 13- **Metabolic downregulated genes in U87MG *GLSiso2*-silenced cells. (A)** Heatmap of expression values for 17 genes involved in the Warburg Effect. Comparison of the expression for *GLSiso2*-silenced cells and NTC, wherein red are up-regulated values and blue down regulated. The logCPM values

were normalized by z-score. The values are expressed as mean of three replicates **** p < 0.0001. (Two–way ANOVA: Bonferroni) **(B)** The differentially expressed genes were plotted in a network according to the biological function (Gene Ontology Resource[3]) by the String Consortium tool. **(C)** Proposed influence of *GLSiso2* inibition in Warburg effect in U87MG cells. **(D)** Lactate expression analysis comparing GLSiso2 silenced cells and NTC. The values are expressed as mean of three replicates of two experiments * p < 0.05.

4.12. *GLSiso2* association with angiogenic process

Considering the findings of angiogenic pathway by transcriptomic analysis of *GLSiso2* silenced U87MG cells, a set of growth factors related to angiogenesis was analyzed using a multiplex assay. The measurements of VEGF-A, TNF-α and ANGPTL2 were significantly lower in the siRNA-*GLSiso2* samples in comparison to the NTC (Figure 14A). Thus, the impact of these decreased growth factors expression on angiogenesis was analyzed by sprouting assay using HUVEC cells. Spheroids of HUVEC cells were harvested with cell media of siRNA*GLSiso2* cells and of NTC cells at D4 of gene silencing. The cell media of HUVEC parental cell harvested with VEGF-A was used as a positive control. Decreased sprouting number formation in the siRNA*GLSiso2* samples compared to the positive control and NTC was observed (Figure 14B, C). The length of the sproutings of HUVEC cells exposed to GLSiso2 silenced cell media was also decreased in comparison to the positive control (Figure 14C), corroborating previous data indicating the involvement of *GLSiso2* in the angiogenic process.
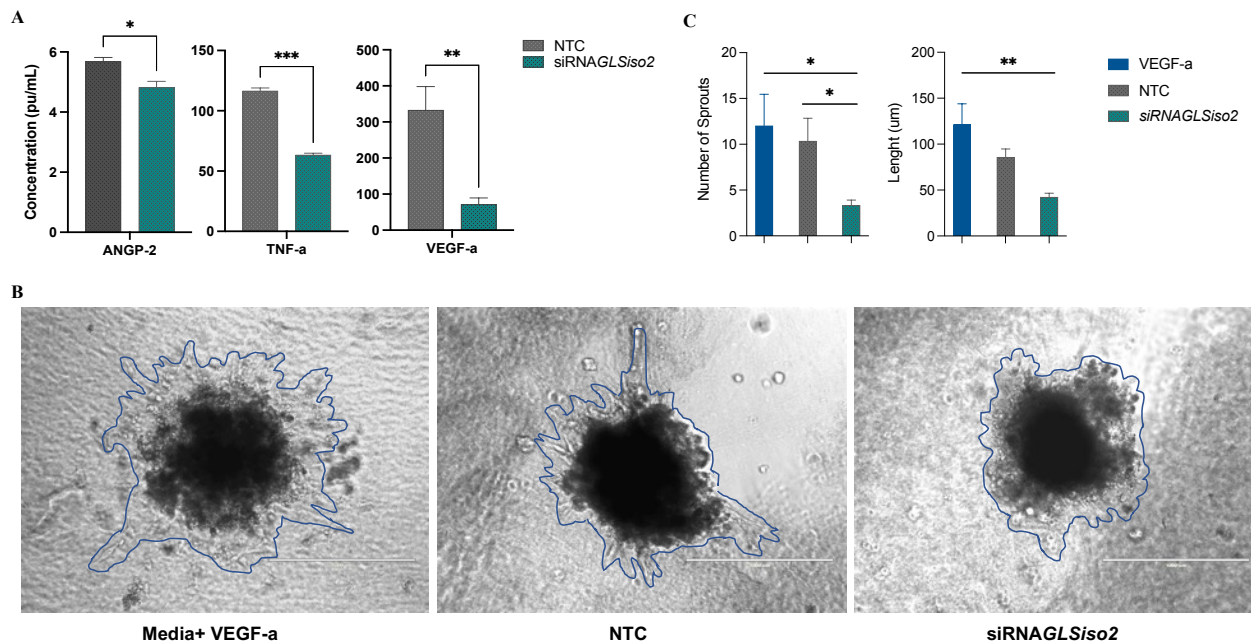
Figure 14- **GLSiso2 participation in angiogenic process. (A)** Analysis of ANGP-2, TNF-a and VEGF-a. Comparison of the expression for *GLSiso2*-silenced cells and NTC. The values are expressed as mean of three replicates of three experiments * $p < 0.05$ ** $p < 0.01$*** $p < 0.001$. (Two–way ANOVA: Bonferroni) **(B)** Photomicrography of HUVEC spheroids after 24 h of treatment with positive control (media+ VEGF-a), NTC and *GLSiso2* cell media at D4 of gene silencing **(C)** Number of sprouting formation and length of sprouting comparing the *GLSiso2* treated spheroids with positive control, and NTC. The values are expressed as mean of three replicates (spheroids) and two experiments * $p < 0.05$ $p < 0.01$**.

5. Discussion

Metabolic reprogramming has been proposed to be a hallmark of cancer (47), and in the present analysis we observed a progressive activation of the glutaminolysis from low grade astrocytoma to GBM. In fact, glutaminolysis has been pointed as one of the major altered metabolic pathways related to tumor growth (41,53). High extracellular Gln concentration has been associated with cell transformation (50), and its metabolism was related to cell survival and tumor growth by maintaining redox balance, bioenergetics and supporting macromolecular biosynthesis (47,60). We have previously reported the upregulation of Gln transporters, ASCT2 and LAT1, in all grades of astrocytoma (61). Here, we showed the upregulation of the mitochondrial isoform of GLS (128), GLSiso2 (GAC), in all grades of astrocytoma at gene and protein levels, and a gradual increase of its expression was observed in parallel to the increment of malignancy. GLSiso2 involvement in cancer progression has been previously reported in prostate cancer and B cell lymphoma (133). GLSiso2 is activated by inorganic phosphate (128) and it is also under c–Myc oncogene influence, through a mechanism involving microRNA (59,133). Oscillation of GLSiso2 expression has been associated with oxygen concentration, with an increase in hypoxic condition (128). Our finding of GLSiso2 higher expression in GBM, the more malignant astrocytoma presenting necrosis, corroborated this previous observation. The cytosolic GLSiso1 (KGA) expression was also higher in more malignant than lower grade astrocytomas. Nevertheless, the high expression observed in NN tissue renders this target less eligible for therapeutic purposes.

The other glutaminase, GLS2, in contrast to GLS with broad distribution among normal tissue, presents a more restricted distribution in liver, brain, pituitary gland and pancreas (134,135). GLS2 expression level was significantly lower in astrocytoma than NN, with the lowest expression in GBM of MS subtype in our cohort. This finding corroborates the tumor suppressor role attributed to GLS2 in previous studies, where inhibition of tumor cell proliferation, colony formation and migration were attributed to GLS2 (60,83,133,136–139). This tumor suppressor activity is dependent on p53 and other related proteins, as p63 and p73 (83). Therefore, concerning the first step of the glutaminolysis pathway, our findings suggested that GLSiso2 plays a key role in tumorigenesis and malignant progression of astrocytoma, whereas GLS2 expression pattern is consistent with tumor suppressor function, being mostly suppressed in the aggressive MS molecular subtype of GBM.

Interestingly, the downflow activation of the glutaminolysis pathway with the conversion of Glu to α–KG through dehydrogenase and transaminase varied according to the astrocytoma grade. A significant downregulation of *GLUD1* and *GPT2* expressions were observed in GBM compared to lower grade astrocytoma in our cohort and confirmed in the TCGA dataset. Particularly, *GPT2* was significantly downregulated in GBM of MS subtype compared to other molecular subtypes. The downregulation of *GPT2* may result in an increase of intracellular Glu availability, which may be directed for GSH synthesis (140).

GSH is a tripeptide formed by glutamic acid, cysteine, and glycine and plays an important role in the maintenance of the intracellular redox balance (141,142). Elevated GSH levels confer resistant to chemotherapy in various types of cancer (143–145) by binding to or reacting with drugs, interacting with ROS, preventing damage to proteins or DNA, and participating in DNA repair processes (143). Moreover, GSH and GSH–related enzymes including ligase (GCLM), transferase (GGT), reductase (GSR) and glutathione S–transferases (GSTM4, GSTO1, MGST1, MGST2) activities may play a role in adaptive detoxification processes in response to the oxidative stress, thus contributing to drug resistance phenotype (141,143).

The increase of intracellular Glu level may favor its release to the extracellular space by a Gln /cysteine antiporter system x c–dependent, which increases intracellular cysteine levels ([Cys]i). In turn, high [Cys]i favors GSH synthesis (140). In fact, the TCGA data analysis showed a significant inverse correlation among *GPT2* expression and expression level of several genes related to GSH synthesis. Particularly, upregulation of *GSTO1*, *MGST2* and *GSR* were correlated significantly to the downregulation of *GPT2* in MS subtype of GBM. The anti–oxidative effect provided by increased synthesis of GSH can balance the elevated generation of ROS due to high metabolic rate presented by GBM cells and favor their survival (146). Such mechanism may be related to the aggressive behavior of GBM of MS molecular subtype.

In contrast, AG2 and AG3 presented higher *GLUD1* expression levels than GBM, and particularly in those cases harboring *IDH1* mutation. Similarly, *GPT2* expression was also higher in AG2 and AG3 cases harboring *IDH1* mutation. Metabolomic studies of *IDH1* mutant cells have revealed alterations in Gln, fatty acid, and citrate synthesis pathways (147,148). *IDH1* mutation was shown to convert α–KG to D–2–hydroxyglutarate, which due to its structural similarities acts as a competitive inhibitor reducing the activity of α–KG–processing enzymes (149). As a feedback, α–KG is replenished by glutaminolysis and TCA cycle, which leads to a decrease in Gln and Glu

levels (150). Therefore, *IDH1*^{mut} gliomas are "glutamate addicted", and the lack of Glu decreases its exchange with Cys through the system XC– (151). The lack of cytoplasmic Cys reduces GSH synthesis, which increases the susceptibility to ROS–induced stress as through radiation therapy or TMZ treatment (151). In this context, reduced Glu contributes to a better outcome presented by gliomas with *IDH1* mutation (127,140). In fact, our correlation analysis among genes related to glutaminolysis and GSH synthesis–related genes demonstrated that *GLUD1* and *GPT2* expression levels inversely correlated to GSH synthesis–related gene expression levels, particularly in *IDH1*^{mut} AG3. Our findings reinforce the hypothesis that decreasing Glu may sensitize *IDH1*^{mut} cells to radiation and ROS–inducing drugs due to reduced GSH synthesis. Indeed, GLS inhibition and *IDH1* mutation were recently demonstrated to present a synthetic lethal relationship under conditions of oxidative stress (127).

Our findings together with TCGA data analysis indicated that AG2 and AG3 harboring *IDH1* mutation may decrease tumor cell fitness by lowering Glu, GSH and resistance to oxidative stress. Interestingly, the end metabolites of these enzymes, ammonia and alanine are measurable by the MR spectroscopy (152–155). Thus, monitoring the waning of *GLUD1* and *GPT2* expression levels by measuring their end substrates by this non–invasive imaging technique may potentially detect the progression of lower grade astrocytomas harboring *IDH1* mutation towards secondary GBM, and it would, therefore, allow a change in therapeutic strategy for these patients. Such hypothesis would be worthwhile to test in future studies.

After studying the glutaminolysis pathway and its impact in tumor astrocytomas we carried out the analysis of the role of the *GLSiso2* isoform in the U87MG cell line, representative of a GBM cell line of MS subtype. As cited before, both isoforms of *GLS* were upregulated in our astrocytoma cohort, with increased expression in parallel to the increase in the astrocytoma malignancy. Interestingly, *GLSiso1* expression was much higher than *GLSiso2* in non-neoplastic brain, which gives advantage to *GLSiso2* as potential therapeutic target. Our results corroborated previous studies reporting GAC variant as the key enzyme for cancer cell growth (128,133,156).

The GLS isozymes, in particular the GAC splice variant, are frequently upregulated in many types of tumors (128,157). Recently, GLS inhibitors, BPTES and 968, have been identified (158,159) and siRNA-mediated knockdown of *GLS* showed to impact severely the proliferation and/or survival of several cancer cell lines, without any detrimental effects on non-tumorigenic cells (99). Here we showed, in U87MG cells, that transient silencing of the *GLSiso2* isoform decreased

cell proliferation, induced cell cycle arrest in G1 phase and sensitized the tumor cells to TMZ treatment. The RNAseq data showed a downregulation in two major GBM-involved pathways: angiogenesis and metabolism.

The hypervascularity is one of the most significant characteristics of GBM. There is a significant correlation between the degree of angiogenesis and prognosis (160,161). Tumor progression is intimately associated with changes to the tumor microenvironment (162), including disruption of the blood brain barrier (BBB), variation of the extracellular matrix (ECM) (163), and other factors that can induce a wide range of interactions between endothelial and stromal cell populations (164). Hypoxic and necrotic conditions distinguish the GBM tumor microenvironment, which supports the formation of new vessels. In these conditions, GBM stem cells (GSCs), promote transdifferentiation of GSCs into ECs, and upregulate the release of pro-angiogenic growth factors, such as VEGF. Notably, tumors presenting high stem cell number are highly angiogenic (164,165). Besides, ECs play a role in barrier formation, conferring specific permeability in different organs, being the tightest in the brain, characterizing the BBB. ECs are stimulated to form new blood vessels by an angiogenic process when tissues or tumors grow. Phalanx ECs must change phenotypically to build vessel sprouts during angiogenesis, inducing the formation of a migratory tip ECs and proliferative stalk ECs that elongate the sprout. Active metabolism to convert nutrients to energy and biomass is essential for ECs in this process of forming new blood vessels (166). One of the main regulators of tumor metabolism and angiogenesis is HIF1α (167). In several cancer types, increased HIF1α expression was correlated with poor clinical prognosis (168). A large body of experimental data shows that manipulations that increases HIF1α expression result in increased tumor growth, vascularization, and metastasis, whereas loss of HIF activity has the opposite effect (169). A therapeutic strategy inhibiting angiogenesis through targeting proteins related to the angiogenic signaling, as VEGF, has been attempted against cancer and other diseases as retinopathies (166,170). However, the results have been limited by low efficacy and/or drug resistance. Our siRNA*GLSiso2* RNAseq results showed a decrease in different growth factors, including VEGFα, TGFα, PDGFβ, and Angiopoietins 2 and 4 that are intimately related to the angiogenic pathway. We also showed a decrease in the number of sprouting when ECs spheroids were cultivated with siRNA*GLSiso2* media indicating that *GLSiso2* was involved in angiogenic process and its silencing in tumor cells may decrease the crosstalk between tumor cells and ECs.

The siRNA*GLSiso2* RNAseq analysis also showed a downregulation in key metabolic genes involved in the glycolysis pathway and Warburg effect. The Warburg effect is characterized by the metabolic shift towards aerobic glycolysis with reprogramming of mitochondrial oxidative phosphorylation, regardless of oxygen availability, a characteristic feature of many types of cancers including gliomas. In addition to the Warburg effect, GBM tumor cells also utilize the TCA/OXPHOS in higher capacity than normal tissue (171). One of the major advantages of the Warburg effect in tumor cells is the production of lactate during aerobic glycolysis. Lactate can induce HIF1α expression, which in turn, drives the expression of several glycolytic enzymes, including phosphofructokinase (PFKM), glucose transporter-1, -3 (GLUT-1, -3), hexokinase II (HK2), lactate dehydrogenase A (LDHA), and aldolase (ALDOA), which are involved in reprogramming aerobic glycolysis (103). The lactate produced by cancer cells is exported to the extracellular space via MCTs and therefore, the extracellular pH significantly decreases in the tumor microenvironment (TME) leading to apoptosis of non-tumor cells and invasion of malignant cells into the normal parenchyma. Lactate also has a role as a potent signaling molecule. This is of particular interest in tumor metabolism, as high-lactate levels are often associated with a worse prognosis (172,173). One of the mechanisms proposed for this poor prognosis is the increase of angiogenesis. Any change in lactate levels lead to immediate balance of pyruvate level through LDH activity and vice versa. Accumulated pyruvate inhibits the formation of 2-oxoglutarate, the molecule responsible for targeting HIF1α for degradation in the proteasome. When lactate (pyruvate) levels increase, HIF1α drives angiogenesis via VEGF expression. Thus, HIF1α stabilization can be driven by lactate independently to hypoxia (174). Several studies have shown the antitumor potential effect of the VEGF-lactate pathway. Interestingly, glycolytic glioma tumor cells showed increased HIF1α levels with exposure to lactate, independent of hypoxia (175). Moreover, oxidative tumor cells activated HIF1α through importation of lactate (176). An *in vivo* study using intraperitoneal lactate administration enhanced xenografted tumor growth, vascularity and metastasis (177), and another *in vivo* study, in Lewis lung carcinoma mice model, showed a twofold reduction of vascularity in less than 2 weeks inhibiting MTCs (178). Our results suggest a decrease of the glycolytic gene expression, with decrease of lactate and VEGFA production, and decrease of both substrates in TME which may lead to decreased angiogenesis.

To summarize our findings, we reported that in GBM particularly in the MS subtype, the downregulation of both genes and proteins (GLUD1 and GPT2) increases the source of glutamate

for GSH synthesis and enhances tumor cell fitness due to increased antioxidative capacity. In contrast, in lower-grade astrocytoma, mainly in those harboring the *IDH1* mutation, the gene expression profile indicates that tumor cells might be sensitized to oxidative stress due to reduced GSH synthesis. Reinforcing the hypothesis that decreasing Glu may sensitize $IDH1^{mut}$ cells to radiation and ROS-inducing drugs due to reduced GSH synthesis. The measurement of GLUD1 and GPT2 metabolic substrates, ammonia, and alanine, by noninvasive MR spectroscopy, may potentially allow the identification of $IDH1^{mut}$ AG2 and AG3 progression towards secondary GBM. Thus, monitoring the waning of *GLUD1*and *GPT2* expression levels by measuring their end substrates by this non-invasive imaging technique may potentially detect the progression of lower grade astrocytomas harboring *IDH1*mutation towards secondary GBM.

We also showed that GLSiso2 upregulation was associated with tumorigenesis and tumor progression in astrocytomas. The *GLSiso2* gene silencing of the U87MG- GBM cell line led to a significant decrease of tumor cell proliferation as well as a cell cycle arrest at G1 phase. Additionally, an enhancement of this finding was achieved on temozolomide-sensitized tumor cells. The RNAseq transcriptome analysis of these *GLSiso2*-silenced cells revealed a differential expression of genes related to blood vessel development, angiogenesis, and tube development with significant FDR values, showing a decrease of the expression in important genes involved in the angiogenesis pathway such as VEGF-a, ANGP2,4, TNF-a in contrast with the control NTC. These findings were confirmed when we evaluated the expression of growth factor in the cell culture media and using the sprouting assay comparing siRNA*GLSiso2* and NTC. The immunohistochemistry analysis in human astrocytoma FFPE samples demonstrated GLS positivity on tumor cells and blood vessels, with higher protein expression in more malignant astrocytoma as well as a higher expression of GLSiso2 in HUVEC cells. We also showed a decreased lactate expression in the silenced cell in comparison to the NTC. Such observation corroborated the transcriptomic finding of *GLSiso2* participation in the EC compartment, connecting genes related to metabolism and angiogenesis and uncovering a new target for therapeutical strategies.

6. Conclusion

In conclusion, *GLSiso2* upregulation was associated with tumorigenesis and tumor progression in astrocytomas. Particularly in GBM, the accumulation of Glu due to *GPT2* and *GLUD1* downregulation correlated to upregulation of genes related to GSH synthesis which could favor tumor cell survival, mostly in the most aggressive MS subtype. In contrast, *GLUD1* may lead to a decrease in GSH synthesis in *IDH1*^mut low-grade astrocytoma increasing the susceptibility to oxidative stress, rendering them more sensitive to radiation therapy and to alkylating therapy. Both GLS isoforms, *GLSiso1* and GLSiso2 presented gradual expression increase in parallel to the increase of astrocytoma malignancy, however, GLSiso2 expression in normal brain tissue was lower than GLSiso1, which rendered GLSiso2 more eligible as therapeutic target. *GLSiso2* silencing in U87MG-GBM cells led to a decrease of tumor cell proliferation, cycle arrest at G1 phase and to increase susceptibility of tumor cells for temozolomide. The RNAseq transcriptome data and functional assays showed the *GLSiso2* association with metabolic shift and decrease of the angiogenic process. In this work, we suggested the monitoring of GLUD1 and GPT2 expression levels by measuring their end metabolites enzymes such as ammonia, and alanine by a non-invasive imaging technique may potentially detect the progression of lower-grade astrocytoma harboring *IDH1*mutation towards secondary GBM. The main findings of this work are described on figure 15. Our results also suggested *GLSiso2* as a potential new therapeutic target for GBM patients.
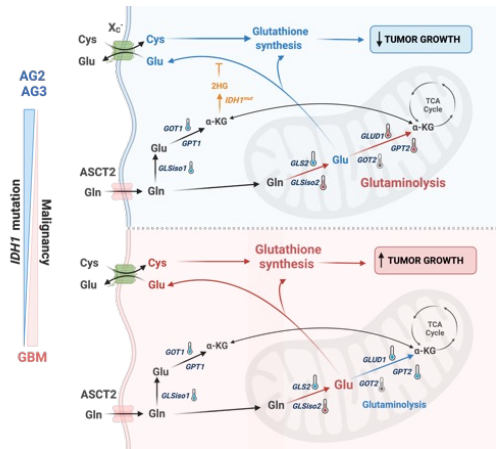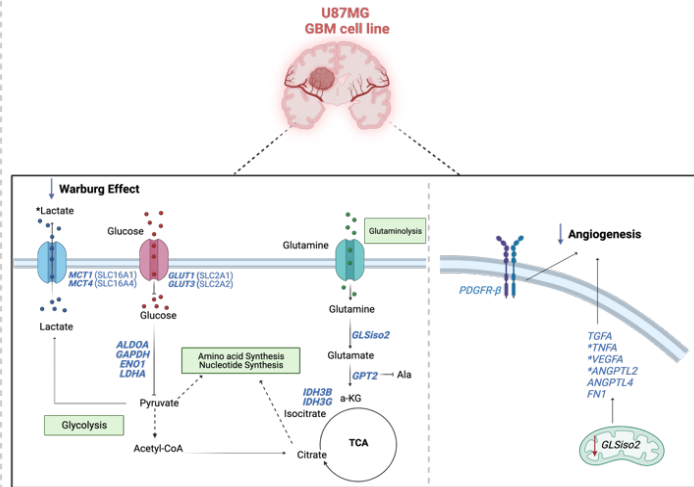
Figure 15. (**A**) Schematic representation of glutaminolysis genes differentially expressed in GBM. GBM presented hyperexpression of *GLSiso2* and hypoexpression of other genes of the glutaminolysis pathway (*GLS2*, *GLUD1*, *GPT2*), leading to Glu accumulation and activation of GSH synthesis. Consequently, enhancing fitness of tumor cells. AG2- and AG3-*IDH1*^mut displayed hyperexpression of *GLSiso2*, *GLUD1,* and *GPT2* with reduction of GSH synthesis, increasing tumor cell susceptibility to radiation and chemotherapy. The downregulated expression is represented by blue thermometers, upregulated by red thermometers, and the non-significant differential expression in gray. Red arrows represent the activation of the pathway and blue arrows represent the inactivation of the pathway. (**B**) Silencing of *GLSiso2* proposed mechanism of action: Metabolic and Angiogenic genes downregulated after *GLSiso2* silencing in comparison with *NTC* in U87MG cells. The downregulated genes are represented in blue. *Substrate measured in tumor cells microenvironment.

7. References

1. Siegel R, Miller K, Jemal A. Cancer statistics , 2015 . CA Cancer J Clin. 2015;65(1):29.

2. INCA. No Title. INSTITUTO NACIONAL DO CANCER 2018.

3. Hanahan D, Weinberg RA. The hallmarks of cancer. Cell [Internet]. 2000 Jan 7;100(1):57–70. Available from: http://www.ncbi.nlm.nih.gov/pubmed/10647931

4. Junttila MR, De Sauvage FJ. Influence of tumour micro-environment heterogeneity on therapeutic response. Nature. 2013;501(7467):346–54.

5. Ostrom QT, Cioffi G, Gittleman H, Patil N, Waite K, Kruchko C, et al. CBTRUS Statistical Report: Primary Brain and Other Central Nervous System Tumors Diagnosed in the United States in 2012–2016. Neuro Oncol [Internet]. 2019 Nov 1;21(Supplement_5):v1–100. Available from: https://academic.oup.com/neuro-oncology/article/21/Supplement_5/v1/5610892

6. Miranda-Filho A, Piñeros M, Soerjomataram I, Deltour I, Bray F. Cancers of the brain and CNS: global patterns and trends in incidence. Neuro Oncol [Internet]. 2016 Aug 29;19(2):now166. Available from: http://neuro-oncology.oxfordjournals.org/lookup/doi/10.1093/neuonc/now166

7. Jones C, Perryman L, Hargrave D. Paediatric and adult malignant glioma: close relatives or distant cousins? Nat Rev Clin Oncol [Internet]. 2012 Jul 29;9(7):400–13. Available from: http://www.nature.com/articles/nrclinonc.2012.87

8. Molinaro AM, Taylor JW, Wiencke JK, Wrensch MR. Genetic and molecular epidemiology of adult diffuse glioma. Nat Rev Neurol [Internet]. 2019 Jul 21;15(7):405–17. Available from: http://www.nature.com/articles/s41582-019-0220-2

9. Sanai N, Alvarez-Buylla A, Berger MS. Neural Stem Cells and the Origin of Gliomas. N Engl J Med [Internet]. 2005 Aug 25;353(8):811–22. Available from: http://www.nejm.org/doi/abs/10.1056/NEJMra043666

10. Wen PY, Weller M, Lee EQ, Alexander BM, Barnholtz-Sloan JS, Barthel FP, et al.

Glioblastoma in adults: A Society for Neuro-Oncology (SNO) and European Society of Neuro-Oncology (EANO) consensus review on current management and future directions. Neuro Oncol. 2020;22(8):1073–113.

11. Barnholtz-Sloan JS, Ostrom QT, Cote D. Epidemiology of Brain Tumors. Neurol Clin [Internet]. 2018;36(3):395–419. Available from: http://dx.doi.org/10.1016/j.ncl.2016.06.014

12. Daubon T, Léon C, Clarke K, Andrique L, Salabert L, Darbo E, et al. Deciphering the complex role of thrombospondin-1 in glioblastoma development. Nat Commun [Internet]. 2019;10(1). Available from: http://dx.doi.org/10.1038/s41467-019-08480-y

13. Daubon T, Hemadou A, Romero Garmendia I, Saleh M. Glioblastoma Immune Landscape and the Potential of New Immunotherapies. Front Immunol. 2020;11(October):1–17.

14. Brennan CW, Verhaak RGWW, McKenna A, Campos B, Noushmehr H, Salama SR, et al. The Somatic Genomic Landscape of Glioblastoma. Cell [Internet]. 2013 Oct;155(2):462–77. Available from: https://linkinghub.elsevier.com/retrieve/pii/S0092867413012087

15. Parsons DW, Jones SS, Zhang X, Lin JC-HC-H, Leary RJ, Angenendt P, et al. An Integrated Genomic Analysis of Human Glioblastoma Multiforme. Science (80-) [Internet]. 2008 Sep 26;321(5897):1807–12. Available from: http://www.sciencemag.org/cgi/doi/10.1126/science.1164382

16. Wu G, Diaz AK, Paugh BS, Rankin SL, Ju B, Li Y, Zhu X, Qu C, Chen X, Zhang J, Easton J, Edmonson M, Ma X, Lu C, Nagahawatte P, Hedlund E, Rusch M, Pounds S, Lin T, Onar-Thomas A, Huether R, Kriwacki R, Parker M, Gupta P, Becksfort J, Wei L, Mulder HL, Bog BS. The genomic landscape of diffuse intrinsic pontine glioma and pediatric non-brainstem high-grade glioma. Nat Genet [Internet]. 2014 May 6;46(5):444–50. Available from: http://www.nature.com/articles/ng.2938

17. Louis DN, Perry A, Reifenberger G, von Deimling A, Figarella-Branger D, Cavenee WK, et al. The 2016 World Health Organization Classification of Tumors of the Central Nervous System: a summary. Acta Neuropathol [Internet]. 2016;131(6):803–20. Available from: http://www.ncbi.nlm.nih.gov/pubmed/27157931

18. Appin CL, Brat DJ. Molecular Genetics of Gliomas. Cancer J [Internet]. 2014;20(1):66–72. Available from: http://content.wkhealth.com/linkback/openurl?sid=WKPTLP:landingpage&an=00130404-201401000-00012

19. Omuro A, DeAngelis LM. Glioblastoma and other malignant gliomas: A clinical review. JAMA - J Am Med Assoc. 2013;310(17):1842–50.

20. Verhaak RGW, Hoadley KA, Purdom E, Wang V, Qi Y, Wilkerson MD, et al. Integrated Genomic Analysis Identifies Clinically Relevant Subtypes of Glioblastoma Characterized by Abnormalities in PDGFRA, IDH1, EGFR, and NF1. Cancer Cell [Internet]. 2010 Jan;17(1):98–110. Available from: https://linkinghub.elsevier.com/retrieve/pii/S1535610809004322

21. Wang Q, Hu B, Hu X, Kim H, Squatrito M, Scarpace L, et al. Tumor Evolution of Glioma-Intrinsic Gene Expression Subtypes Associates with Immunological Changes in the Microenvironment. Cancer Cell [Internet]. 2017 Jul;32(1):42-56.e6. Available from: https://linkinghub.elsevier.com/retrieve/pii/S1535610817302532

22. Cohen AL, Holmen SL, Colman H. IDH1 and IDH2 Mutations in Gliomas. Curr Neurol Neurosci Rep [Internet]. 2013 May 27;13(5):345. Available from: http://link.springer.com/10.1007/s11910-013-0345-4

23. Phillips HS, Kharbanda S, Chen R, Forrest WF, Soriano RH, Wu TD, et al. Molecular subclasses of high-grade glioma predict prognosis, delineate a pattern of disease progression, and resemble stages in neurogenesis. Cancer Cell [Internet]. 2006 Mar;9(3):157–73. Available from: https://linkinghub.elsevier.com/retrieve/pii/S1535610806000560

24. Sidaway P. Glioblastoma subtypes revisited. Nat Rev Clin Oncol [Internet]. 2017 Oct 1;14(10):587–587. Available from: http://www.nature.com/articles/nrclinonc.2017.122

25. Weller M. Angiogenesis in glioblastoma: just another moving target? Brain [Internet]. 2010 Apr 1;133(4):955–6. Available from: https://academic.oup.com/brain/article-lookup/doi/10.1093/brain/awq063

26. El Hallani S, Boisselier B, Peglion F, Rousseau A, Colin C, Idbaih A, et al. A new alternative mechanism in glioblastoma vascularization: tubular vasculogenic mimicry. Brain [Internet]. 2010 Apr 1;133(4):973–82. Available from: https://academic.oup.com/brain/article-lookup/doi/10.1093/brain/awq044

27. Talasila KM, Røsland G V., Hagland HR, Eskilsson E, F|ønes IH, Fritah S, et al. The angiogenic switch leads to a metabolic shift in human glioblastoma. Neuro Oncol [Internet]. 2016 Sep 3;now175. Available from: http://neuro-oncology.oxfordjournals.org/lookup/doi/10.1093/neuonc/now175

28. Venneti S, Thompson CB. Metabolic Reprogramming in Brain Tumors. Annu Rev Pathol Mech Dis [Internet]. 2017 Jan 24;12(1):515–45. Available from: http://www.annualreviews.org/doi/10.1146/annurev-pathol-012615-044329

29. Vander Heiden MG, DeBerardinis RJ. Understanding the Intersections between Metabolism and Cancer Biology. Cell [Internet]. 2017 Feb;168(4):657–69. Available from: https://linkinghub.elsevier.com/retrieve/pii/S009286741631755X

30. Han S, Liu Y, Cai SJ, Qian M, Ding J, Larion M, et al. IDH mutation in glioma: molecular mechanisms and potential therapeutic targets. Br J Cancer [Internet]. 2020 May 26;122(11):1580–9. Available from: https://www.nature.com/articles/s41416-020-0814-x

31. Leighton F, Poole B, Lazarow PB, De Duve C. THE SYNTHESIS AND TURNOVER OF RAT LIVER PEROXISOMES. J Cell Biol [Internet]. 1969 May 1;41(2):521–35. Available from: https://rupress.org/jcb/article/41/2/521/17350/THE-SYNTHESIS-AND-TURNOVER-OF-RAT-LIVER

32. Pirozzi CJ, Yan H. The implications of IDH mutations for cancer development and therapy. Nat Rev Clin Oncol [Internet]. 2021 Oct 15;18(10):645–61. Available from: https://www.nature.com/articles/s41571-021-00521-0

33. Claus EB, Walsh KM, Wiencke JK, Molinaro AM, Wiemels JL, Schildkraut JM, et al. Survival and low-grade glioma: the emergence of genetic information. Neurosurg Focus [Internet]. 2015 Jan;38(1):E6. Available from: https://thejns.org/view/journals/neurosurg-focus/38/1/article-pE6.xml

34. Sanson M, Marie Y, Paris S, Idbaih A, Laffaire J, Ducray F, et al. Isocitrate Dehydrogenase 1 Codon 132 Mutation Is an Important Prognostic Biomarker in Gliomas. J Clin Oncol [Internet]. 2009 Sep 1;27(25):4150–4. Available from: https://ascopubs.org/doi/10.1200/JCO.2009.21.9832

35. Labussiere M, Boisselier B, Mokhtari K, Di Stefano A-L, Rahimian A, Rossetto M, et al. Combined analysis of TERT, EGFR, and IDH status defines distinct prognostic glioblastoma classes. Neurology [Internet]. 2014 Sep 23;83(13):1200–6. Available from: https://www.neurology.org/lookup/doi/10.1212/WNL.0000000000000814

36. Camelo-Piragua S, Jansen M, Ganguly A, Kim JC, Cosper AK, Dias-Santagata D, et al. A Sensitive and Specific Diagnostic Panel to Distinguish Diffuse Astrocytoma From Astrocytosis: Chromosome 7 Gain With Mutant Isocitrate Dehydrogenase 1 and p53. J Neuropathol Exp Neurol [Internet]. 2011 Feb 1;70(2):110–5. Available from: https://academic.oup.com/jnen/article-lookup/doi/10.1097/NEN.0b013e31820565f9

37. Reuss DE, Mamatjan Y, Schrimpf D, Capper D, Hovestadt V, Kratz A, et al. IDH mutant diffuse and anaplastic astrocytomas have similar age at presentation and little difference in survival: a grading problem for WHO. Acta Neuropathol [Internet]. 2015 Jun 12;129(6):867–73. Available from: http://link.springer.com/10.1007/s00401-015-1438-8

38. Schumacher T, Bunse L, Pusch S, Sahm F, Wiestler B, Quandt J, et al. A vaccine targeting mutant IDH1 induces antitumour immunity. Nature [Internet]. 2014 Aug 21;512(7514):324–7. Available from: https://www.nature.com/articles/nature13387

39. Hanahan D, Weinberg RA. Hallmarks of Cancer: The Next Generation. Cell [Internet]. 2011 Mar;144(5):646–74. Available from: http://dx.doi.org/10.1016/j.cell.2011.02.013

40. Vijayakumar SN, Sethuraman S, Krishnan UM. Metabolic pathways in cancers: key targets and implications in cancer therapy. RSC Adv [Internet]. 2015;5(52):41751–62. Available from: http://www.scopus.com/inward/record.url?eid=2-s2.0-84929340650&partnerID=tZOtx3y1

41. Strickland M, Stoll EA. Metabolic Reprogramming in Glioma. Front Cell Dev Biol [Internet]. 2017;5(April). Available from:

http://journal.frontiersin.org/article/10.3389/fcell.2017.00043/full

42.   Marie SKN, Shinjo SMO. Metabolism and brain cancer. Clinics (Sao Paulo) [Internet]. 2011;66 Suppl 1:33–43. Available from: http://www.ncbi.nlm.nih.gov/pubmed/23320861

43.   Cairns RA, Harris IS, Mak TW. Regulation of cancer cell metabolism. Nat Rev Cancer [Internet]. 2011 Feb;11(2):85–95. Available from: http://www.ncbi.nlm.nih.gov/pubmed/21258394

44.   Smith B, Schafer XL, Ambeskovic A, Spencer CM, Land H, Munger J. Addiction to Coupling of the Warburg Effect with Glutamine Catabolism in Cancer Cells. Cell Rep [Internet]. 2016 Oct;17(3):821–36. Available from: https://linkinghub.elsevier.com/retrieve/pii/S2211124716312840

45.   Liberti M V., Locasale JW. The Warburg Effect: How Does it Benefit Cancer Cells? Trends Biochem Sci [Internet]. 2016;41(3):211–8. Available from: http://dx.doi.org/10.1016/j.tibs.2015.12.001

46.   Vander Heiden MG, Cantley LC, Thompson CB. Understanding the Warburg effect: the metabolic requirements of cell proliferation. Science. 2009 May;324(5930):1029–33.

47.   Pavlova NN, Thompson CB. The Emerging Hallmarks of Cancer Metabolism. Cell Metab [Internet]. 2016 Jan;23(1):27–47. Available from: https://linkinghub.elsevier.com/retrieve/pii/S155041311500621X

48.   Bi J, Chowdhry S, Wu S, Zhang W, Masui K, Mischel PS. Altered cellular metabolism in gliomas — an emerging landscape of actionable co-dependency targets. Nat Rev Cancer [Internet]. 2020;20(1):57–70. Available from: http://dx.doi.org/10.1038/s41568-019-0226-5

49.   Warburg O. The Metabolism of Carcinoma Cells. J Cancer Res [Internet]. 1925 Mar 1;9(1):148–63. Available from: http://cancerres.aacrjournals.org/cgi/doi/10.1158/jcr.1925.148

50.   Jin L, Kang S. Glutaminolysis as a target for cancer therapy. Oncogene. 2016;35(28):3619–25.

51. Herranz D. Glutaminolysis gets the spotlight in cancer. 2017;8(7):10761–2.

52. DeBerardinis RJ, Mancuso A, Daikhin E, Nissim I, Yudkoff M, Wehrli S, et al. Beyond aerobic glycolysis: Transformed cells can engage in glutamine metabolism that exceeds the requirement for protein and nucleotide synthesis. Proc Natl Acad Sci [Internet]. 2007 Dec 4;104(49):19345–50. Available from: http://www.pnas.org/cgi/doi/10.1073/pnas.0709747104

53. Cluntun AA, Lukey MJ, Cerione RA, Locasale JW. Glutamine Metabolism in Cancer: Understanding the Heterogeneity. Trends in Cancer [Internet]. 2017;3(3):169–80. Available from: http://dx.doi.org/10.1016/j.trecan.2017.01.005

54. Durán R V., Oppliger W, Robitaille AM, Heiserich L, Skendaj R, Gottlieb E, et al. Glutaminolysis Activates Rag-mTORC1 Signaling. Mol Cell [Internet]. 2012 Aug;47(3):349–58. Available from: https://linkinghub.elsevier.com/retrieve/pii/S1097276512004881

55. Nicklin P, Bergman P, Zhang B, Triantafellow E, Wang H, Nyfeler B, et al. Bidirectional Transport of Amino Acids Regulates mTOR and Autophagy. Cell [Internet]. 2009 Feb;136(3):521–34. Available from: http://linkinghub.elsevier.com/retrieve/pii/S0092867408015195

56. Son J, Lyssiotis CA, Ying H, Wang X, Hua S, Ligorio M, et al. Glutamine supports pancreatic cancer growth through a KRAS-regulated metabolic pathway. Nature [Internet]. 2013 Apr 27;496(7443):101–5. Available from: http://www.nature.com/articles/nature12040

57. van der Vos KE, Eliasson P, Proikas-Cezanne T, Vervoort SJ, van Boxtel R, Putker M, et al. Modulation of glutamine metabolism by the PI(3)K–PKB–FOXO network regulates autophagy. Nat Cell Biol [Internet]. 2012 Aug 22;14(8):829–37. Available from: http://www.nature.com/articles/ncb2536

58. Altman BJ, Stine ZE, Dang C V. From Krebs to clinic: glutamine metabolism to cancer therapy. Nat Publ Gr [Internet]. 2016;16(10):619–34. Available from: http://dx.doi.org/10.1038/nrc.2016.71

59. Márquez J, Alonso FJ, Matés JM, Segura JA, Martín-Rufián M, Campos-Sandoval JA. Glutamine Addiction In Gliomas. Neurochem Res. 2017;42(6):1735–46.

60. Obara-Michlewska M, Szeliga M. Targeting glutamine addiction in Gliomas. Cancers (Basel). 2020;12(2).

61. Alves MJF, Uno M, Silva R da, Oba-Shinjo SM, Marie SKN. The expression of the aminoacid transporters ASCT2 (SLC1A5) and LAT1 (SLC7A5) in astrocytomas. Med Express [Internet]. 2016;3(6):1–8. Available from: http://www.gnresearch.org/doi/10.5935/MedicalExpress.2016.06.05

62. Vander Heiden MG. Targeting cancer metabolism: a therapeutic window opens. Nat Rev Drug Discov [Internet]. 2011 Sep;10(9):671–84. Available from: http://www.nature.com/articles/nrd3504

63. Daye D, Wellen KE. Metabolic reprogramming in cancer: Unraveling the role of glutamine in tumorigenesis. Semin Cell Dev Biol [Internet]. 2012 Jun;23(4):362–9. Available from: https://linkinghub.elsevier.com/retrieve/pii/S1084952112000341

64. Ralph J. DeBerardinis, M.D. and TC. Q's next: The diverse functions of glutamine in metabolism, cell biology and cancer. 2010;29(3):313–24.

65. Koch G. A tale of two glutaminases: homologous enzymes with distinct roles in tumorigenesis. Med Chem Res. 2017;71(10):643.

66. Luengo A, Gui DY, Vander Heiden MG. Targeting Metabolism for Cancer Therapy. Cell Chem Biol [Internet]. 2017 Sep;24(9):1161–80. Available from: https://linkinghub.elsevier.com/retrieve/pii/S2451945617303264

67. Jacque N, Ronchetti AM, Larrue C, Meunier G, Birsen R, Willems L, et al. Targeting glutaminolysis has antileukemic activity in acute myeloid leukemia and synergizes with BCL-2 inhibition. Blood [Internet]. 2015 Sep 10;126(11):1346–56. Available from: https://ashpublications.org/blood/article/126/11/1346/34377/Targeting-glutaminolysis-has-antileukemic-activity

68. Xiang Y, Stine ZE, Xia J, Lu Y, O'Connor RS, Altman BJ, et al. Targeted inhibition of tumor-specific glutaminase diminishes cell-autonomous tumorigenesis. J Clin Invest

[Internet]. 2015 Jun 1;125(6):2293–306. Available from: http://www.jci.org/articles/view/75836

69. Amores-Sánchez MI, Medina MÁ. Glutamine, as a Precursor of Glutathione, and Oxidative Stress. Mol Genet Metab [Internet]. 1999 Jun;67(2):100–5. Available from: https://linkinghub.elsevier.com/retrieve/pii/S1096719299928573

70. Kennedy L, Sandhu JK, Harper M-E, Cuperlovic-Culf M. Role of Glutathione in Cancer: From Mechanisms to Therapies. Biomolecules [Internet]. 2020 Oct 9;10(10):1429. Available from: https://www.mdpi.com/2218-273X/10/10/1429

71. Franklin CC, Backos DS, Mohar I, White CC, Forman HJ, Kavanagh TJ. Structure, function, and post-translational regulation of the catalytic and modifier subunits of glutamate cysteine ligase. Mol Aspects Med [Internet]. 2009 Feb;30(1–2):86–98. Available from: https://linkinghub.elsevier.com/retrieve/pii/S0098299708000630

72. Muir A, Danai L V, Gui DY, Waingarten CY, Lewis CA, Vander Heiden MG. Environmental cystine drives glutamine anaplerosis and sensitizes cancer cells to glutaminase inhibition. Elife [Internet]. 2017 Aug 15;6. Available from: https://elifesciences.org/articles/27713

73. Timmerman LA, Holton T, Yuneva M, Louie RJ, Padró M, Daemen A, et al. Glutamine Sensitivity Analysis Identifies the xCT Antiporter as a Common Triple-Negative Breast Tumor Therapeutic Target. Cancer Cell [Internet]. 2013 Oct;24(4):450–65. Available from: https://linkinghub.elsevier.com/retrieve/pii/S1535610813003668

74. Harris IS, Treloar AE, Inoue S, Sasaki M, Gorrini C, Lee KC, et al. Glutathione and Thioredoxin Antioxidant Pathways Synergize to Drive Cancer Initiation and Progression. Cancer Cell [Internet]. 2015 Feb;27(2):211–22. Available from: https://linkinghub.elsevier.com/retrieve/pii/S153561081400470X

75. Cramer SL, Saha A, Liu J, Tadi S, Tiziani S, Yan W, et al. Systemic depletion of L-cyst(e)ine with cyst(e)inase increases reactive oxygen species and suppresses tumor growth. Nat Med [Internet]. 2017 Jan 21;23(1):120–7. Available from: http://www.nature.com/articles/nm.4232

76. Lv H, Zhen C, Liu J, Yang P, Hu L, Shang P. Unraveling the Potential Role of Glutathione in Multiple Forms of Cell Death in Cancer Therapy. Oxid Med Cell Longev [Internet]. 2019 Jun 10;2019:1–16. Available from: https://www.hindawi.com/journals/omcl/2019/3150145/

77. Wang Z, Ding Y, Wang X, Lu S, Wang C, He C, et al. Pseudolaric acid B triggers ferroptosis in glioma cells via activation of Nox4 and inhibition of xCT. Cancer Lett [Internet]. 2018 Aug;428:21–33. Available from: https://linkinghub.elsevier.com/retrieve/pii/S030438351830288X

78. Lewerenz J, Hewett SJ, Huang Y, Lambros M, Gout PW, Kalivas PW, et al. The Cystine/Glutamate Antiporter System x c − in Health and Disease: From Molecular Mechanisms to Novel Therapeutic Opportunities. Antioxid Redox Signal [Internet]. 2013 Feb 10;18(5):522–55. Available from: http://www.liebertpub.com/doi/10.1089/ars.2011.4391

79. Moreira Franco YE, Alves MJ, Uno M, Moretti IF, Trombetta-Lima M, de Siqueira Santos S, et al. Glutaminolysis dynamics during astrocytoma progression correlates with tumor aggressiveness. Cancer Metab [Internet]. 2021 Dec 28;9(1):18. Available from: https://cancerandmetabolism.biomedcentral.com/articles/10.1186/s40170-021-00255-8

80. Matés JM, Segura JAA, Martín-Rufián M, Campos-Sandoval JAA, Alonso FJJ, Márquez J, et al. Glutaminase isoenzymes as key regulators in metabolic and oxidative stress against cancer. Curr Mol Med [Internet]. 2013 May 1;13(4):514–34. Available from: http://www.eurekaselect.com/openurl/content.php?genre=article&issn=1566-5240&volume=13&issue=4&spage=514

81. Katt WP, Lukey MJ, Cerione RA. A tale of two glutaminases: homologous enzymes with distinct roles in tumorigenesis. Future Med Chem [Internet]. 2017 Feb;9(2):223–43. Available from: https://www.future-science.com/doi/10.4155/fmc-2016-0190

82. Szeliga M, Obara-Michlewska M. Glutamine in neoplastic cells: Focus on the expression and roles of glutaminases. Neurochem Int. 2009;55(1–3):71–5.

83. Hu W, Zhang C, Wu R, Sun Y, Levine A, Feng Z. Glutaminase 2, a novel p53 target gene

regulating energy metabolism and antioxidant function. Proc Natl Acad Sci [Internet]. 2010 Apr 20;107(16):7455–60. Available from: http://www.pnas.org/cgi/doi/10.1073/pnas.1001006107

84. Szeliga M, Bogacińska-Karaś M, Rózycka A, Hilgier W, Marquez J, Albrecht J. Silencing of GLS and overexpression of GLS2 genes cooperate in decreasing the proliferation and viability of glioblastoma cells. Tumor Biol. 2014;35(3):1855–62.

85. PÉREZ-GÓMEZ C, CAMPOS-SANDOVAL JA, ALONSO FJ, SEGURA JA, MANZANARES E, RUIZ-SÁNCHEZ P, et al. Co-expression of glutaminase K and L isoenzymes in human tumour cells. Biochem J [Internet]. 2005 Mar 15;386(3):535–42. Available from: https://portlandpress.com/biochemj/article/386/3/535/78703/Co-expression-of-glutaminase-K-and-L-isoenzymes-in

86. Szeliga M, Sidoryk M, Matyja E, Kowalczyk P, Albrecht J. Lack of expression of the liver-type glutaminase (LGA) mRNA in human malignant gliomas. Neurosci Lett [Internet]. 2005 Feb;374(3):171–3. Available from: https://linkinghub.elsevier.com/retrieve/pii/S0304394004013357

87. Yu D, Shi X, Meng G, Chen J, Yan C, Jiang Y, et al. Kidney-type glutaminase (GLS1) is a biomarker for pathologic diagnosis and prognosis of hepatocellular carcinoma. Oncotarget [Internet]. 2015 Apr 10;6(10):7619–31. Available from: https://www.oncotarget.com/lookup/doi/10.18632/oncotarget.3196

88. Szeliga M, Matyja E, Obara M, Grajkowska W, Czernicki T, Albrecht J. Relative Expression of mRNAS Coding for Glutaminase Isoforms in CNS Tissues and CNS Tumors. Neurochem Res [Internet]. 2008 May 17;33(5):808–13. Available from: http://link.springer.com/10.1007/s11011-012-9356-0

89. TURNER A, McGIVAN JD. Glutaminase isoform expression in cell lines derived from human colorectal adenomas and carcinomas. Biochem J [Internet]. 2003 Mar 1;370(2):403–8. Available from: https://portlandpress.com/biochemj/article/370/2/403/40052/Glutaminase-isoform-expression-in-cell-lines

90. Potente M, Gerhardt H, Carmeliet P. Basic and Therapeutic Aspects of Angiogenesis. Cell [Internet]. 2011 Sep;146(6):873–87. Available from: http://linkinghub.elsevier.com/retrieve/pii/S0092867411010099

91. Rohlenova K, Veys K, Miranda-Santos I, De Bock K, Carmeliet P. Endothelial Cell Metabolism in Health and Disease. Trends Cell Biol [Internet]. 2018 Mar;28(3):224–36. Available from: https://linkinghub.elsevier.com/retrieve/pii/S0962892417302015

92. De Bock K, Georgiadou M, Schoors S, Kuchnio A, Wong BW, Cantelmo AR, et al. Role of PFKFB3-driven glycolysis in vessel sprouting. Cell. 2013;154(3):651–63.

93. Cantelmo AR, Pircher A, Kalucka J, Carmeliet P. Vessel pruning or healing: endothelial metabolism as a novel target? Expert Opin Ther Targets [Internet]. 2017;21(3):239–47. Available from: https://doi.org/10.1080/14728222.2017.1282465

94. Holash J, Maisonpierre PC, Compton D, Boland P, Alexander CR, Zagzag D, et al. Vessel Cooption, Regression, and Growth in Tumors Mediated by Angiopoietins and VEGF. Science (80-) [Internet]. 1999 Jun 18;284(5422):1994–8. Available from: https://www.science.org/doi/10.1126/science.284.5422.1994

95. Brem S. The Role of Vascular Proliferation in the Growth of Brain Tumors. Neurosurgery [Internet]. 1976 Jan;23(Supplement 1):440–53. Available from: https://journals.lww.com/00006123-197601001-00037

96. Du R, Lu K V., Petritsch C, Liu P, Ganss R, Passegué E, et al. HIF1α Induces the Recruitment of Bone Marrow-Derived Vascular Modulatory Cells to Regulate Tumor Angiogenesis and Invasion. Cancer Cell [Internet]. 2008 Mar;13(3):206–20. Available from: https://linkinghub.elsevier.com/retrieve/pii/S153561080800041X

97. Nico B, Crivellato E, Guidolin D, Annese T, Longo V, Finato N, et al. Intussusceptive microvascular growth in human glioma. Clin Exp Med [Internet]. 2010 Jun;10(2):93–8. Available from: http://link.springer.com/10.1007/s10238-009-0076-7

98. Hardee ME, Zagzag D. Mechanisms of Glioma-Associated Neovascularization. Am J Pathol [Internet]. 2012 Oct;181(4):1126–41. Available from: https://linkinghub.elsevier.com/retrieve/pii/S0002944012005081

99.   Wang R, Chadalavada K, Wilshire J, Kowalik U, Hovinga KE, Geber A, et al. Glioblastoma stem-like cells give rise to tumour endothelium. Nature [Internet]. 2010 Dec 21;468(7325):829–33. Available from: http://www.nature.com/articles/nature09624

100. Cheng L, Huang Z, Zhou W, Wu Q, Donnola S, Liu JK, et al. Glioblastoma Stem Cells Generate Vascular Pericytes to Support Vessel Function and Tumor Growth. Cell [Internet]. 2013 Mar;153(1):139–52. Available from: https://linkinghub.elsevier.com/retrieve/pii/S0092867413002109

101. Ricci-Vitiani L, Pallini R, Biffoni M, Todaro M, Invernici G, Cenci T, et al. Tumour vascularization via endothelial differentiation of glioblastoma stem-like cells. Nature [Internet]. 2010 Dec 9;468(7325):824–8. Available from: http://www.nature.com/articles/nature09557

102. Pérez-Escuredo J, Dadhich RK, Dhup S, Cacace A, Van Hée VF, De Saedeleer CJ, et al. Lactate promotes glutamine uptake and metabolism in oxidative cancer cells. Cell Cycle [Internet]. 2016 Jan 2;15(1):72–83. Available from: https://www.tandfonline.com/doi/full/10.1080/15384101.2015.1120930

103. Bao X, Zhang J, Huang G, Yan J, Xu C, Dou Z, et al. The crosstalk between HIFs and mitochondrial dysfunctions in cancer development. Cell Death Dis [Internet]. 2021 Feb 26;12(2):215. Available from: https://www.nature.com/articles/s41419-021-03505-1

104. Dasgupta A, Wu D, Tian L, Xiong PY, Dunham-Snary KJ, Chen K, et al. Mitochondria in the Pulmonary Vasculature in Health and Disease: Oxygen-Sensing, Metabolism, and Dynamics. In: Comprehensive Physiology [Internet]. Wiley; 2020. p. 713–65. Available from: https://onlinelibrary.wiley.com/doi/10.1002/cphy.c190027

105. Hayashi Y, Yokota A, Harada H, Huang G. Hypoxia/pseudohypoxia-mediated activation of hypoxia-inducible factor-1α in cancer. Cancer Sci [Internet]. 2019 May 23;110(5):1510–7. Available from: https://onlinelibrary.wiley.com/doi/10.1111/cas.13990

106. Brizel DM, Schroeder T, Scher RL, Walenta S, Clough RW, Dewhirst MW, et al. Elevated tumor lactate concentrations predict for an increased risk of metastases in head-and-neck cancer. Int J Radiat Oncol [Internet]. 2001 Oct;51(2):349–53. Available from:

https://linkinghub.elsevier.com/retrieve/pii/S0360301601016303

107. Walenta S, Salameh A, Lyng H, Evensen JF, Mitze M, Rofstad EK, et al. Correlation of high lactate levels in head and neck tumors with incidence of metastasis. Am J Pathol [Internet]. 1997 Feb;150(2):409–15. Available from: http://www.ncbi.nlm.nih.gov/pubmed/9033256

108. McFate T, Mohyeldin A, Lu H, Thakar J, Henriques J, Halim ND, et al. Pyruvate Dehydrogenase Complex Activity Controls Metabolic and Malignant Phenotype in Cancer Cells. J Biol Chem [Internet]. 2008 Aug;283(33):22700–8. Available from: https://linkinghub.elsevier.com/retrieve/pii/S0021925820748039

109. Hunt TK, Aslam RS, Beckert S, Wagner S, Ghani QP, Hussain MZ, et al. Aerobically Derived Lactate Stimulates Revascularization and Tissue Repair via Redox Mechanisms. Antioxid Redox Signal [Internet]. 2007 Aug;9(8):1115–24. Available from: http://www.liebertpub.com/doi/10.1089/ars.2007.1674

110. Goetze K. Lactate enhances motility of tumor cells and inhibits monocyte migration and cytokine release. Int J Oncol [Internet]. 2011 May 25; Available from: http://www.spandidos-publications.com/10.3892/ijo.2011.1055

111. Rafii S, Lyden D, Benezra R, Hattori K, Heissig B. Vascular and haematopoietic stem cells: novel targets for anti-angiogenesis therapy? Nat Rev Cancer [Internet]. 2002 Nov 1;2(11):826–35. Available from: https://www.nature.com/articles/nrc925

112. Niu G, Chen X. Vascular Endothelial Growth Factor as an Anti-Angiogenic Target for Cancer Therapy. Curr Drug Targets [Internet]. 2010 Aug 1;11(8):1000–17. Available from: http://www.eurekaselect.com/openurl/content.php?genre=article&issn=1389-4501&volume=11&issue=8&spage=1000

113. Kaplan RN, Riba RD, Zacharoulis S, Bramley AH, Vincent L, Costa C, et al. VEGFR1-positive haematopoietic bone marrow progenitors initiate the pre-metastatic niche. Nature [Internet]. 2005 Dec;438(7069):820–7. Available from: https://www.nature.com/articles/nature04186

114. Jain RK, di Tomaso E, Duda DG, Loeffler JS, Sorensen AG, Batchelor TT. Angiogenesis

in brain tumours. Nat Rev Neurosci [Internet]. 2007 Aug;8(8):610–22. Available from: https://www.nature.com/articles/nrn2175

115. Jain RK. Normalization of Tumor Vasculature: An Emerging Concept in Antiangiogenic Therapy. Science (80-) [Internet]. 2005 Jan 7;307(5706):58–62. Available from: https://www.science.org/doi/10.1126/science.1104819

116. Soda Y, Myskiw C, Rommel A, Verma IM. Mechanisms of neovascularization and resistance to anti-angiogenic therapies in glioblastoma multiforme. J Mol Med [Internet]. 2013 Apr 20;91(4):439–48. Available from: http://link.springer.com/10.1007/s00109-013-1019-z

117. Gilbert MR, Dignam JJ, Armstrong TS, Wefel JS, Blumenthal DT, Vogelbaum MA, et al. A Randomized Trial of Bevacizumab for Newly Diagnosed Glioblastoma. N Engl J Med [Internet]. 2014 Feb 20;370(8):699–708. Available from: http://www.nejm.org/doi/10.1056/NEJMoa1308573

118. Chinot OL, Wick W, Mason W, Henriksson R, Saran F, Nishikawa R, et al. Bevacizumab plus Radiotherapy–Temozolomide for Newly Diagnosed Glioblastoma. N Engl J Med [Internet]. 2014 Feb 20;370(8):709–22. Available from: http://www.nejm.org/doi/10.1056/NEJMoa1308345

119. Louis DN, Ohgaki H, Wiestler OD, Cavenee WK, Burger PC, Jouvet A, et al. The 2007 WHO classification of tumours of the central nervous system. Acta Neuropathol. 2007;114(2):97–109.

120. Valente V, Teixeira SA, Neder L, Okamoto OK, Oba-Shinjo SM, Marie SK, et al. Selection of suitable housekeeping genes for expression analysis in glioblastoma using quantitative RT-PCR. BMC Mol Biol [Internet]. 2009;10(1):17. Available from: http://bmcmolbiol.biomedcentral.com/articles/10.1186/1471-2199-10-17

121. Livak KJ, Schmittgen TD. Analysis of Relative Gene Expression Data Using Real-Time Quantitative PCR and the 2−ΔΔCT Method. Methods [Internet]. 2001 Dec;25(4):402–8. Available from: https://linkinghub.elsevier.com/retrieve/pii/S1046202301912629

122. Dobin A, Davis CA, Schlesinger F, Drenkow J, Zaleski C, Jha S, et al. Sequence analysis.

2013;29(1):15–21.

123. Li B, Dewey CN. RSEM : accurate transcript quantification from RNA-Seq data with or without a reference genome. 2011;

124. Ritchie ME, Phipson B, Wu D, Hu Y, Law CW, Shi W, et al. limma powers differential expression analyses for RNA-sequencing and microarray studies. 2015;43(7).

125. DeLuca DS, Levin JZ, Sivachenko A, Fennell T, Nazaire M-D, Williams C, et al. RNA-SeQC: RNA-seq metrics for quality control and process optimization. Bioinformatics [Internet]. 2012 Jun 1;28(11):1530–2. Available from: https://academic.oup.com/bioinformatics/article/28/11/1530/267467

126. Galatro TF, Sola P, Moretti IF, Miura FK, Oba-Shinjo SM, Marie SK, et al. Correlation between molecular features and genetic subtypes of Glioblastoma: critical analysis in 109 cases. Med Express [Internet]. 2017;4(5). Available from: http://www.gnresearch.org/doi/10.5935/MedicalExpress.2017.05.05

127. McBrayer SK, Mayers JR, DiNatale GJ, Shi DD, Khanal J, Chakraborty AA, et al. Transaminase Inhibition by 2-Hydroxyglutarate Impairs Glutamate Biosynthesis and Redox Homeostasis in Glioma. Cell [Internet]. 2018 Sep;175(1):101-116.e25. Available from: https://linkinghub.elsevier.com/retrieve/pii/S0092867418310997

128. Cassago A, Ferreira APS, Ferreira IM, Fornezari C, Gomes ERM, Greene KS, et al. Mitochondrial localization and structure-based phosphate activation mechanism of Glutaminase C with implications for cancer metabolism. Proc Natl Acad Sci [Internet]. 2012;109(4):1092–7. Available from: http://www.pnas.org/cgi/doi/10.1073/pnas.1112495109

129. Weis SM, Cheresh DA. Tumor angiogenesis: molecular pathways and therapeutic targets. Nat Med [Internet]. 2011 Nov 7;17(11):1359–70. Available from: http://www.nature.com/articles/nm.2537

130. Gene Ontology Data Archive [Internet]. Available from: https://zenodo.org/record/2529950#.YoW7zajMKUk

131. KEGG Pathway Database [Internet]. Available from: http://david.abcc.ncifcrf.gov

132. Li L, Liang Y, Kang L, Liu Y, Gao S, Chen S, et al. Transcriptional Regulation of the Warburg Effect in Cancer by SIX1. Cancer Cell [Internet]. 2018 Mar;33(3):368-385.e7. Available from: https://linkinghub.elsevier.com/retrieve/pii/S1535610818300102

133. Gao P, Tchernyshyov I, Chang T-C, Lee Y-S, Kita K, Ochi T, et al. c-Myc suppression of miR-23a/b enhances mitochondrial glutaminase expression and glutamine metabolism. Nature [Internet]. 2009 Apr 15;458(7239):762–5. Available from: http://www.nature.com/articles/nature07823

134. Curthoys NP. Regulation of Glutaminase Activity and Glutamine Metabolism. Annu Rev Nutr. 1995;15(1):133–59.

135. Ardlie KG, Deluca DS, Segre A V., Sullivan TJ, Young TR, Gelfand ET, et al. The Genotype-Tissue Expression (GTEx) pilot analysis: Multitissue gene regulation in humans. Science (80-) [Internet]. 2015 May 8;348(6235):648–60. Available from: https://www.sciencemag.org/lookup/doi/10.1126/science.1262110

136. Suzuki S, Tanaka T, Poyurovsky M V., Nagano H, Mayama T, Ohkubo S, et al. Phosphate-activated glutaminase (GLS2), a p53-inducible regulator of glutamine metabolism and reactive oxygen species. Proc Natl Acad Sci [Internet]. 2010 Apr 20;107(16):7461–6. Available from: http://www.pnas.org/cgi/doi/10.1073/pnas.1002459107

137. Szeliga M, Bogacińska-Karaś M, Kuźmicz K, Rola R, Albrecht J. Downregulation of GLS2 in glioblastoma cells is related to DNA hypermethylation but not to the p53 status. Mol Carcinog. 2016;55(9):1309–16.

138. Xiao D, Ren P, Su H, Yue M, Xiu R, Hu Y, et al. Myc promotes glutaminolysis in human neuroblastoma through direct activation of glutaminase 2. Oncotarget [Internet]. 2015 Dec 1;6(38). Available from: http://www.oncotarget.com/fulltext/5821

139. Wang J-B, Erickson JW, Fuji R, Ramachandran S, Gao P, Dinavahi R, et al. Targeting mitochondrial glutaminase activity inhibits oncogenic transformation. Cancer Cell [Internet]. 2010 Sep 14;18(3):207–19. Available from: http://www.ncbi.nlm.nih.gov/pubmed/20832749

140. Maus A, Peters GJ. Glutamate and α-ketoglutarate: key players in glioma metabolism.

Amino Acids [Internet]. 2017 Jan 17;49(1):21–32. Available from: http://link.springer.com/10.1007/s00726-016-2342-9

141. Forman HJ, Zhang H, Rinna A. Glutathione: Overview of its protective roles, measurement, and biosynthesis. Mol Aspects Med [Internet]. 2009 Feb;30(1–2):1–12. Available from: https://linkinghub.elsevier.com/retrieve/pii/S0098299708000617

142. Meister A. [1] Glutathione metabolism. In 1995. p. 3–7. Available from: https://linkinghub.elsevier.com/retrieve/pii/0076687995511067

143. Traverso N, Ricciarelli R, Nitti M, Marengo B, Furfaro AL, Pronzato MA, et al. Role of glutathione in cancer progression and chemoresistance. Oxid Med Cell Longev. 2013;2013.

144. Rocha CRR, Garcia CCM, Vieira DB, Quinet A, de Andrade-Lima LC, Munford V, et al. Glutathione depletion sensitizes cisplatin- and temozolomide-resistant glioma cells in vitro and in vivo. Cell Death Dis [Internet]. 2014 Oct 30;5(10):e1505–e1505. Available from: http://www.nature.com/articles/cddis2014465

145. Estrela JM, Ortega A, Obrador E. Glutathione in Cancer Biology and Therapy. Crit Rev Clin Lab Sci [Internet]. 2006 Jan 10;43(2):143–81. Available from: http://www.tandfonline.com/doi/full/10.1080/10408360500523878

146. Nguyen T-L, Durán R V. Glutamine metabolism in cancer therapy. Cancer Drug Resist [Internet]. 2018; Available from: http://cdrjournal.com/article/view/2787

147. Borodovsky A, Seltzer MJ, Riggins GJ. Altered cancer cell metabolism in gliomas with mutant IDH1 or IDH2. Curr Opin Oncol [Internet]. 2012 Jan;24(1):83–9. Available from: http://content.wkhealth.com/linkback/openurl?sid=WKPTLP:landingpage&an=00001622-201201000-00015

148. Garrett M, Sperry J, Braas D, Yan W, Le TM, Mottahedeh J, et al. Metabolic characterization of isocitrate dehydrogenase (IDH) mutant and IDH wildtype gliomaspheres uncovers cell type-specific vulnerabilities. Cancer Metab [Internet]. 2018 Dec 17;6(1):4. Available from: https://cancerandmetabolism.biomedcentral.com/articles/10.1186/s40170-018-0177-4

149. Peeters TH, Lenting K, Breukels V, van Lith SAM, van den Heuvel CNAM, Molenaar R,

et al. Isocitrate dehydrogenase 1-mutated cancers are sensitive to the green tea polyphenol epigallocatechin-3-gallate. Cancer Metab [Internet]. 2019 Dec 20;7(1):4. Available from: https://cancerandmetabolism.biomedcentral.com/articles/10.1186/s40170-019-0198-7

150. Ohka F, Ito M, Ranjit M, Senga T, Motomura A, Motomura K, et al. Quantitative metabolome analysis profiles activation of glutaminolysis in glioma with IDH1 mutation. Tumor Biol. 2014;35(6):5911–20.

151. van Lith SAM, Navis AC, Verrijp K, Niclou SP, Bjerkvig R, Wesseling P, et al. Glutamate as chemotactic fuel for diffuse glioma cells: Are they glutamate suckers? Biochim Biophys Acta - Rev Cancer [Internet]. 2014 Aug;1846(1):66–74. Available from: https://linkinghub.elsevier.com/retrieve/pii/S0304419X14000407

152. Albers MJ, Bok R, Chen AP, Cunningham CH, Zierhut ML, Zhang VY, et al. Hyperpolarized 13C Lactate, Pyruvate, and Alanine: Noninvasive Biomarkers for Prostate Cancer Detection and Grading. Cancer Res [Internet]. 2008 Oct 15;68(20):8607–15. Available from: http://cancerres.aacrjournals.org/cgi/doi/10.1158/0008-5472.CAN-08-0749

153. Brindle KM, Bohndiek SE, Gallagher FA, Kettunen MI. Tumor imaging using hyperpolarized 13C magnetic resonance spectroscopy. Magn Reson Med [Internet]. 2011 Aug;66(2):505–19. Available from: http://doi.wiley.com/10.1002/mrm.22999

154. Crisi G. 1 H MR Spectroscopy of Meningiomas at 3.0T: The Role of Glutamate-Glutamine Complex and Glutathione. Neuroradiol J [Internet]. 2011 Dec;24(6):846–53. Available from: http://journals.sagepub.com/doi/10.1177/197140091102400603

155. Hazany S, Hesselink JR, Healy JF, Imbesi SG. Utilization of glutamate/creatine ratios for proton spectroscopic diagnosis of meningiomas. Neuroradiology [Internet]. 2007 Feb 4;49(2):121–7. Available from: http://link.springer.com/10.1007/s00234-006-0167-z

156. Ascenção CFR, Nagampalli RSK, Islam Z, Pinheiro MP, Menezes dos Reis L, Pauletti BA, et al. N-terminal phosphorylation of glutaminase C decreases its enzymatic activity and cancer cell migration. Biochimie [Internet]. 2018 Nov;154:69–76. Available from: https://linkinghub.elsevier.com/retrieve/pii/S0300908418302177

157. Huang F, Zhang Q, Ma H, Lv Q, Zhang T. Expression of glutaminase is upregulated in colorectal cancer and of clinical significance. Int J Clin Exp Pathol [Internet]. 2014;7(3):1093–100. Available from: http://www.ncbi.nlm.nih.gov/pubmed/24696726

158. Robinson MM, McBryant SJ, Tsukamoto T, Rojas C, Ferraris D V, Hamilton SK, et al. Novel mechanism of inhibition of rat kidney-type glutaminase by bis-2-(5-phenylacetamido-1,2,4-thiadiazol-2-yl)ethyl sulfide (BPTES). Biochem J [Internet]. 2007 Sep 15;406(3):407–14. Available from: http://www.ncbi.nlm.nih.gov/pubmed/17581113

159. Gross MI, Demo SD, Dennison JB, Chen L, Chernov-Rogan T, Goyal B, et al. Antitumor Activity of the Glutaminase Inhibitor CB-839 in Triple-Negative Breast Cancer. Mol Cancer Ther [Internet]. 2014 Apr;13(4):890–901. Available from: http://mct.aacrjournals.org/lookup/doi/10.1158/1535-7163.MCT-13-0870

160. Norden AD, Drappatz J, Wen PY. Antiangiogenic therapies for high-grade glioma. Nat Rev Neurol [Internet]. 2009 Nov 13;5(11):610–20. Available from: http://www.nature.com/articles/nrneurol.2009.159

161. Ling C, Pouget C, Rech F, Pflaum R, Treffel M, Bielle F, et al. Endothelial Cell Hypertrophy and Microvascular Proliferation in Meningiomas Are Correlated with Higher Histological Grade and Shorter Progression-Free Survival. J Neuropathol Exp Neurol [Internet]. 2016 Dec;75(12):1160–70. Available from: https://academic.oup.com/jnen/article-lookup/doi/10.1093/jnen/nlw095

162. Rascher G, Fischmann A, Kröger S, Duffner F, Grote E-H, Wolburg H. Extracellular matrix and the blood-brain barrier in glioblastoma multiforme: spatial segregation of tenascin and agrin. Acta Neuropathol [Internet]. 2002 Jul 28;104(1):85–91. Available from: http://link.springer.com/10.1007/s00401-002-0524-x

163. Novak U, Kaye AH. Extracellular matrix and the brain: components and function. J Clin Neurosci [Internet]. 2000 Jul;7(4):280–90. Available from: https://linkinghub.elsevier.com/retrieve/pii/S0967586899902126

164. Hambardzumyan D, Bergers G. Glioblastoma: Defining Tumor Niches. Trends in Cancer [Internet]. 2015 Dec;1(4):252–65. Available from:

https://linkinghub.elsevier.com/retrieve/pii/S2405803315000564

165. Tatla AS, Justin AW, Watts C, Markaki AE. A vascularized tumoroid model for human glioblastoma angiogenesis. Sci Rep [Internet]. 2021 Oct 1;11(1):19550. Available from: https://www.nature.com/articles/s41598-021-98911-y

166. Eelen G, de Zeeuw P, Treps L, Harjes U, Wong BW, Carmeliet P. Endothelial Cell Metabolism. Physiol Rev [Internet]. 2018 Jan 1;98(1):3–58. Available from: http://physrev.physiology.org/lookup/doi/10.1152/physrev.00001.2017

167. Hashimoto T, Shibasaki F. Hypoxia-Inducible Factor as an Angiogenic Master Switch. Front Pediatr [Internet]. 2015 Apr 24;3. Available from: http://journal.frontiersin.org/article/10.3389/fped.2015.00033/abstract

168. Semenza GL. Evaluation of HIF-1 inhibitors as anticancer agents. Drug Discov Today [Internet]. 2007 Oct;12(19–20):853–9. Available from: https://linkinghub.elsevier.com/retrieve/pii/S1359644607003248

169. Semenza GL. Defining the role of hypoxia-inducible factor 1 in cancer biology and therapeutics. Oncogene [Internet]. 2010 Feb 4;29(5):625–34. Available from: https://www.nature.com/articles/onc2009441

170. Missiaen R, Morales-Rodriguez F, Eelen G, Carmeliet P. Targeting endothelial metabolism for anti-angiogenesis therapy: A pharmacological perspective. Vascul Pharmacol [Internet]. 2017;90:8–18. Available from: http://dx.doi.org/10.1016/j.vph.2017.01.001

171. Agnihotri S, Zadeh G. Metabolic reprogramming in glioblastoma: the influence of cancer metabolism on epigenetics and unanswered questions. Neuro Oncol [Internet]. 2016 Feb;18(2):160–72. Available from: https://academic.oup.com/neuro-oncology/article-lookup/doi/10.1093/neuonc/nov125

172. Lunt SY, Vander Heiden MG. Aerobic Glycolysis: Meeting the Metabolic Requirements of Cell Proliferation. Annu Rev Cell Dev Biol [Internet]. 2011 Nov 10;27(1):441–64. Available from: http://www.annualreviews.org/doi/10.1146/annurev-cellbio-092910-154237

173. Yamasaki F, Kurisu K, Kajiwara Y, Watanabe Y, Takayasu T, Akiyama Y, et al. Magnetic

resonance spectroscopic detection of lactate is predictive of a poor prognosis in patients with diffuse intrinsic pontine glioma. Neuro Oncol [Internet]. 2011 Jul 1;13(7):791–801. Available from: https://academic.oup.com/neuro-oncology/article-lookup/doi/10.1093/neuonc/nor038

174. Goodwin ML, Gladden LB, Nijsten MWN, Jones KB. Lactate and Cancer: Revisiting the Warburg Effect in an Era of Lactate Shuttling. Front Nutr [Internet]. 2015 Jan 5;1. Available from: http://journal.frontiersin.org/article/10.3389/fnut.2014.00027/abstract

175. Lu H, Forbes RA, Verma A. Hypoxia-inducible Factor 1 Activation by Aerobic Glycolysis Implicates the Warburg Effect in Carcinogenesis. J Biol Chem [Internet]. 2002 Jun;277(26):23111–5. Available from: https://linkinghub.elsevier.com/retrieve/pii/S0021925819666767

176. De Saedeleer CJ, Copetti T, Porporato PE, Verrax J, Feron O, Sonveaux P. Lactate Activates HIF-1 in Oxidative but Not in Warburg-Phenotype Human Tumor Cells. Bai Y, editor. PLoS One [Internet]. 2012 Oct 17;7(10):e46571. Available from: https://dx.plos.org/10.1371/journal.pone.0046571

177. Bonuccelli G, Tsirigos A, Whitaker-Menezes D, Pavlides S, Pestell RG, Chiavarina B, et al. Ketones and lactate "fuel" tumor growth and metastasis. Cell Cycle [Internet]. 2010 Sep 5;9(17):3506–14. Available from: http://www.tandfonline.com/doi/abs/10.4161/cc.9.17.12731

178. Sonveaux P, Végran F, Schroeder T, Wergin MC, Verrax J, Rabbani ZN, et al. Targeting lactate-fueled respiration selectively kills hypoxic tumor cells in mice. J Clin Invest [Internet]. 2008 Nov 20; Available from: http://www.jci.org/articles/view/36843

7. Appendix

PARECER CONSUBSTANCIADO DO CEP

DADOS DA EMENDA

Título da Pesquisa: ESTUDO DO MECANISMO DE AÇÃO DO SILENCIAMENTO DO GENE GLS ISO 2 (GAC)

Pesquisador: Suely Kazue Nagahashi Marie

Área Temática: Genética Humana:
(Trata-se de pesquisa envolvendo Genética Humana que não necessita de análise ética por parte da CONEP;);

Versão: 4

CAAE: 90324718.0.0000.0065

Instituição Proponente: Faculdade de Medicina da Universidade de São Paulo

Patrocinador Principal: FUNDACAO DE AMPARO A PESQUISA DO ESTADO DE SAO PAULO

DADOS DO PARECER

Número do Parecer: 3.687.639

Apresentação do Projeto:

Este projeto visa a caracterização do mecanismo de ação induzido pelo silenciamento da GLS isoforma 2, nas linhagens tumorais de glioblastoma (U87MG e A172) afim de elucidar melhor esta via e consequentemente buscar uma alternativa terapêutica para pacientes acometidos com astrocitomas de alto grau. O estudo já esta aprovado por este CEP e os investigadores enviam solicitação para inclusão de um centro no exterior para o desenvolvimento de parte do projeto. Incluiu-se carta de aceite do orientador externo e carta de solicitação ao CEP. Não haverá alteração do projeto nem envio de amostras humanas/animais.

Objetivo da Pesquisa:

Solicitamos a inclusão de um centro no exterior para o desenvolvimento de parte do projeto. Incluiu-se carta de aceite do orientador externo e carta de solicitação ao CEP. Não haverá alteração do projeto nem envio de amostras humanas/animais.

Avaliação dos Riscos e Benefícios:

não se aplica

Continuação do Parecer: 3.687.639

Comentários e Considerações sobre a Pesquisa:

Anexado carta de aceite do orientador externo e carta de solicitação ao CEP.

Há informação de que não haverá alteração do projeto nem envio de amostras humanas/animais.

Considerações sobre os Termos de apresentação obrigatória:

Anexado carta de aceite do orientador externo e carta de solicitação ao CEP.

Há informação de que não haverá alteração do projeto nem envio de amostras humanas/animais.

Recomendações:

sem recomendações

Conclusões ou Pendências e Lista de Inadequações:

aprovado

Considerações Finais a critério do CEP:

Este parecer foi elaborado baseado nos documentos abaixo relacionados:

Tipo Documento	Arquivo	Postagem	Autor	Situação
Informações Básicas do Projeto	PB_INFORMAÇÕES_BÁSICAS_1461161_E1.pdf	30/10/2019 14:38:07		Aceito
Outros	InclusaoDeInstituicaoInternacional.PDF	30/10/2019 14:35:59	Suely Kazue Nagahashi Marie	Aceito
Outros	YollandaMoreiraAcceptanceLetterfromChanlaboratorySeptember2019TimothyChan.pdf	29/10/2019 12:09:57	Suely Kazue Nagahashi Marie	Aceito
Parecer Anterior	PARECERCIBIO.PDF	03/08/2018 14:07:56	Suely Kazue Nagahashi Marie	Aceito
Cronograma	CRONOGRAMADOPROJETO.pdf	25/07/2018 13:48:01	Suely Kazue Nagahashi Marie	Aceito
Projeto Detalhado / Brochura Investigador	PROJETODOUTORADO1.pdf	25/07/2018 13:47:10	Suely Kazue Nagahashi Marie	Aceito
Folha de Rosto	suelymarieyollandafr0001.pdf	21/05/2018 15:25:13	Suely Kazue Nagahashi Marie	Aceito
Outros	suelymarieyollandacep0001.pdf	21/05/2018 15:24:23	Suely Kazue Nagahashi Marie	Aceito

Situação do Parecer:

Aprovado

Necessita Apreciação da CONEP:

USP - FACULDADE DE MEDICINA DA UNIVERSIDADE DE SÃO PAULO - FMUSP

Não

SAO PAULO, 06 de Novembro de 2019

_____

Assinado por:
Maria Aparecida Azevedo Koike Folgueira
(Coordenador(a))

Cancer & Metabolism

Glutaminolysis dynamics during astrocytoma progression correlates with tumor aggressiveness

Yollanda E. Moreira Franco[1*†], Maria Jose Alves[1†], Miyuki Uno[1], Isabele Fattori Moretti[1], Marina Trombetta-Lima[1,2], Suzana de Siqueira Santos[3], Ancely Ferreira dos Santos[4], Gabriel Santos Arini[4], Mauricio S. Baptista[4], Antonio Marcondes Lerario[5], Sueli Mieko Oba-Shinjo[1] and Suely Kazue Nagahashi Marie[1]

Abstract

Background: Glioblastoma is the most frequent and high-grade adult malignant central nervous system tumor. The prognosis is still poor despite the use of combined therapy involving maximal surgical resection, radiotherapy, and chemotherapy. Metabolic reprogramming currently is recognized as one of the hallmarks of cancer. Glutamine metabolism through glutaminolysis has been associated with tumor cell maintenance and survival, and with antioxidative stress through glutathione (GSH) synthesis.

Methods: In the present study, we analyzed the glutaminolysis-related gene expression levels in our cohort of 153 astrocytomas of different malignant grades and 22 non-neoplastic brain samples through qRT-PCR. Additionally, we investigated the protein expression profile of the key regulator of glutaminolysis (GLS), glutamate dehydrogenase (GLUD1), and glutamate pyruvate transaminase (GPT2) in these samples. We also investigated the glutathione synthase (GS) protein profile and the GSH levels in different grades of astrocytomas. The differential gene expressions were validated in silico on the TCGA database.

Results: We found an increase of glutaminase isoform 2 gene (*GLSiso2*) expression in all grades of astrocytoma compared to non-neoplastic brain tissue, with a gradual expression increment in parallel to malignancy. Genes coding for *GLUD1* and *GPT2* expression levels varied according to the grade of malignancy, being downregulated in glioblastoma, and upregulated in lower grades of astrocytoma (AGII–AGIII). Significant low GLUD1 and GPT2 protein levels were observed in the mesenchymal subtype of GBM.

(Continued on next page)

* Correspondence: yollanda.moreiraf@usp.br
†Yollanda E. Moreira Franco and Maria Jose Alves contributed equally to this work.
[1]Laboratory of Molecular and Cellular Biology (LIM 15), Department of Neurology, Faculdade de Medicina FMUSP, Universidade de São Paulo, São Paulo 01246–903, Brazil
Full list of author information is available at the end of the article

(Continued from previous page)

Conclusions: In glioblastoma, particularly in the mesenchymal subtype, the downregulation of both genes and proteins (GLUD1 and GPT2) increases the source of glutamate for GSH synthesis and enhances tumor cell fitness due to increased antioxidative capacity. In contrast, in lower-grade astrocytoma, mainly in those harboring the *IDH1* mutation, the gene expression profile indicates that tumor cells might be sensitized to oxidative stress due to reduced GSH synthesis. The measurement of *GLUD1* and *GPT2* metabolic substrates, ammonia, and alanine, by noninvasive MR spectroscopy, may potentially allow the identification of *IDH1*[mut] AGII and AGIII progression towards secondary GBM.

Keywords: Glutaminolysis, GBM, Low-grade astrocytoma, IDH1 mutation, Astrocytoma progression

Background

Cancer is among the leading causes of death worldwide [1]. Although the tumors of the central nervous system (CNS) are less frequent, representing about 3% of all tumors, they are among the most aggressive [2, 3]. Gliomas, which originate from glial cells or their precursors, represent more than 80% of primary brain tumors [4–6]. Glioblastoma (GBM), the most frequent adult malignant glioma and classified as a WHO grade IV astrocytoma, has been stratified according to the molecular profile as proneural, classical, and mesenchymal subtypes [7, 8], which partially predict the clinical outcome. The proneural subtype characterized by the presence of *IDH* mutation has been associated with a better prognosis [9], while the mesenchymal subtype with *NF1* or *RB1* mutations has presented the worst outcome, with an average overall survival of 8–11 months [10]. More recently, an impact of the mutational landscape on the response to immunotherapy and on the acquired resistance to temozolomide (TMZ) has been demonstrated in gliomas [11].

The capacity of cancer cells to reprogram their metabolisms to support rapid proliferation is another cancer hallmark with prognostic impact [12, 13]. Interestingly, metabolic enzymes with high catalytic activity are found upregulated in different kinds of tumor and are associated with poor survival [14]. Glutamine (Gln) metabolism is upregulated by various oncogenic signaling pathways [15] and is relevant in cancer development due to its involvement in mTOR signaling, autophagy, and antioxidative stress and as a source of glutathione (GSH) and for anaplerosis [12, 13, 16]. Moreover, Gln uptake and the rate of glutaminolysis are known to be related to tumor growth [17–19]. Besides, we previously have observed that Gln transporters are upregulated in astrocytoma [20]. The dependence of cancer cells on Gln makes glutaminolysis an attractive cancer therapy target [15, 21–23]. Gln is a non-essential amino acid, consumed largely by proliferating cancer cells in vitro, which are often dependent on extracellular Gln for survival [24]. Gln carbon contributes to aspartate, glutamate (Glu), and tricarboxylic acid (TCA) cycle metabolites via glutaminolysis [15]. High rates of glutaminolysis support

rapid proliferation by supplying precursors to low-flux biosynthetic pathways [24]. Current attempts to target glutaminolysis clinically have focused largely on inhibiting glutaminase. Chemical inhibitors have been found to decrease cancer cell proliferation in both in vitro/in vivo models [25–27].

The metabolic ending of glutamine–derived Glu is, apart from α–ketoglutarate (α–KG), lactate and GSH being an important nitrogen donor for cell growth and proliferation [28, 29]. Additionally, studies about *IDH* mutation showed significantly reduced levels of Gln and Glu levels were, which implies replenishment of α–KG by glutaminolysis. Consequently, wild-type (wt) gliomas presented high levels of intracellular Glu, which is released via the Gln/cysteine antiporter System X_C^- in exchange for cysteine. GSH is considered a potent antioxidant and the main factor responsible for treatment resistance in gliomas or other neoplastic cells [30, 31]. Therapeutic attempts have been aimed at GSH depletion by inhibiting the X_C^- transporter [32], which is responsible for counter–transport of Glu and cysteine– a substrate–limiting GSH synthesis [30, 31]. This exchange is favorable for the cancer cells because Cys is a major component of the antioxidant GSH, which in turn is an antagonist of reactive oxygen species (ROS) [28].

In the present study, we analyzed the expression profile of the genes related to glutaminolysis in different grades of astrocytomas and, more specifically, in the molecular subtypes of GBM, and lower malignant grades of astrocytoma regarding *IDH1* mutation status. We searched for differential features of glutaminolysis related to GBM aggressiveness and malignant progression of low-grade astrocytomas with *IDH1* mutation, which may help to better characterize the metabolic features associated with GBM aggressiveness and to tumor malignant progression.

Methods

Tissue sample and ethical statement

Samples were snap-frozen in liquid nitrogen immediately following surgical removal and macro dissected before RNA extraction. A 4-μm-thick cryosection of each sample was stained with hematoxylin-eosin and analyzed

under a light microscope for assessment of necrotic, cellular debris, and NN areas (in tumoral samples). For gene expression, we analyzed 153 human astrocytoma samples stratified according to the WHO classification (2007) [33] as 23 astrocytomas grade I (AGI), 26 astrocytomas grade II (AGII), 18 astrocytomas grade III (AGIII), and 86 GBM. Non-neoplastic brain samples (NN) were used as control (22 cases). For the GLS protein analysis, NN (5), AGI (4), AGII (4), AGIII (2), and GBM (6) were evaluated. For GLUD1 and GPT2 protein analysis, we explored AGII-*IDH*^{wt} (4), AGII-*IDH*^{mut} (6), GBM of mesenchymal subtype (GBM-MS) (7), and GBM of proneural subtype (GBM-PN) (5) samples. For glutathione synthetase (GS) protein analysis, we explored AGII-*IDH*^{wt} (4), AGII-*IDH*^{mut} (4), GBM-MS (4), and GBM-PN (4). Tumor samples were obtained from surgery of patients treated by the Neurosurgery Group of Department of Neurology at Hospital das Clinicas at the School of Medicine of University of São Paulo, from 2000 to 2007. NN brain tissue samples were collected from epilepsy patients subjected to temporal lobectomy.

Cell culture
The U87MG cell line was acquired from ATCC and authenticated by short tandem repeats (STR) analysis using GenePrint 10 System (Promega, Madison, WI). Cells were cultured in monolayer with DMEM medium (Dulbecco's modified Eagle's medium, Thermo Fisher Scientific, Carlsbad, CA), 10% fetal bovine serum, and 100 μg/ml streptomycin and 100 IU/ml penicillin.

RNA extraction and cDNA synthesis
Total RNA was extracted from frozen tissues (tumor and NN) using the RNeasy Mini Kit (Qiagen, Hilden, Germany) following the manufacturer's instructions. The RNA concentration and purity were evaluated by NanoDrop, and ratios of 260/280 measures ranging from 1.8 to 2.0 were considered satisfactory for purity standards. RNA quality was checked by electrophoresis in agarose gel. A conventional reverse transcription reaction was performed to yield single-stranded cDNA. The first strand of cDNA was synthesized from 1 μg of total RNA previously treated with 1 unit of DNase I (FPLC–pure, GE Healthcare, Uppsala, Sweden) using random and oligo (dT) primers, RNase inhibitor, and SuperScript III reverse transcriptase according to the manufacturer's recommendations (Thermo Fisher Scientific). The resulting cDNA was subsequently treated with 1 unit of RNase H (GE Healthcare), diluted with TE buffer, and stored at − 20 °C until later use.

Analysis of gene expression by quantitative real-time PCR (qRT–PCR)
The relative expression levels of genes involved in the glutaminolysis pathway *GLS, GLSiso1, GLSiso2, GLS2,* *GLUD1, GOT1, GOT2,* and *GPT2* were analyzed by qRT–PCR, using the SYBR Green approach. The expression of *ASCT2* and *LAT1* genes were previously described by our group [20]. A geometric mean of three suitable reference genes was used for normalizing the quantitative data: hypoxanthine phosphoribosyltransferase (*HPRT*), glucuronidase beta (*GUSβ*), and TATA box binding protein (*TBP*) [34]. The primers were designed to amplify 80–120 bp amplicons, with a melting temperature of 60 °C and were synthesized by IDT (Integrated DNA Technologies, Coralville, IA). The primers information is described in Table 1.

To ensure the efficiency of amplification and analysis of melting curves, which gave a single peak for all PCR products, standard curves with varying concentrations of the primer pairs of each gene were performed. The optimal primer concentration was determined as the lower concentration which did not affect the cycle threshold (Ct) and displayed the maximum amplification efficiency while minimizing non-specific amplification. Additionally, the amplified PCR product sizes were checked by agarose gel electrophoresis. The SYBR Green I amplification mixtures (12 μl) were composed of cDNA, Power SYBR Green I Master Mix (Thermo Fisher Scientific), and the reverse and forward primers. The qRT–PCR was done in duplicate using the ABI Prism 7500 (Thermo Fisher Scientific) as follows: 2 min at 50 °C, 10 min of polymerase activation at 95 °C, and 40 cycles of 15 s at 95 °C and 1 min at 60 °C. The following equation was applied to calculate gene expression in tumor and NN tissue samples: $2^{-\Delta Ct}$, where ΔCt = Ct of a specific gene–geometric mean Ct of housekeeping genes [35].

Analysis of protein expression by western blotting
The samples and U87MG cells were homogenized with RIPA lysis buffer (50 mM Tris–HCl, 1% NP–40, 0.25% Na deoxycholate, 150 mM NaCl, 1 mM EDTA) supplemented with a cocktail of protease inhibitors (Sigma–Aldrich, St Louis, MO). The protein concentration was determined using the Bradford reagent. All samples (20 μg protein) were resolved by electrophoresis on 4–12% gradient gels in SDS–PAGE using electrophorese buffer NuPAGE MOPS SDS (Thermo Fisher Scientific) and transferred onto PVDF membrane by iBlot Dry Blotting System (Thermo Fisher Scientific). Then the remaining binding sites of the membranes were blocked with skimmed milk powder solution at 5% diluted in Tris-buffered saline and 0.1%Tween 20 (TBST). Subsequently, the membranes were incubated overnight with the primary antibody, anti–GLS (1:1,000), anti-GS (1:2,000) from Abcam (Cambridge, MA), and anti-GLUD1, anti-GPT2 (1:1,000) from Thermo Fisher and then diluted in TBST with 5% bovine serum albumin (BSA) solution. β–

Table 1 The primer sequences and the concentration used in qRT–PCR

Genes	Forward primer (5′–3′)	Reverse Primer (5′–3′)	Concentration (nM)
GLS	CAGGGCAGTTTGCTTTCCAT	GAGACCAGCACATCATACCCAT	200
GLSiso1	GCAGAGGGTCATGTTGAAGTTGT	GGTGTCCAAAGTGCAGTGCTT	200
GLSiso2	ATCCTCGAAGAGAAGGTGGTGA	GCAAGTTCTTGTTGGAGACTTTCA	400
GLS2	ATCCTCGAAGAGAAGGTGGTGA	ATGGCTGACAAGGCAAACCT	200
GLUD1	TGGCATACACAATGGAGCGT	TCTCAATGGCATTAACATAGGCA	400
GOT1	CTGTGCCCAGTCCTTCTCCA	GATGCTCTCAGGTTCTTTTCCAA	400
GOT2	CTTGAGGTTGGAGACCAGTTGAGT	GATTGCTGCTGCCATTCTGA	400
GPT2	GGCTTTGGGCAGAGGGAA	TCACGCGTACTTCTCCAGGAA	200
HPRT	TGAGGATTTGGAAAGGGTGT	GAGCACACAGAGGGCTACAA	200
GUSβ	AAATACGTGGTTGGAGAGCTCATT	CCGAGTGAAGATCCCCTTTTTA	400
TBP	AGGATAAGAGAGCCACGAACCA	CTTGCTGCCAGTCTGGACTGT	200

actin (1:5.000) (Sigma–Aldrich) was used as a loading control. The membranes were incubated with peroxidase-conjugated secondary antibody anti-rabbit and anti-mouse (1:5.000) (Sigma–Aldrich), also diluted in TBST 5% BSA. The protein levels were detected using the chemiluminescence detection method (Western Lightning Plus–ECL, Enhanced Chemiluminescence Substrate, Perkin Elmer, Waltham, MA). The detection of the chemiluminescent signal was performed in the Photo QuantLAS 4000 mini (GE Healthcare) photo documentation system and the bands were analyzed and quantified using ImageJ software (obtained from imagej.nih.gov/ij/download/).

GSH measurement

Tissue samples were resuspended in PSB–0.5% NP40 (pH 6) and homogenized in syringes with an insulin needle 10 times. An aliquot of each sample was separated for protein quantification. Eighty microliters were processed with 250 μL of cold GSH extraction buffer ($KClO_4$ 50 mM; EDTA 10 mM; H_3PO_4 0.1% (v/v), pH 5) and 40 μL of cold metaphosphoric acid 5% (v/v). The samples were vortexed for 1 min and centrifuged at 8000×g (10 min, 4 °C). The supernatants were used as 1:10 dilutions. GSH was measured using a fluorometric detection assay kit (ab138881, Abcam) assay according to the manufacturer's instructions. This assay is based on the fluorescent properties of thiol green, which is a non-fluorescent dye that becomes strongly fluorescent upon reacting directly with GSH. The fluorescence intensity was evaluated at an excitation wavelength of 490 nm and an emission wavelength of 520 nm using a 96-well plate in a spectrofluorometer (SpectraMAX M2, Molecular Devices, Sunnyvale, CA). GSH concentration was calculated by interpolation of a standard curve and results were expressed as pmol/μg of total protein.

TCGA data analysis

The gene expression from the RNAseq GBM dataset was downloaded (Genomics Data Commons Data Portal—https://portal.gdc.cancer.gov/) and normalized by DEseq R software. Normalized read counts were converted to a z-score for heat map visualization.

Statistical analysis

Statistical analysis was conducted with SPSS for Windows, version 20.0 (IBM Corporation, Armonk, NY), and GraphPad Prism (version 5.02, San Diego, CA). Comparisons were considered statistically significant when $p < 0.05$. The non-parametric Kruskal-Wallis and post hoc Dunn tests were used to analyze the differences in mRNA relative expression in different grades of astrocytomas. The correlation analysis between gene expression values was assessed by the non-parametric Spearman-rho correlation test. The variation of specificity and sensibility of gene expression levels was analyzed using the receiver operating characteristic (ROC) curve. Among the continuous variables categorized through the ROC curve, the value with the best sensitivity and specificity was chosen as the cut-off value. The area under the ROC curve (AUC) was used to measure how the expression levels could distinguish between two groups. The gene expressions were classified as hyper or hypoexpressed based on this cut-off value. The comparison of protein expression analysis was carried by two-way ANOVA and Bonferroni post-test.

Results

GAC (GLSiso2) expression increases in parallel to astrocytoma malignancy

Once Gln is transported into cells by ASCT2 (SLC1A5) and LAT1 (SLC7A5), it is converted to Glu by glutaminases (GLS and GLS2). This is a critical step, as Glu does not efficiently cross the blood-brain barrier, and brain

interstitial Glu concentration is maintained essentially through its synthesis [36–38]. *GLS* presents two isoforms: *KGA* (*GLSiso1,* cytosolic) and *GAC* (*GLSiso2,* mitochondrial). The *GLS*iso2 is derived from an alternative exon splicing at the 3′–end terminal, excluding the ankyrin repeats at the C–terminus coded by the last four exons of the *GLSiso1* transcript. Thus, the *GLSiso2* is shorter than the *GLSiso1*, with a distinct C–terminal [39]. Expression analysis of transcript coding for the key enzymes involved in glutaminolysis, *GLSiso1*, *GLSiso2*, *GLS2*, *GLUD1*, *GOT1*, *GOT2*, and *GPT2* was performed in our series of astrocytomas of different malignant grades and NN brain samples. Interestingly, although no significant differential expression of the total *GLS* transcripts was observed among different grades of astrocytoma compared to NN, a significant *GLSiso2* (*GAC*) hyperexpression was observed in all grades of astrocytoma when compared to NN ($p < 0.0001$ Kruskal–Wallis test, and $p < 0.001$ Dunn test), with the highest expression levels detected in a set of GBM samples (Fig. 1a). Of note, *GLSiso2* expression increased in parallel to the grade of malignancy ($p < 0.0001$ AGII vs. AGIII, $p < 0.05$ AGII vs. GBM, $p < 0.05$ AGIII vs. GBM; Dunn test) which reflected an increase of its correlation with the gene expression levels of the glutaminolysis pathway from NN to GBM (Fig. 1a). When gene expression level correlations were analyzed, *GLSiso2* expression correlated weakly only with *GPT2* expression in NN, while no correlation was detected in AGI. *GLSiso2* correlated negatively with *GLS2*, *GOT1*, and *GOT2* in AGII and positively with *GLS2* and *GLSiso1* in AGIII, whereas *GLSiso2* correlated positively with all genes of the glutaminolysis pathway in GBM (Fig. 1b). All statistically significant values are demonstrated in Supplemental Table 1. Additionally, as shown in Fig. 2, the *GLSiso2* expression levels presented high discriminatory power to distinguish between GBM and NN samples by ROC curve analysis (AUC = 0.919; 95% CI, 0.867–0.971) and between GBM and AGII, although with lower discriminatory power (AUC = 0.675; 95% CI, 0.569–0.781).

In contrast, *GLSiso1 mRNA* expression was significantly lower in AGI, AGII, and GBM compared to NN ($p < 0.0001$ Kruskal–Wallis test, and $p < 0.05$ Dunn´s test) (Fig. 1a), with discriminatory power to distinguish between GBM and NN (AUC = 0.796; 95% CI, 0.1–0.308). No significant difference in its expression was detected in a pairwise comparison among different grades of astrocytoma. However, we observed a strong positive correlation between *GLSiso1* and *GLS2* in AGII and with *GLSiso2* in AGIII, as well as with *GLSiso2*, *GLUD1*, *GOT1*, *GOT2,* and *GPT2* in GBM cases. Similarly, *GLS2* hypoexpression was observed in astrocytoma of all malignant grades compared to NN ($p < 0.0001$ Kruskal-Wallis test, and $p < 0.00001$ for all astrocytoma grades

and NN Dunn test), and its expression level presented the power to distinguish between GBM and NN (AUC = 0.791; 95% CI, 0.000–0.06) and to distinguish between GBM and AGII, but with lower discriminatory power (AUC = 0.65; 95% CI, 0.221–0.48).

GLS isoforms expression was also investigated at the protein level, and we confirmed a differential expression of GLSiso1 and GLSiso2 in NN and astrocytomas of different malignant grades (Fig. 3). Whereas GLSiso1 was present in all NN and diffusely infiltrative astrocytoma (grade II to IV) samples, with higher abundance in NN samples in comparison to GBM samples ($p < 0.001$ ANOVA two–way, with Bonferroni post-test). In contrast, GLSiso2 was mostly detected in GBM cases and only slightly detected in NN samples. GLS isoforms were detected in the U87MG cell line—a GBM mesenchymal subtype cell line (Fig. 3).

GPT2 downregulation in the GBM mesenchymal subtype correlated to upregulation of genes involved in GSH synthesis

Once Glu is synthesized it can be converted to α–KG, an intermediate of the TCA cycle, by glutamate dehydrogenase (GLUD1) and glutamate transaminases, as glutamate oxaloacetate transaminases (GOT1–cytosolic and GOT2–mitochondrial) and glutamate pyruvate transaminases (GPT1–cytosolic and GPT2–mitochondrial), which transfer amino groups from oxaloacetate or from pyruvate to generate α–KG and aspartate or alanine, respectively [17]. The expression levels of *GLUD1*, *GOT1*, *GOT2*, and *GPT2* were differentially expressed in astrocytomas compared to NN ($p < 0.0001$ Kruskal–Wallis test for *GLUD1*, *GOT1*, and *GPT2* and $p < 0.002$ for *GOT2*) (Fig. 1a). Interestingly, *GLUD1* expression was significantly decreased in GBM compared to AGII ($p < 0.005$ Dunn test), and its expression level presented discriminatory power to distinguish between GBM and NN (ROC AUC = 0.770; 95% CI, 0.128–0.332) and between GBM and AGII (ROC AUC = 0.742; 95% CI, 0.147–0.368) (Fig. 2).

In contrast, *GOT2* expressions increased according to malignancy ($p < 0.001$ AGII vs. AGIII and $p < 0.01$ AGII vs. GBM, Dunn test) (Fig. 1a) and presented discriminatory power to distinguish between GBM and AGII (AUC = 0.709; 95% CI, 0.608–0.810) (Fig. 2). *GPT2* expression also increased significantly according to malignancy (AGI relative to AGII $p < 0.001$, to AGIII $p < 0.0001$, to GBM $p < 0.05$; AGII vs AGIII $p < 0.05$, AGIII vs GBM $p < 0.005$; Dunn test), besides, the only different expression level in comparison with NN was AGIII ($p < 0.0001$) (Fig. 1a). Although *GOT1* expression levels differed significantly between NN and astrocytoma, with discriminatory power to distinguish GBM from NN (ROC AUC = 0.902; 95% CI, 0.038–0.159), no significant

Fig. 1 Expression analysis of genes coding for glutaminolysis in astrocytomas of different malignant grades. **a** *GLSiso1, GLSiso2, GLS, GLS2, GLUD1, GOT1, GOT2,* and *GPT2* expression levels in non-neoplastic brain tissue (NN) compared to pilocytic astrocytoma (AGI), low-grade astrocytoma (AGII), anaplastic astrocytoma (AGIII), and glioblastoma (GBM). The expression levels differ significantly among the groups for all genes analyzed (**p = 0.002, ***p < 0.0001, Kruskal-Wallis test) and between NN and each tumor group (post hoc Dunn test, where ****p < 0.0001, ***p < 0.0005, **p < 0.005, and *p < 0.05. The significant comparison between the groups is represented by different symbols: NN (*), AGI (α), AGII ($), and AGIII (#). Horizontal bars show the median of each group. The results are presented on a log10 scale. **b** Correlation matrix showing the gene expression correlations with each other in all groups analyzed. Positive correlations are shown in blue and negative correlations in dark orange. The color intensiveness and the size of the circle are proportional to the value of *r* by the Spearman test. Only the correlations with *p* < 0.05 are plotted

difference of *GOT1* expression levels was detected among the astrocytoma grades of malignancy (Fig. 1a).

Considering the natural history of malignancy progression of malignancy from AGII to GBM, an upregulation of *GLSiso2, GOT2,* and *GPT2* expression levels were observed, in contrast to the downregulation of *GLUD1*. However, a large spreading of their expressions was detected in GBM, consistent with the well-known heterogeneity observed in GBM. Therefore, we analyzed the expression levels in GBM cases classified according to the molecular subtypes in proneural (PN), classical (CS), and mesenchymal (MS) subtypes [40]. Our cohort comprised 14 PN, 38 CS, and 14 MS cases. We found a statistical difference for *GLS2* expression among the groups

(*p* < 0.005, Kruskal–Wallis test) and comparing two groups: PN vs MS (*p* < 0.05, Dunn test) and CS vs MS (*p* < 0.05, Dunn test), with lower expression detected in the MS subtype (Supplemental Figure 1).

To validate these findings, we analyzed gene expression in silico in a larger database. The TCGA GBM database with gene expression from RNAseq comprising 37 PN (8 G-CIMP and 29 non-G-CIMP), 38 CS, and 48 MS cases. *GPT2* expression levels varied significantly among the GBM subtypes (*p* < 0.0001, Kruskal–Wallis test) with lower levels in MS than G-CIMP (*p* < 0.0005), PN (*p* < 0.05), and CS (*p* < 0.05, Dunn test). *GLUD1* expression levels also varied significantly amongst GBM subtypes (*p* = 0.05, Kruskal–Wallis test) with significant

Variables	Area under the ROC Curve	Std. Error	*p* Value
GLS2	0.971	0.01	.000
GLSiso2	0.919	0.02	.000
GOT1	0.902	0.03	.000
GLSiso1	0.796	0.05	.000
GLUD1	0.770	0.05	.000

Variables	Area under the ROC Curve	Std. Error	*p* Value
GOT2	0.709	0.000	.000
GLUD1	0.742	0.001	.000
GLSiso2	0.675	0.021	.000
GLS2	0.650	0.007	.000

Fig. 2 ROC curves for glutaminolysis pathway gene expressions. ROC curves for *GLSiso1*, *GLSiso2*, *GLS2*, *GLUD1*, and *GOT1* and *GOT2* expression levels, showing sensitivity and specificity of gene expression. The AUC values represent the accuracy of the individual gene for distinguishing between GBM and non–neoplastic tissue in **a**, and between GBM and AGII samples in **b**
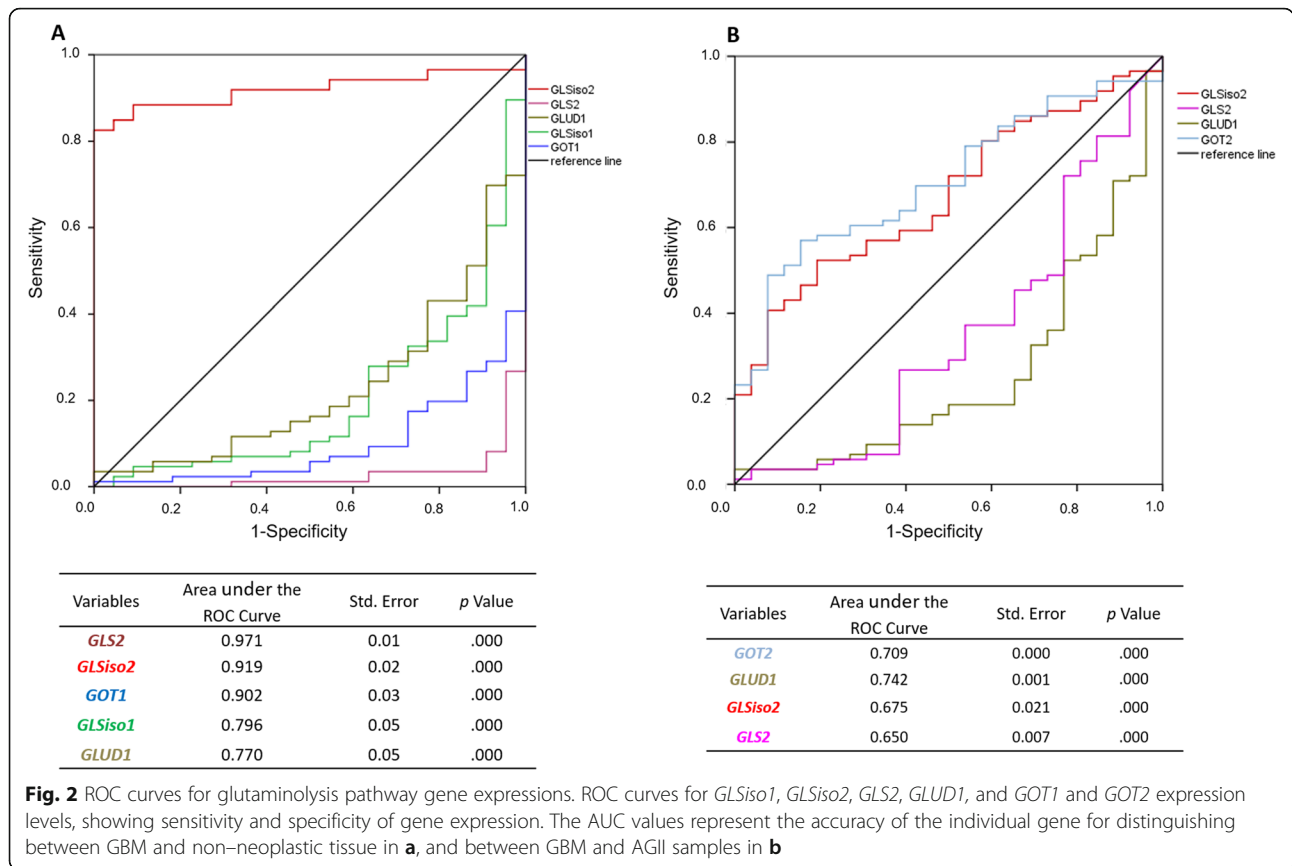
higher levels in G-CIMP compared to PN ($p < 0.01$) and to MS ($p < 0.005$, Dunn test). Although no statistical significance was observed of *GLS* expression among GBM subtypes, a trend of increase of its expression was noted in the MS subtype (Fig. 4a). The expression levels of *GLS* isoforms were not available in this dataset. The TCGA data analysis showed the downregulation of *GLUD1* and *GPT2* involved in the conversion of Glu to α–KG. *GLUD1* differed statistically in G–CIMP to MS ($p < 0.01$). Particularly, *GPT2* differed when comparing
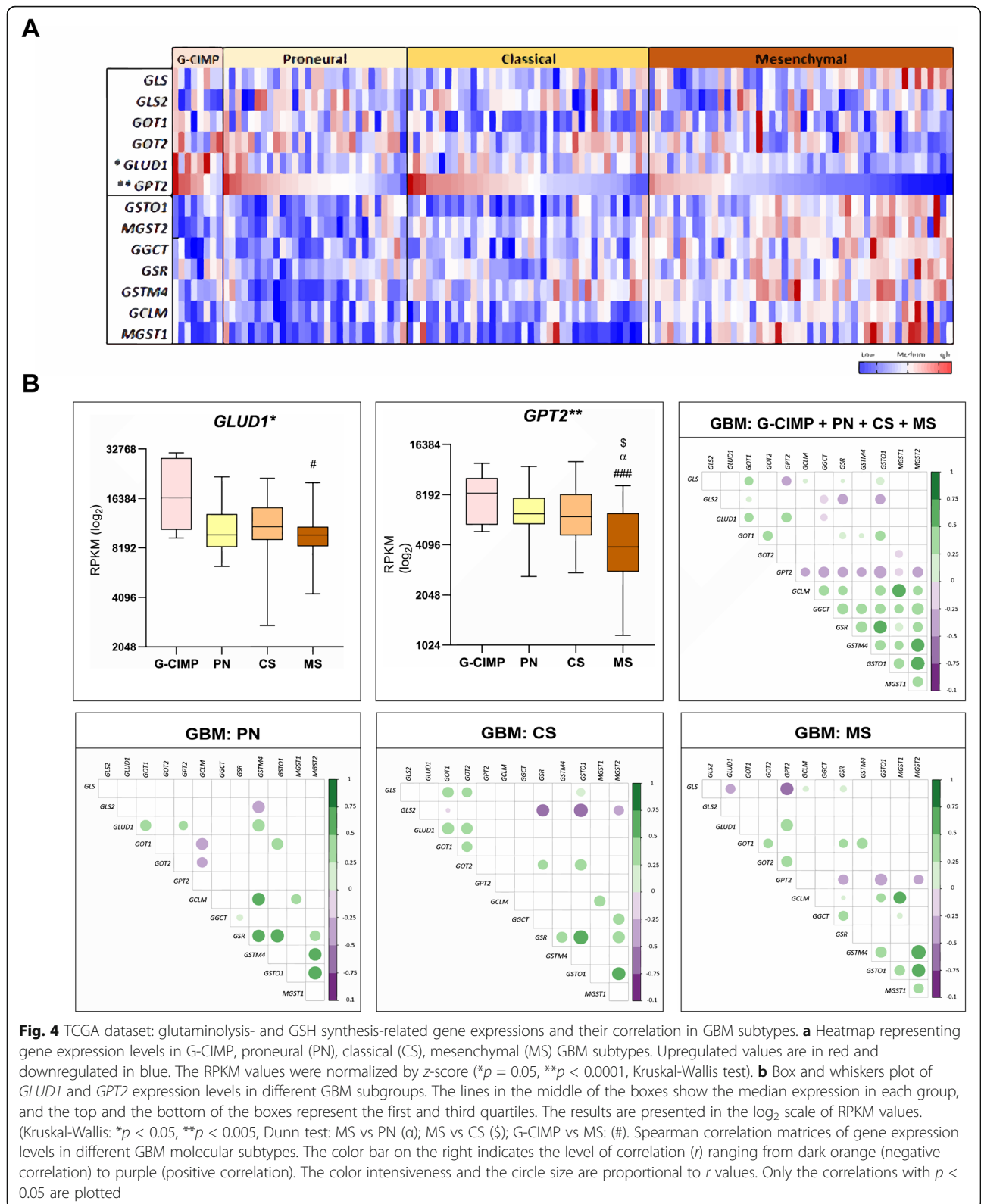
all groups with the MS subtype of GBM (G–CIMP–MS $p < 0.001$; PN–MS $p < 0.01$; CS–MS $p < 0.05$).

The downregulation of both genes *GLUD1* and *GPT2* suggest that the intracellular availability of Glu is increased, especially in the MS subtype of GBM, which led us to investigate another important Glu metabolism pathway: GHS. To this purpose, we selected the genes related to GSH pathway, glutamate-cysteine ligase modifier subunit (*CGLM*), gamma–glutamylcyclotransferase (*GGCT*), glutathione S–transferase mu 4 (*GSTM4*),

Fig. 3 GLS isoforms expression profile during astrocytoma progression and U87MG human GBM cells. **a** Western blot analysis of the expression of GLS isoforms in non-neoplastic (NN), pilocytic astrocytoma (AGI), low-grade astrocytoma (AGII), anaplastic astrocytoma (AGIII), glioblastoma (GBM), and U87MG GBM cell line. GLSiso1 and GLSiso2 are indicated by green arrow and red arrows, respectively. β-actin was used as a loading control. **b** Quantification of the protein relative to β-actin protein by ImageJ, represented by mean values ± standard deviation. The graph is representative of at least two replicates of one experiment. ***$p < 0.001$, Two-way ANOVA, Bonferroni post-test

Fig. 4 TCGA dataset: glutaminolysis- and GSH synthesis-related gene expressions and their correlation in GBM subtypes. **a** Heatmap representing gene expression levels in G-CIMP, proneural (PN), classical (CS), mesenchymal (MS) GBM subtypes. Upregulated values are in red and downregulated in blue. The RPKM values were normalized by z-score (*p = 0.05, **p < 0.0001, Kruskal-Wallis test). **b** Box and whiskers plot of *GLUD1* and *GPT2* expression levels in different GBM subgroups. The lines in the middle of the boxes show the median expression in each group, and the top and the bottom of the boxes represent the first and third quartiles. The results are presented in the log$_2$ scale of RPKM values. (Kruskal-Wallis: *p < 0.05, **p < 0.005, Dunn test: MS vs PN (α); MS vs CS ($); G-CIMP vs MS: (#). Spearman correlation matrices of gene expression levels in different GBM molecular subtypes. The color bar on the right indicates the level of correlation (r) ranging from dark orange (negative correlation) to purple (positive correlation). The color intensiveness and the circle size are proportional to r values. Only the correlations with p < 0.05 are plotted

glutathione S–transferase omega 1 (*GSTO1*), microsomal glutathione S–transferase 1 (*MGST1*), and microsomal glutathione S–transferase 2 (*MSGT2*) and analyzed the expression levels in the GBM database of TCGA (Fig. 4a). Additionally, the expression values were correlated to the expression data of glutaminolysis genes (Fig. 4b). The seven genes related to GSH synthesis presented differential expression levels among the GBM molecular subtypes, with statistical differences for all genes ($p < 0.0005$, Kruskal–Wallis test). Particularly, the expression of these genes was higher in the MS subtype compared to the other subtypes (Supplemental Figure 2). Moreover, the gene expression levels of GSH synthesis were highly correlated among themselves when all groups of GBM were analyzed together (GBM: G–CIM+PN+CS+ MS), and interestingly, an inverse correlation was noted with *GPT2* expression. Particularly in the MS subtype, *GPT2* expression correlated inversely to the expression levels of *GSTO1, GSR,* and *MGST2*, suggesting the possibility of Glu not converted to α–KG being used for GHS synthesis (Fig. 4b). All statistically significant values are demonstrated on Supplemental Table 2.

GLUD1 upregulation in *IDH1*[mut] AGIII correlated to downregulation of genes involved in GSH synthesis

G-CIMP cases of PN molecular subtype of GBM presented the higher *GLUD1* and *GPT2* expression levels when compared to the other subgroups. Additionally, genes related to GSH synthesis presented the lowest expression levels in G-CIMP cases. These data and the information that increased conversion of Gln to Glu has been described in glioma cells harboring *IDH1* mutation [41] motivated us to investigate the *IDH*1 mutation status influence in the expression levels of genes involved in the glutaminolysis pathway and GSH. Gene expression levels previously analyzed in GBM cases were also analyzed in AGII and AGIII cases of TCGA, separating cases with and without *IDH1* mutation (Fig. 5a). In our cohort, 20 AGII out of 26 cases (77%) presented *IDH1* mutation, and 11 out of 18 AGIII cases harbored *IDH1* mutation (61%). Interestingly, upregulated *GLUD1* and *GPT2* expressions were observed in *IDH1*[mut] AGII cases, with a significant difference compared to *IDH1*[wt] AGII cases for *GPT2* expression ($p < 0.05$, Mann-Whitney test), and a trend of increase for *GLUD1* (Fig. 5b). In a larger TCGA dataset, with 51 *IDH1*[mut] AGII out of 63 cases (86%), and 80 *IDH1*[mut] AGIII out of 129 cases (63%), a significant higher *GLUD1* and *GPT2* expression levels were observed both in AGII and AGIII harboring *IDH1* mutation when compared to cases without *IDH1* mutation ($p < 0.01$ and $p < 0.0001$ for *GLUD1* in AGII and AGIII respectively; $p < 0.01$ and $p < 0.001$ for *GPT2* in AGII and AGIII, respectively, Mann-Whitney test) (Fig. 5b). Expression analyses of expression levels of all
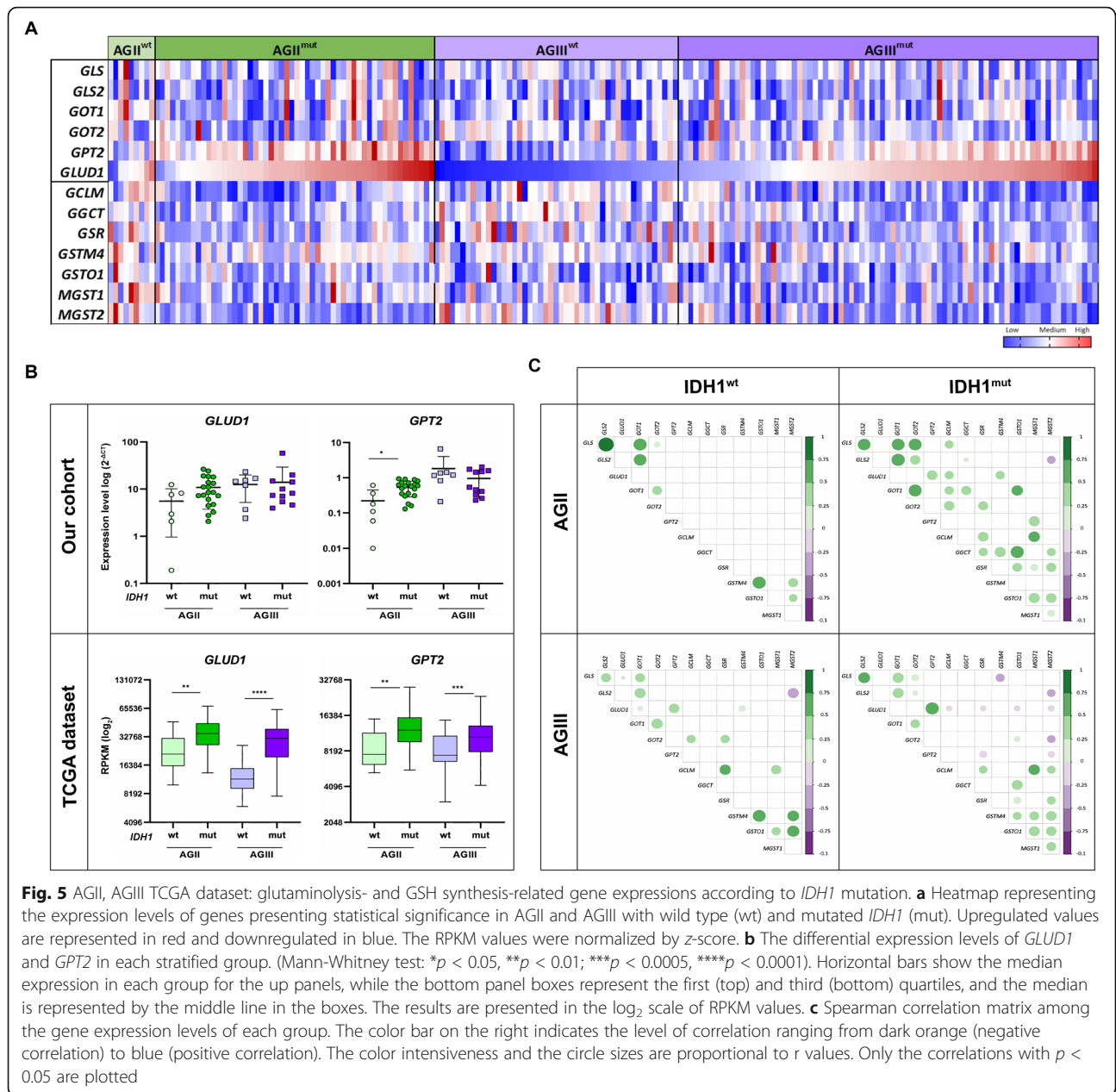
genes presented in the correlation matrix demonstrated that *IDH1*[mut] AGII cases presented activation of both glutaminolysis and GSH synthesis in contrast to *IDH1*[wt] AGII, with an inverse correlation between *GLS2* and *MSGT2* expressions in *IDH1*[mut] AGII (Fig. 5c). On the other hand, *IDH1*[mut] AGIII cases presented a significantly high correlation between *GLUD1* and *GPT2* expression levels, and inverse correlations with several genes related to GSH synthesis. Of note, the *GLUD1* expression level was inversely correlated to *GSR, GCLM, GSTO1,* and *GSMT2* expression levels, indicating the downregulation of these gene expressions when *GLUD1* was upregulated in AGIII cases with *IDH1* mutation (Fig. 5c). All statistically significant values are demonstrated on Supplemental Table 3.

GLUD1 and GPT2 protein downregulation in GBM-MS and GLUD1 downregulation in AGII-IDH[wt] correlated with upregulation of GS activity

The GBM-MS presented low expression of GLUD1 and GPT2 protein levels when compared to the GBM-PN cases ($p < 0.05$ and $p < 0.001$, respectively). Although statistical significance was not reached, AGII-IDH[wt] presented low GLUD1 protein level (Fig. 6a, b). Additionally, we evaluated whether the level of these proteins correlated with glutathione synthetase (GS) expression. Interestingly, a significant increase of GS expression was observed in GBM-MS and AGII-*IDH*[wt] in comparison with GBM-PN and AGII-*IDH*[mut] ($p < 0.01$ and $p = 0.05$, respectively) (Fig. 6c, d). We also found a trend of increased levels of GSH in GBM-MS (*IDH*[wt]) samples in contrast to more uniform low GSH levels in GBM-PN (*IDH*[mut]) (Supplemental Figure 3).
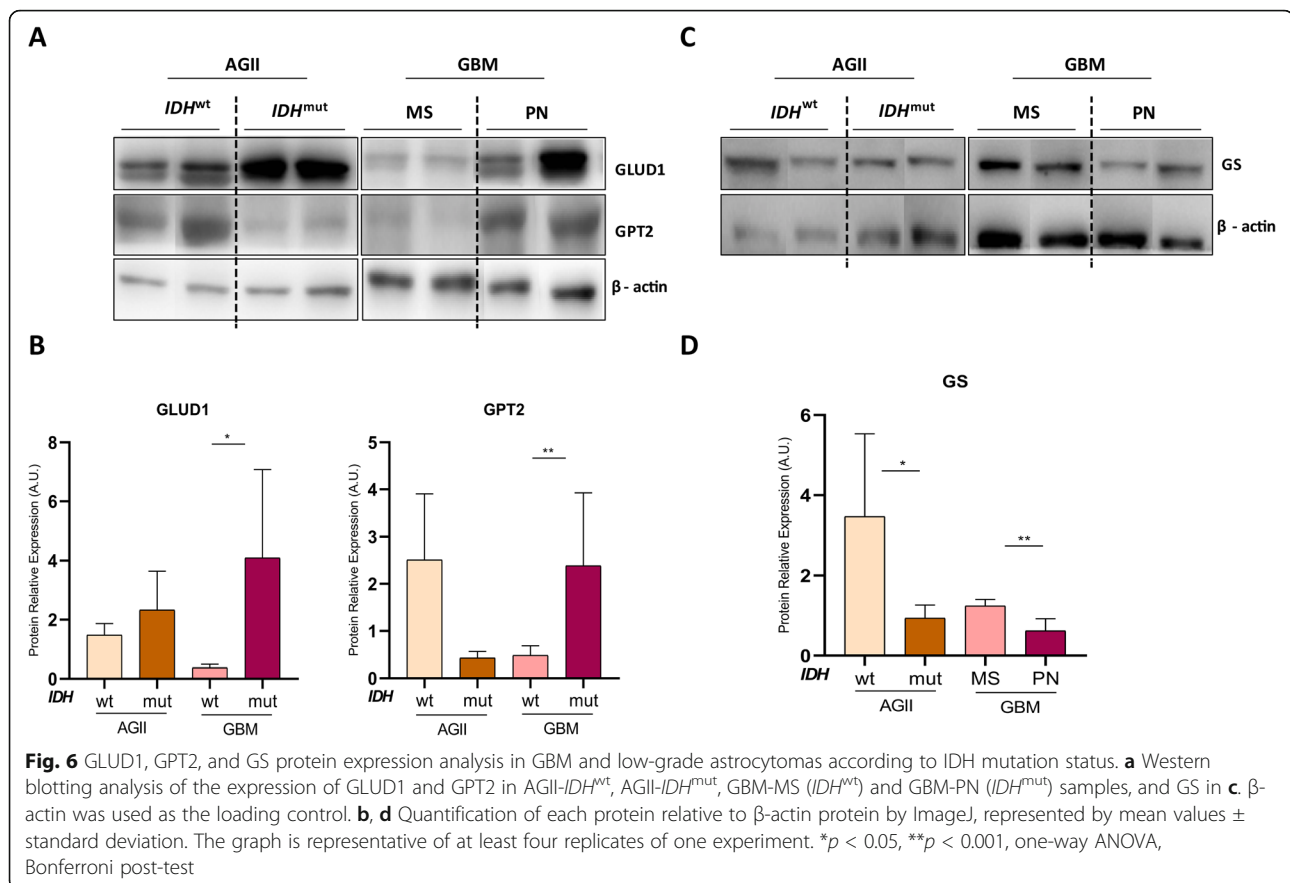
Discussion

Metabolic reprogramming has been proposed to be a hallmark of cancer [42], and in the present analysis, we observed a progressive activation of the glutaminolysis from low-grade astrocytoma to GBM. Glutaminolysis has been pointed to as one of the major altered metabolic pathways related to tumor growth [12, 16]. High extracellular Gln concentration has been associated with cell transformation [17], and its metabolism was related to cell survival and tumor growth by maintaining redox balance, bioenergetics, and supporting macromolecular biosynthesis [28, 42]. We have previously reported the upregulation of Gln transporters, *ASCT2* and *LAT1*, in all grades of astrocytoma [20]. Here, we showed the upregulation of the mitochondrial isoform of *GLS* [39], *GLSiso2* (*GAC*), in all grades of astrocytoma at gene and protein levels, and a gradual increase of its expression was observed in parallel to the increment of malignancy. GLSiso2 involvement in cancer progression has been previously reported in prostate cancer and B cell

Fig. 5 AGII, AGIII TCGA dataset: glutaminolysis- and GSH synthesis-related gene expressions according to *IDH1* mutation. **a** Heatmap representing the expression levels of genes presenting statistical significance in AGII and AGIII with wild type (wt) and mutated *IDH1* (mut). Upregulated values are represented in red and downregulated in blue. The RPKM values were normalized by z-score. **b** The differential expression levels of *GLUD1* and *GPT2* in each stratified group. (Mann-Whitney test: *$p < 0.05$, **$p < 0.01$; ***$p < 0.0005$, ****$p < 0.0001$). Horizontal bars show the median expression in each group for the up panels, while the bottom panel boxes represent the first (top) and third (bottom) quartiles, and the median is represented by the middle line in the boxes. The results are presented in the log$_2$ scale of RPKM values. **c** Spearman correlation matrix among the gene expression levels of each group. The color bar on the right indicates the level of correlation ranging from dark orange (negative correlation) to blue (positive correlation). The color intensiveness and the circle sizes are proportional to r values. Only the correlations with $p < 0.05$ are plotted

lymphoma [43]. GLSiso2 is activated by inorganic phosphate [39] and it is also under c−*Myc* oncogene influence, through a mechanism involving miRNA [43, 44]. The c-Myc can also upregulate the GLS isoforms KGA and GAC at protein levels increasing the levels of intracellular glutamate in Epstein-Barr virus-infected cells [68]. Oscillation of GLSiso2 expression has been associated with oxygen concentration, with an increase in hypoxic conditions [39]. Our finding of GLSiso2 higher expression in GBM, the more malignant astrocytoma presenting necrosis, corroborated these previous observations. The cytosolic GLSiso1 (KGA) expression was also higher in more malignant than lower-grade

astrocytomas. Nevertheless, the high expression observed in NN tissue renders this target less eligible for therapeutic purposes.

The other glutaminase, *GLS2*, in contrast to *GLS* with broad distribution among normal tissue, presents a more restricted distribution in the liver, brain, pituitary gland, and pancreas [45, 46]. The *GLS2* expression level was significantly lower in astrocytoma than NN, with the lowest expression in GBM of MS subtype in our cohort. This finding corroborates the tumor suppressor role attributed to *GLS2* in previous studies, where inhibition of tumor cell proliferation, colony formation, and migration were attributed to *GLS2* [28, 43, 47–51]. This tumor

Fig. 6 GLUD1, GPT2, and GS protein expression analysis in GBM and low-grade astrocytomas according to IDH mutation status. **a** Western blotting analysis of the expression of GLUD1 and GPT2 in AGII-*IDH*wt, AGII-*IDH*mut, GBM-MS (*IDH*wt) and GBM-PN (*IDH*mut) samples, and GS in **c**. β-actin was used as the loading control. **b, d** Quantification of each protein relative to β-actin protein by ImageJ, represented by mean values ± standard deviation. The graph is representative of at least four replicates of one experiment. *$p < 0.05$, **$p < 0.001$, one-way ANOVA, Bonferroni post-test

suppressor activity is dependent on p53 and other related proteins, as p63 and p73 [48]. Therefore, concerning the first step of the glutaminolysis pathway, our findings suggested that *GLSiso2* plays a key role in tumorigenesis and malignant progression of astrocytoma, whereas the *GLS2* expression pattern is consistent with tumor suppressor function, being mostly suppressed in the aggressive MS molecular subtype of GBM.

Interestingly, the downflow activation of the glutaminolysis pathway with the conversion of Glu to α–KG through dehydrogenase and transaminase varied according to the astrocytoma grade. Significant downregulation of *GLUD1* and *GPT2* expressions were observed in GBM compared to lower-grade astrocytoma in our cohort and confirmed in the TCGA dataset. Particularly, *GPT2* was significantly downregulated in GBM of MS subtype compared to other molecular subtypes. We also observed this downregulation of GLUD1 and GPT2 at the protein level in GBM-MS subtype. The downregulation of these proteins may increase intracellular Glu availability, which may be directed for GSH synthesis [52].

GSH is a tripeptide formed by glutamic acid, cysteine, and glycine and plays an important role in the maintenance of the intracellular redox balance [53, 54]. Elevated

GSH levels confer resistance to chemotherapy in various types of cancer [55–57] by binding to or reacting with drugs, interacting with ROS, preventing damage to proteins or DNA, and participating in DNA repair processes [55]. Moreover, GSH- and GSH-related enzymes including synthetase (GS), ligase (GCLM), transferase (GGT), reductase (GSR), and glutathione S–transferases (GSTM4, GSTO1, MGST1, MGST2) activities may play a role in adaptive detoxification processes in response to the oxidative stress, thus contributing to drug resistance phenotype [53, 54].

The increase of intracellular Glu level may favor its release to the extracellular space by a Gln/cysteine antiporter system x c–dependent, which increases intracellular cysteine levels ([Cys]i). In turn, high [Cys]i favors GSH synthesis [52]. The TCGA data analysis showed a significant inverse correlation among *GPT2* expression and expression level of several genes related to GSH synthesis. Particularly, upregulation of *GSTO1*, *MGST2*, and *GSR* were correlated significantly to the downregulation of *GPT2* in the MS subtype of GBM. Also, we observed a significant increase of the GS protein and a trend of an increase of GSH protein level in the GBM-MS in comparison with the GBM-PN samples. The antioxidative effect provided by increased synthesis of GSH can balance the elevated generation of ROS due to the high metabolic

rate presented by GBM cells and favor their survival [58]. Such mechanism may be related to the aggressive behavior of GBM of MS molecular subtype.

In contrast, AGII and AGIII presented higher *GLUD1* expression levels than GBM, and particularly in those cases harboring *IDH1* mutation, and a similar trend was observed at the protein level, although this observation needs to be extended for additional cases to reach statistical significance. Similarly, *GPT2* expression was also

higher in AGII and AGIII cases harboring *IDH1* mutation, but this finding was not confirmed at the protein level in our studied cohort. However, GS protein level was significantly lower in AGII-IDH^{mut} compared to AGII-IDH^{wt}, suggesting that low-grade astrocytomas harboring IDH mutation may be more susceptible to ROS induced stress. Metabolomic studies of *IDH1* mutant cells have revealed alterations in Gln, fatty acid, and citrate synthesis pathways [59, 60]. *IDH1* mutation was
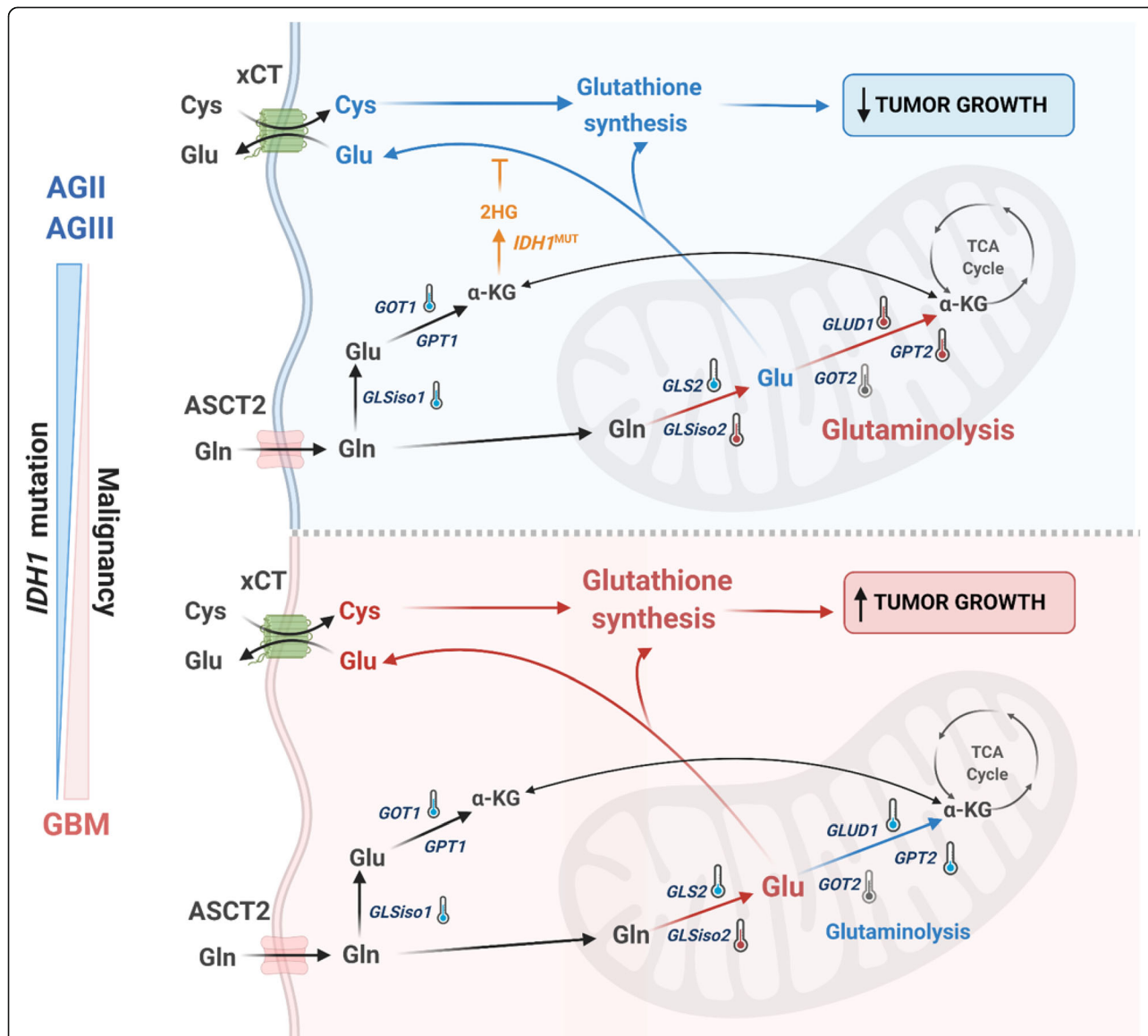
Fig. 7 Schematic representation of glutaminolysis genes differentially expressed in GBM. GBM cases presented hyperexpression of *GLSiso2* and hypoexpression of other genes of the glutaminolysis pathway (*GLSiso1, GLS2, GLUD1, GPT2*), (downregulation of GLUD1 and GPT2 was confirmed at protein level) leading to an accumulation of Glu and activation of GSH synthesis and consequently inducing tumor cell proliferation and survival. On the other hand, AGII and AGIII *IDH1*^{mut} display hyperexpression of *GLSiso2, GLUD1*, and *GPT2* (upregulation of GLUD1 was confirmed at protein level) leading to activation of glutaminolysis pathway and fueling the TCA cell cycle. Additionally, in *IDH1*^{mut} cases, a decrease in Glu availability sensitizes the tumor cells to oxidative stress leading to slow tumor growth. The downregulated expression is represented by blue thermometers, upregulated by red thermometers, and the non-significant differential expression in gray. Red arrows represent the activation of the pathway and blue arrows represent the inactivation of the pathway

shown to convert α–KG to D–2–hydroxyglutarate, which due to its structural similarities acts as a competitive inhibitor reducing the activity of α–KG–processing enzymes [61]. As feedback, α–KG is replenished by glutaminolysis and TCA cycle, which leads to a decrease in Gln and Glu levels [62]. Therefore, *IDH*^mut gliomas are "glutamate addicted", and the lack of Glu decreases its exchange with Cys through the system X_C^- [63]. The lack of cytoplasmic Cys reduces GSH synthesis, which increases the susceptibility to ROS–induced stress as through radiation therapy or TMZ treatment [63]. In this context, reduced Glu contributes to a better outcome presented by gliomas with *IDH1* mutation [41, 52]. Our correlation analysis among genes related to glutaminolysis and GSH synthesis-related genes demonstrated that *GLUD1* and *GPT2* expression levels inversely correlated to GSH synthesis-related gene expression levels, particularly in *IDH1*^mut AGIII. Our findings reinforce the hypothesis that decreasing Glu may sensitize *IDH1*^mut cells to radiation and ROS-inducing drugs due to reduced GSH synthesis. Indeed, GLS inhibition and *IDH1* mutation were recently demonstrated to present a synthetic lethal relationship under conditions of oxidative stress [41].

Our findings together with TCGA data analysis indicated that AGII and AGIII harboring *IDH1* mutation may decrease tumor cell fitness by lowering Glu, GSH, and resistance to oxidative stress. Interestingly, the end metabolites of these enzymes, ammonia, and alanine are measurable by the MR spectroscopy [64–67]. Thus, monitoring the waning of *GLUD1* and *GPT2* expression levels by measuring their end substrates by this non-invasive imaging technique may potentially detect the progression of lower-grade astrocytomas harboring *IDH1* mutation towards secondary GBM, and it would, therefore, allow a change in the therapeutic strategy for these patients. Such hypothesis would be worthwhile to test in future studies.

Conclusion

In conclusion, *GLSiso2* upregulation was associated with tumorigenesis and tumor progression in astrocytomas. Particularly in GBM, the accumulation of Glu due to *GPT2* and *GLUD1* downregulation correlated to upregulation of genes related to GSH synthesis which could favor tumor cell survival, mostly in the most aggressive MS subtype. In contrast, *GLUD1* may lead to a decrease in GSH synthesis in *IDH1*^mut low-grade astrocytomas increasing the susceptibility to oxidative stress, rendering them more sensitive to radiation therapy and to alkylating therapy (Fig. 7).

Abbreviations

GBM: Glioblastoma; AGI: Astrocytoma grade I; AGII: Astrocytoma grade II; AGIII: Astrocytoma grade III; NN: Non-neoplastic; Gln: Glutamine;

Glu: Glutamate; TCA: Tricarboxylic acid; α–KG: Alpha ketoglutarate; GSH: Glutathione; GLS: Glutaminase; GLS2: Glutaminase 2; GLSiso1: Glutaminase isoform 1; GLSiso2: Glutaminase isoform 2; GLUD1: Glutamate dehydrogenase 1; GOT1: Glutamate oxaloacetate transaminase 1; GOT2: Glutamate oxaloacetate transaminase 2; GPT1: Glutamate pyruvate transaminase 1; GPT2: Glutamate pyruvate transaminase 2; TCGA: The Cancer Genome Atlas; IDH: Isocitrate dehydrogenase; IDH1: Isocitrate dehydrogenase 1; IDH1^MUT: Isocitrate dehydrogenase 1 mutation; IDH^WT: Isocitrate dehydrogenase wild type; CNS: Central nervous system; WHO: World Health Organization; NF1: Neurofibromin 1; RB1: Retinoblastoma 1; TMZ: Temozolomide; qRT–PCR: Quantitative reverse transcription PCR; ASCT2 (SLC1A5): Solute carrier family 1 member 5; LAT1 (SLC7A5): Solute carrier family 7 member 5; HPRT: Hypoxanthine phosphoribosyltransferase; GUSβ: Glucuronidase beta; TBP: TATA box binding protein; PCR: Polymerase chain reaction; ATCC: American Type Culture Collection; mRNA: Messenger RNA; ROC: Receiver operating characteristic; PN: Proneural; CS: Classical; MS: Mesenchymal; G–CIMP: Glioma CpG island methylator phenotype; CGLM: Glutamate–cysteine ligase modifier subunit; GGCT: Gamma–glutamylcyclotransferase; GSTM4: Glutathione S–transferase mu 4; GSTO1: Glutathione S–transferase omega 1; MGST1: Microsomal glutathione S–transferase 1; MGST2: Microsomal glutathione S–transferase 2; GSR: Glutathione–disulfide reductase; GS: Glutathione synthetase; ROS: Reactive oxygen species; MR: Magnetic resonance

Supplementary Information

The online version contains supplementary material available at https://doi.org/10.1186/s40170-021-00255-8.

Additional file 1: Figure S1. Expression analysis of genes related to glutaminolysis in different molecular subtypes of GBM in our cohort. A: Heatmap of *GLSiso1, GLSiso2, GLS, GLS2, GOT1, GOT2, GPT2,* and *GLUD1* mRNA expression levels in different molecular subtypes of GBM (PN: proneural, CS: classical, MS: mesenchymal). Upregulated values are in red and downregulated in blue. The RPKM values were normalized by z-score. B: *GLS2* expression differed significantly among the subtypes (Kruskal-Wallis, $p < 0.005$, **$p < 0.05$, Dunn test). Horizontal bars show the median relative expression in each group.

Additional file 2: Figure S2. Expression analysis of GPT2 and genes related to glutathione synthesis in different molecular subgroups of GBM from TCGA RNAseq dataset. Box and whiskers plot of *GPT2, GCLM, GGCT, GSR, GSTM4, GSTO1, MGST1,* and *MGST2* expression levels in G-CIMP, proneural (PN), classical (CS), and mesenchymal (MS) GBM cases. The top and the bottom of boxes represent the first and third quartiles, respectively, and the lines in the middle the median of the groups. Kruskal-Wallis: *$p < 0.05$, **$p < 0.005$, ***$p < 0.0005$, Dunn test: CS vs PN (#); MS vs PN (¶); MS vs CS ($); G-CIMP vs MS: (‡); G-CIMP vs CS: (@). The results are presented in the log2 scale of RPKM values.

Additional file 3: Figure S3 Analysis of Reduced Glutathione (GSH) levels in AGII*IDH*^wt, AGII*IDH*^mut, GBM-MS (*IDH*^wt) and PN (*IDH*^mut). GSH levels [pmol/μg of total protein] analysis of low-grade astrocytoma *IDH*^wt, low grade astrocytoma *IDH*^mut, Glioblastoma^wt –Mesenchymal, and glioblastoma IDH^mut –Proneural). Results are presented as mean ± standard deviation (n ≥ 3 samples of each group).

Additional file 4: Supplemental Table S1. Correlations values of the glutaminolysis pathway genes in all grades of astrocytoma.

Additional file 5: Supplemental Table S2. Correlations values of the glutaminolysis and GSH pathway genes in the subtypes of GBM.

Additional file 6: Supplemental Table S3. Correlations values of the glutaminolysis and GSH pathway genes in AGII and AGIII with *IDH1* wild type (*IDH1*^wt) and mutated *IDH1* (*IDH1*^mut).

Availability of data and materials
Normalized gene expression data are available from the corresponding author on request. The results shown here are in part based upon data generated by the TCGA Research Network: https://www.cancer.gov/tcga.

Declarations

Ethics approval and consent to participate
The procedures were performed with informed and approved consents according to the Institutional Ethical Committee guidelines at the Hospital das Clinicas of the School of Medicine of University of São Paulo (691/05).

Consent for publication
Not applicable

Competing interests
The authors declare that they have no competing interests.

Author details
[1]Laboratory of Molecular and Cellular Biology (LIM 15), Department of Neurology, Faculdade de Medicina FMUSP, Universidade de São Paulo, São Paulo 01246–903, Brazil. [2]Department of Molecular Pharmacology, University of Groningen, 9713 Av, Groningen, The Netherlands. [3]School of Applied Mathematics, Fundação Getulio Vargas, Rio de Janeiro 22250-900, Brazil. [4]Institute of Chemistry, Department of Biochemistry, Universidade de São Paulo, CEP, São Paulo 05508-000, Brazil. [5]Department of Internal Medicine, Division of Metabolism, Endocrinology, and Diabetes, University of Michigan, Ann Arbor, Michigan, USA.

References
1. Siegel RL, Miller KD, Jemal A. Cancer statistics, 2019. CA Cancer J Clin. 2019; 69(1):7–34.
2. Dolecek TA, Propp JM, Stroup NE, Kruchko C. CBTRUS Statistical report: primary brain and central nervous system tumors diagnosed in the United States in 2005-2009. Neuro Oncol. 2012;14(suppl 5):v1–49.
3. Miranda-Filho A, Piñeros M, Soerjomataram I, Deltour I, Bray F. Cancers of the brain and CNS: global patterns and trends in incidence. Neuro Oncol. 2016;19(2):now166.
4. Jones C, Perryman L, Hargrave D. Paediatric and adult malignant glioma: close relatives or distant cousins? Nat Rev Clin Oncol. 2012;9(7):400–13.
5. Molinaro AM, Taylor JW, Wiencke JK, Wrensch MR. Genetic and molecular epidemiology of adult diffuse glioma. Nat Rev Neurol. 2019;15(7):405–17.
6. Sanai N, Alvarez-Buylla A, Berger MS. Neural stem cells and the origin of gliomas. N Engl J Med. 2005;353(8):811–22.
7. Wang Q, Hu B, Hu X, Kim H, Squatrito M, Scarpace L, et al. Tumor evolution of glioma-intrinsic gene expression subtypes associates with immunological changes in the microenvironment. Cancer Cell. 2017;32(1):42–56 e6.
8. Verhaak RGW, Hoadley KA, Purdom E, Wang V, Qi Y, Wilkerson MD, et al. Integrated Genomic Analysis Identifies Clinically Relevant Subtypes of Glioblastoma Characterized by Abnormalities in PDGFRA, IDH1, EGFR, and NF1. Cancer Cell. 2010;17(1):98–110.
9. Yan H, Parsons DW, Jin G, McLendon R, Rasheed BA, Yuan W, et al. IDH1 and IDH2 mutations in gliomas. N Engl J Med. 2009;360(8):765–73.
10. Sidaway P. Glioblastoma subtypes revisited. Nat Rev Clin Oncol. 2017;14(10): 587–7.
11. Touat M, Li YY, Boynton AN, Spurr LF, Iorgulescu JB, Bohrson CL, et al. Mechanisms and therapeutic implications of hypermutation in gliomas. Nature. 2020;580(7804):517–23.
12. Strickland M, Stoll EA. Metabolic Reprogramming in Glioma. Front Cell Dev Biol. 2017;5.
13. Vander Heiden M, Cantley L, Thompson C. Understanding the Warburg effect: The metabolic Requiremetns of cell proliferation. Science (80). 2009; 324(5930):1029–33.
14. Oruganty K, Campit SE, Mamde S, Lyssiotis CA, Chandrasekaran S. Common biochemical properties of metabolic genes recurrently dysregulated in tumors. Cancer Metab. 2020;8(1):1–15.
15. Altman BJ, Stine ZE, Dang CV. From Krebs to clinic: glutamine metabolism to cancer therapy. Nat Publ Gr. 2016;16(10):619–34.
16. Cluntun AA, Lukey MJ, Cerione RA, Locasale JW. Glutamine metabolism in cancer: understanding the heterogeneity. Trends in Cancer. 2017;3(3): 169–80.
17. Jin L, Kang S. Glutaminolysis as a target for cancer therapy. Oncogene. 2016; 35(28):3619–25.
18. DeBerardinis RJ, Sayed N, Ditsworth D, Thompson CB. Brick by brick: metabolism and tumor cell growth. Curr Opin Genet Dev. 2008;18(1):54–61.
19. Herranz D. Glutaminolysis gets the spotlight in cancer. 2017;8(7):10761–2.
20. Alves MJF, Uno M, da Silva R, Oba-Shinjo SM, Marie SKN. The expression of the aminoacid transporters ASCT2 (SLC1A5) and LAT1 (SLC7A5) in astrocytomas. Med Express. 2016;3(6):1–8.
21. Vander Heiden MG. Targeting cancer metabolism: a therapeutic window opens. Nat Rev Drug Discov. 2011;10(9):671–84.
22. Daye D, Wellen KE. Metabolic reprogramming in cancer: unraveling the role of glutamine in tumorigenesis. Semin Cell Dev Biol. 2012;23(4):362–9.
23. Ralph J. DeBerardinis, and TC. Q's next: The diverse functions of glutamine in metabolism, cell biology and cancer. 2010;29(3):313–324.
24. Luengo A, Gui DY, Vander Heiden MG. Targeting metabolism for cancer therapy. Cell Chem Biol. 2017;24(9):1161–80.
25. Gross MI, Demo SD, Dennison JB, Chen L, Chernov-Rogan T, Goyal B, et al. Antitumor activity of the glutaminase inhibitor CB-839 in triple-negative breast cancer. Mol Cancer Ther. 2014;13(4):890–901.
26. Jacque N, Ronchetti AM, Larrue C, Meunier G, Birsen R, Willems L, et al. Targeting glutaminolysis has antileukemic activity in acute myeloid leukemia and synergizes with BCL-2 inhibition. Blood. 2015;126(11): 1346–56.
27. Xiang Y, Stine ZE, Xia J, Lu Y, O'Connor RS, Altman BJ, et al. Targeted inhibition of tumor-specific glutaminase diminishes cell-autonomous tumorigenesis. J Clin Invest. 2015;125(6):2293–306.
28. Obara-Michlewska M, Szeliga M. Targeting glutamine addiction in Gliomas. Cancers (Basel). 2020;12:2.
29. Walker MC, van der Donk WA. The many roles of glutamate in metabolism. J Ind Microbiol Biotechnol. 2016;43(2–3):419–30.
30. Lv H, Zhen C, Liu J, Yang P, Hu L, Shang P. Unraveling the potential role of glutathione in multiple forms of cell death in cancer therapy. Oxid Med Cell Longev. 2019;2019:1–16.
31. Wang Z, Ding Y, Wang X, Lu S, Wang C, He C, et al. Pseudolaric acid B triggers ferroptosis in glioma cells via activation of Nox4 and inhibition of xCT. Cancer Lett. 2018;428:21–33.
32. Lewerenz J, Hewett SJ, Huang Y, Lambros M, Gout PW, Kalivas PW, et al. The cystine/glutamate antiporter system x c − in health and disease: from molecular mechanisms to novel therapeutic opportunities. Antioxid Redox Signal. 2013;18(5):522–55.
33. Louis DN, Ohgaki H, Wiestler OD, Cavenee WK, Burger PC, Jouvet A, et al. The 2007 WHO classification of tumours of the central nervous system. Acta Neuropathol. 2007;114(2):97–109.
34. Valente V, Teixeira SA, Neder L, Okamoto OK, Oba-Shinjo SM, Marie SK, et al. Selection of suitable housekeeping genes for expression analysis in glioblastoma using quantitative RT-PCR. BMC Mol Biol. 2009;10(1):17.
35. Livak KJ, Schmittgen TD. Analysis of relative gene expression data using real-time quantitative PCR and the 2−ΔΔCT method. Methods. 2001;25(4): 402–8.

36. Matés JM, Segura JA, Campos-Sandoval JA, Lobo C, Alonso L, Alonso FJ, et al. Glutamine homeostasis and mitochondrial dynamics. Int J Biochem Cell Biol. 2009;41(10):2051–61.

37. Katt WP, Cerione RA. Glutaminase regulation in cancer cells: A druggable chain of events. Drug Discov Today. 2014;19(4):450–7.

38. Vijayakumar SN, Sethuraman S, Krishnan UM. Metabolic pathways in cancers: key targets and implications in cancer therapy. RSC Adv. 2015;5(52):41751–62.

39. Cassago A, Ferreira APS, Ferreira IM, Fornezari C, Gomes ERM, Greene KS, et al. Mitochondrial localization and structure-based phosphate activation mechanism of Glutaminase C with implications for cancer metabolism. Proc Natl Acad Sci. 2012;109(4):1092–7.

40. Galatro TF, et al. Correlation between molecular features and genetic subtypes of Glioblastoma: critical analysis in 109 cases. Med. Express. 2017;4.

41. McBrayer SK, Mayers JR, DiNatale GJ, Shi DD, Khanal J, Chakraborty AA, et al. Transaminase inhibition by 2-hydroxyglutarate impairs glutamate biosynthesis and redox homeostasis in glioma. Cell. 2018;175(1):101–16 e25.

42. Pavlova NN, Thompson CB. The emerging hallmarks of cancer metabolism. Cell Metab. 2016;23(1):27–47.

43. Gao P, Tchernyshyov I, Chang T-C, Lee Y-S, Kita K, Ochi T, et al. c-Myc suppression of miR-23a/b enhances mitochondrial glutaminase expression and glutamine metabolism. Nature. 2009 Apr 15;458(7239):762–5.

44. Márquez J, Alonso FJ, Matés JM, Segura JA, Martín-Rufián M, Campos-Sandoval JA. Glutamine Addiction In Gliomas. Neurochem Res. 2017;42(6):1735–46.

45. Curthoys NP. Regulation of glutaminase activity and glutamine metabolism. Annu Rev Nutr. 1995;15(1):133–59.

46. Ardlie KG, Deluca DS, Segre AV, Sullivan TJ, Young TR, Gelfand ET, et al. The genotype-tissue expression (GTEx) pilot analysis: multitissue gene regulation in humans. Science. 2015;348(6235):648–60.

47. Suzuki S, Tanaka T, Poyurovsky MV, Nagano H, Mayama T, Ohkubo S, et al. Phosphate-activated glutaminase (GLS2), a p53-inducible regulator of glutamine metabolism and reactive oxygen species. Proc Natl Acad Sci. 2010;107(16):7461–6.

48. Hu W, Zhang C, Wu R, Sun Y, Levine A, Feng Z. Glutaminase 2, a novel p53 target gene regulating energy metabolism and antioxidant function. Proc Natl Acad Sci. 2010;107(16):7455–60.

49. Szeliga M, Bogacińska-Karaś M, Kuźmicz K, Rola R, Albrecht J. Downregulation of GLS2 in glioblastoma cells is related to DNA hypermethylation but not to the p53 status. Mol Carcinog. 2016;55(9):1309–16.

50. Xiao D, Ren P, Su H, Yue M, Xiu R, Hu Y, et al. Myc promotes glutaminolysis in human neuroblastoma through direct activation of glutaminase 2. Oncotarget. 2015;6:38.

51. Wang J-B, Erickson JW, Fuji R, Ramachandran S, Gao P, Dinavahi R, et al. Targeting mitochondrial glutaminase activity inhibits oncogenic transformation. Cancer Cell. 2010;18(3):207–19.

52. Maus A, Peters GJ. Glutamate and α-ketoglutarate: key players in glioma metabolism. Amino Acids. 2017;49(1):21–32.

53. Forman HJ, Zhang H, Rinna A. Glutathione: Overview of its protective roles, measurement, and biosynthesis. Mol Aspects Med. 2009;30(1–2):1–12.

54. Meister A. Glutathione metabolism. In 1995. p. 3–7.

55. Traverso N, Ricciarelli R, Nitti M, Marengo B, Furfaro AL, Pronzato MA, et al. Role of glutathione in cancer progression and chemoresistance. Oxid Med Cell Longev. 2013.

56. Rocha CRR, Garcia CCM, Vieira DB, Quinet A, de Andrade-Lima LC, Munford V, et al. Glutathione depletion sensitizes cisplatin- and temozolomide-resistant glioma cells in vitro and in vivo. Cell Death Dis. 2014;5(10):e1505–5.

57. Estrela JM, Ortega A, Obrador E. Glutathione in cancer biology and therapy. Crit Rev Clin Lab Sci. 2006;43(2):143–81.

58. Nguyen T-L, Durán R V. Glutamine metabolism in cancer therapy. Cancer Drug Resist. 2018;

59. Borodovsky A, Seltzer MJ, Riggins GJ. Altered cancer cell metabolism in gliomas with mutant IDH1 or IDH2. Curr Opin Oncol. 2012;24(1):83–9.

60. Garrett M, Sperry J, Braas D, Yan W, Le TM, Mottahedeh J, et al. Metabolic characterization of isocitrate dehydrogenase (IDH) mutant and IDH wildtype gliomaspheres uncovers cell type-specific vulnerabilities. Cancer Metab. 2018;6(1):4.

61. Peeters TH, Lenting K, Breukels V, van Lith SAM, van den Heuvel CNAM, Molenaar R, et al. Isocitrate dehydrogenase 1-mutated cancers are sensitive to the green tea polyphenol epigallocatechin-3-gallate. Cancer Metab. 2019;7(1):4.

62. Ohka F, Ito M, Ranjit M, Senga T, Motomura A, Motomura K, et al. Quantitative metabolome analysis profiles activation of glutaminolysis in glioma with IDH1 mutation. Tumor Biol. 2014;35(6):5911–20.

63. van Lith SAM, Navis AC, Verrijp K, Niclou SP, Bjerkvig R, Wesseling P, et al. Glutamate as chemotactic fuel for diffuse glioma cells: Are they glutamate suckers? Biochim Biophys Acta - Rev Cancer. 2014;1846(1):66–74.

64. Albers MJ, Bok R, Chen AP, Cunningham CH, Zierhut ML, Zhang VY, et al. Hyperpolarized 13C lactate, pyruvate, and alanine: noninvasive biomarkers for prostate cancer detection and grading. Cancer Res. 2008;68(20):8607–15.

65. Brindle KM, Bohndiek SE, Gallagher FA, Kettunen MI. Tumor imaging using hyperpolarized 13C magnetic resonance spectroscopy. Magn Reson Med. 2011;66(2):505–19.

66. Crisi G. 1 H MR Spectroscopy of meningiomas at 3.0T: the role of glutamate-glutamine complex and glutathione. Neuroradiol J. 2011;24(6):846–53.

67. Hazany S, Hesselink JR, Healy JF, Imbesi SG. Utilization of glutamate/creatine ratios for proton spectroscopic diagnosis of meningiomas. Neuroradiology. 2007;49(2):121–7.

68. Krishna G, Soman Pillai V, Valiya Veettil M. Upregulation of GLS1 isoforms KGA and GAC facilitates mitochondrial metabolism and cell proliferation in Epstein–Barr virus infected cells. Viruses. 2020;12:811.

Publisher's Note